ABSTRACT

Title of Dissertation: EFFECT OF GLASS JOINS ON PERFORMANCE OF LAYERED DENTAL CERAMIC SYSTEMS

Mey A.Saied, Doctorate of Philosophy 2009

Dissertation Directed by: Associate Professor Isabel K. Lloyd
Department of Materials Science and Engineering

Layered structures can be used to address the competing needs of systems like dental crown restorations where the exterior needs to be aesthetic and the interior needs to be strong and fatigue resistant. Dental crowns typically have an aesthetic porcelain veneer layered on a strong, fatigue resistant ceramic or metallic core. In current restorations, even when the core is shaped by a computer-aided design and manufacturing (CAD/CAM) or solid-freeform fabrication processes, the veneer is applied in sequential layers. This process is labor intensive, time consuming and may not optimize the long-term performance properties of the veneer layer. If the core and veneer layers were to be independently fabricated and then joined, their individual and the veneer-core system performance could be optimized. Some groups have explored the possibility of joining with filled epoxies, which is easier, but may

not be long-lasting. In this project we explore the possibility of using more durable glassy joins. Dense, thermal-expansion-matched (to the core and veneer glass) joins can be fired at temperatures far enough below the melting and/or slumping temperatures to join veneers to cores without degradation. In this study, we design and fabricate joining glasses for bonding porcelain veneers to ceramic cores, specifically to dental aluminas and zirconias. We study the chemical bonding and mechanical integrity of the resulting layers. Finally, we assess the effects of glass joins on performance of layered dental ceramic systems.

EFFECT OF GLASS JOINS ON PERFORMANCE OF LAYERED DENTAL CERAMIC SYSTEMS

By

Mey A. Saied

Dissertation submitted to the Faculty of the Graduate School of the
University of Maryland, College Park in partial fulfillment
of the requirements for the degree of
Doctor of Philosophy
2009

Advisory Committee:
Associate Professor Isabel K. Lloyd, Chair/Advisor
Dr. Brian R. Lawn, Co-advisor
Professor Lourdes Salamanca-Riba
Professor Manfred Wuttig
Associate Professor F. Patrick McCluskey

Dedication

For my father, Abdullah, my mother, Fathia, my brother Hatim and especially my niece, Iman, the future.

Acknowledgements

I would like to thank Dr. Isabel K. Lloyd for supervising me throughout these very interesting and intellectually stimulating last five years. She helped to inspire my curiosity for this subject matter. In particular her collaboration with Dr. Brian Lawn on my behalf was a pivotal part of my completion. Thank you for the late nights, and for your dedication to my progress.

I would also like to thank Dr. Brian Lawn, NIST for being a wonderful co-advisor, for his expert advice on mechanical properties and his outstanding logic. He gave me unequivocal assistance, energy, and advice and treated like family, understanding my strengths and weaknesses, and having faith in me even when I faltered. I owe him a great deal, and will miss him terribly.

I wish to extend my deep gratitude to Dr. James Lee for his help and advice throughout. He is a joy for anyone lucky enough to work with him. In him I have a brother, a colleague and a friend. At NIST, I would also like to thank Dr. Wolfgang Haller, Mr. George Quinn, and Mr. Ed Parry.

To Dr. Dianne Rekow, New York University College of Dentistry, for taking a chance on me, pointing me in the right direction, and putting in so much effort and energy to help me succeed—many thanks. I promise to pay it forward. Also at NYU, I would also like to thank Dr. Van Thompson, Dr. Yu Zhang, Dr. Paolo Coelho and Ms. Elizabeth Clarke for their constant support, assistance and friendship.

I would like to thank Dr. Otto Wilson of Catholic University for his advice, support, and friendship. His input on sol-gel processing was invaluable, as were his

introductions to the Vitreous State Laboratory (VSL) group at Catholic University. Also at VSL, I would like to thank Dr. Isabelle Muller, Dr. Fernando Perez-Cardenas and the staff there who were essential for the glass processing segment of this project.

At the University of Maryland, my gratitude is due to Dr. Kathleen Hart, who always listened and stepped in to make things happen, Dr. Robert Briber, for helping whenever funding hiccups occurred and Dr. Phil Piccoli, for his friendly assistance with electron microscopy.

I am thankful for financial support from the NRSA Minority pre-doctoral fellowship award grant NIDCR 5F31DE017297.

Finally, I would like to thank my family for their continued patience, encouragement and faith even when they are so far away. My father, who opened my eyes to the world, the possibilities, gave everything he could and helped me see that nothing could hold me back. My mother, who withstood the storm of traditions, and opened her mind, and fought for me always. My brother, who was my friend first, my protector second, and who always believed in me. I would be nothing without you.

Table of Contents

List of Tables

List of Figures

Chapter 1: Introduction

1.1 Background and Approach

Dental restorations involve repairing or replacing dentition that has been lost due to disease or injury. Several considerations must be taken into account when such restorations are made. Mechanical properties must be sufficient to withstand the functional stresses of chewing and, in extreme cases, to bruxing/grinding. Chewing may involve loads of several hundreds of N, over 10^6 cycles/5 years, in a hostile oral environment, making restorations vulnerable to failure. The hostile environment includes aqueous chemistry, saliva pH, thermal stresses (hot coffee and ice-cream), and complex loading. This requires high-strength materials for long life. The hardness and Young's modulus of the replacement materials must be similar to natural dentition; any departure may adversely affect load transfer and lead to failure. And the materials should also be sufficiently tough to avoid fracture. In addition to these requirements are the needs for a good cementation of a crown replacement to the remaining tooth. Most important in the context of dentistry, there is the demand for aesthetics, requiring matching of natural teeth in color, hue (tone), value (saturation) and chroma (lightness), opacity, metamerism and fluorescence. All this constitutes a significant materials challenge.

Of primary interest to this study is the need to find new ways to fabricate dental crowns. Currently, there is a trend toward all-ceramic systems, because of

aesthetics, bioinertness and biocompatibility. Traditional metal/alloy-based crowns are losing favor. But all-ceramic systems pose a problem. It is almost impossible to find a single ceramic that provides the essential combination of strength and aesthetics, so modern crowns are generally fabricated by painting an aesthetic porcelain veneer onto a hard, stiff and tough ceramic alumina or zirconia base. This approach has several drawbacks. It is time- and labor-intensive, and demands a highly skilled technician. Errors in sintering times and temperatures can introduce flaws (pores, cracks) that lead to premature failures. There is an interesting materials challenge here, to produce an alternative economic processing route.

Our approach is to introduce a different method of making all-ceramic crowns, whereby a porcelain veneer and ceramic core can be fabricated independently and subsequently fused with a strong join. The prospect is of cheaper, better and more durable crowns. We will investigate this approach in this study using glass as a bonding agent. Glass joining has a solid history in several technologies, notably in glass seals and glazes, electronic packaging, fuels cell technology, etc. Adjacent veneer and core ceramic layers could be fabricated independently via solid free-form techniques or CAD/CAM methods, and sintered according to material specifications. Then, the two layers could be fused using a thermally sintered glass join, with melting and wetting below the softening temperature of the veneer.

1.2 The Challenge

To our knowledge, the performance of glass joins has not been systematically evaluated in systems that relate to dental crown fabrication. There are many

challenges to putting such an approach into practice. (i) One must be able to prepare veneer and core ceramics routinely and independently. This is the realm of traditional ceramic science, and is well documented. (ii) Then one must demonstrate that these layers can be fused with an appropriate glass. The glass must wet the two ceramic components. The glass join must have good thermal fit to both the veneer and the core, so as to avoid deleterious residual stresses from thermal expansion mismatch and must be bioinert or biocompatible. (iii) One must understand the chemical nature of the join, and characterize it. Generally, the join is expected to form an atomically mixed interdiffusion layer. The degree of interdiffusion, interdiffusion chemistry and thermomechanical properties are all expected to influence the overall mechanical performance of the joins. (iv) Finally, one must then test the strength of the join, to demonstrate its resilience under comparative oral operational conditions, incorporating a hostile environment and fatigue loading. Throughout the fabrication process, it is important to remain aware of clinical relevance, to ensure that the technology is transferable to dental practice.

1.3 Outline of Thesis

The thesis will follow the following route. Chapter 2 will outline how suitable glasses are chosen to match veneering porcelains and ceramic cores. For this, matching of thermal expansion coefficients is vital, to avoid residual stresses in the finished product. The chapter will describe how commercial glasses were tested to meet this need, and then rejected because of incompatibility concerns. It will then

describe how new glass compositions were designed and fabricated to overcome these incompatibility issues. Sol gel processing will form the underlying processing route, with the prospective advantage of low-temperature manufacture. Various tests for assessing the glass properties will then be described, including degree of wetting, crazing and pore formation.

Chapter 3 will deal with the methodology for joining veneer and core layers by glass fusion. Glasses with a range of compositions will be investigated, and tested to see how well they bond the adjacent layers. Different firing temperatures and times for glasses of different compositions will be explored, to determine optimum bonding conditions. Simple mechanical screening tests for deciding whether any given layer combination is suitable for more detailed study will be described. Optical microscopy of veneer/glass/core sections will be used to determine the integrity of the fused interfaces. Microprobe analysis for determining the nature of interdiffusion layers at the interface boundaries will be presented.

In Chapter 4, the mechanical integrity of the glass joins will be examined in greater depth. For this, a Vickers indentation probe method developed at NIST will be employed. This method introduces small controlled cracks at prescribed locations in the veneer/glass/core sections, close to and away from the interfaces of interest. This is a simple but powerful way to examine local fracture properties of complex systems. The indentations are aligned so that a lead crack is made to approach the glass join interface—if the crack arrests at the boundary, or penetrates it, without deflecting along the interface, then the system is deemed to be adequately strong for the specific application in mind. A quantitative analysis of this mechanical testing

procedure will be presented.

Finally, in Chapter 5, future directions will be discussed.

Chapter 2: Design & Processing of Tailored Glasses

2.1 Introduction

Dental crowns are used to repair badly damaged teeth. They are traditionally fabricated by fusing hand-layered porcelain veneer onto metal or, more recently, ceramic cores. In current restorations, even when the core is shaped by CAD/CAM (or solid freeform fabrication processes), the veneer is applied in sequential layers. Many problems are associated with this method of veneer application, including high expense, labor-intensive multiple layers, which may degrade the long-term performance. Fabricating veneers and core separately—e.g. computer-aided design and manufacturing, including robocasting by [1]—would appear to have some advantages. Some workers [2-5] have explored the possibility of joining with filled epoxy resins. This is an easy solution, but the interfaces tend to be weak and susceptible to degradation over time.

In this study our aim is to explore the possibility of using more durable joins, specifically glass interlayers. This method requires higher temperatures, so more attention must be paid to residual stress issues. However, it offers the prospect of much stronger and more chemically inert structures. There is a wide literature on the use of glasses for joining, but dentistry imposes some stringent constraints. For instance, it is important that the glass be matched in CTE (coefficient of thermal expansion) to that of the veneer and core, to minimize spurious stresses. Also, there

is a limit to the operating temperatures for joining, to ensure that the integrity of the veneering porcelain is not compromised. Additionally, there are issues of toxicity. And finally, the glass must resist large numbers of stress cycles under adverse chemical conditions (fatigue). Thus lead-containing glasses, while widely used as glass seals, are not a viable possibility for any form of human prostheses. All this means paying a great deal of attention to glass compositions and processing methodologies.

In this chapter we will lay out the procedure for selecting, designing and fabricating joining glasses for porcelain veneers to ceramic cores, specifically to dental aluminas and zirconias. We will provide a background outlining fabrication procedures, both general and specific. Then we will describe our experimental approach to the problem, with a detailed description of processing in relation to the particular veneer/core combination under consideration. Finally, we will describe various techniques used to characterize the materials produced, in preparation for layer joining in the next chapter.

2.2 Background

As indicated, layered structures can be used to address the competing needs of systems like dental crown restorations where the exterior needs to be aesthetic and the interior needs to be strong and fatigue resistant. Dental crowns typically have an aesthetic porcelain veneer layered onto a strong, fatigue-resistant ceramic or metallic core [6], before being cemented onto the supporting tooth dentin structure layer, as

shown in Figs. 2.1 and 2.2. The veneer-layering process is labor intensive, time consuming and may not optimize the long-term performance properties of the veneer.

If the core and veneer layers were independently fabricated and then joined, their individual performance could be optimized. Glass joining methods are widely used in other areas including lighting [7,8], fuel cells [9,10] and hermetic seals for electronic packaging [11,12]. In principle, dense, CTE matched veneer/core joins could be fired at temperatures far enough below the softening temperature, T_s, of the veneer without degradation. Initial work in our laboratory has shown that this approach is feasible for ceramics used in dental restorations [13-16].

Traditional glass processing makes use of glass compositions to match requisite properties such as softening temperature, thermal expansion, electronic properties, opacity, etc. Examples of glass sealant use include hermetic sealing [7], electronic packaging [17] and solid oxide fuel cells [9,18]. The most widely used method is by mixing oxide powders with melting, fining, annealing and quenching [19,20]. Other methods include sol-gel and wet chemical processing, with the advantage of lower-temperature manufacture (avoiding the need for platinum crucibles), greater control over material homogeneity and small-batch processing [21-23]. This last approach has large appeal in the context of dental material joining, and so we adopt it here.

2.3 Materials Selection

The first step was to determine which glass compositions we need to use. We

need to match glass composition in terms of important properties, most importantly CTE and T_g (glass transition temperature). Our glasses were formulated using property-dependent additivity factors developed by several early workers to tailor CTE [24-29], viscosity [30-34] and T_g (glass transition temperature) [35,36]. Compositions were then made by sol-gel processing and glass-melting techniques, and tested for CTE and T_g using dilatometry and thermomechanical analysis (TMA), and then used to join layers of common veneer/ core combinations.

2.3.1 Choice of core and veneer materials

For alumina-based core-veneer bilayers, experiments were carried out on core material from two sources: one, an alumina used as substrates in the electronic industry (AD90, Coors, Golden, CO); and two, a dental alumina from Nobel BioCare (Procera, Nobel BioCare AB, Stockholm, Sweden). The first of these was chosen because it was available cheaply in quantity, the second for its dental relevance. For zirconia-based bilayers, Cyrtina Dental zirconia, (Biozyram, Cyrtina Dental, Netherlands) was selected. Materials were obtained as blocks, cut to size approximately 10 mm square and 1–3 mm thick. Blocks were ground to 0.2–0.7 mm thickness, and surfaces were polished flat and parallel to 1 μm finish using diamond paste. Zirconia samples were finished with colloidal silica suspension to remove any strain-induced transformations.

Body porcelain veneer powders were procured so as to match the CTE for the core materials.

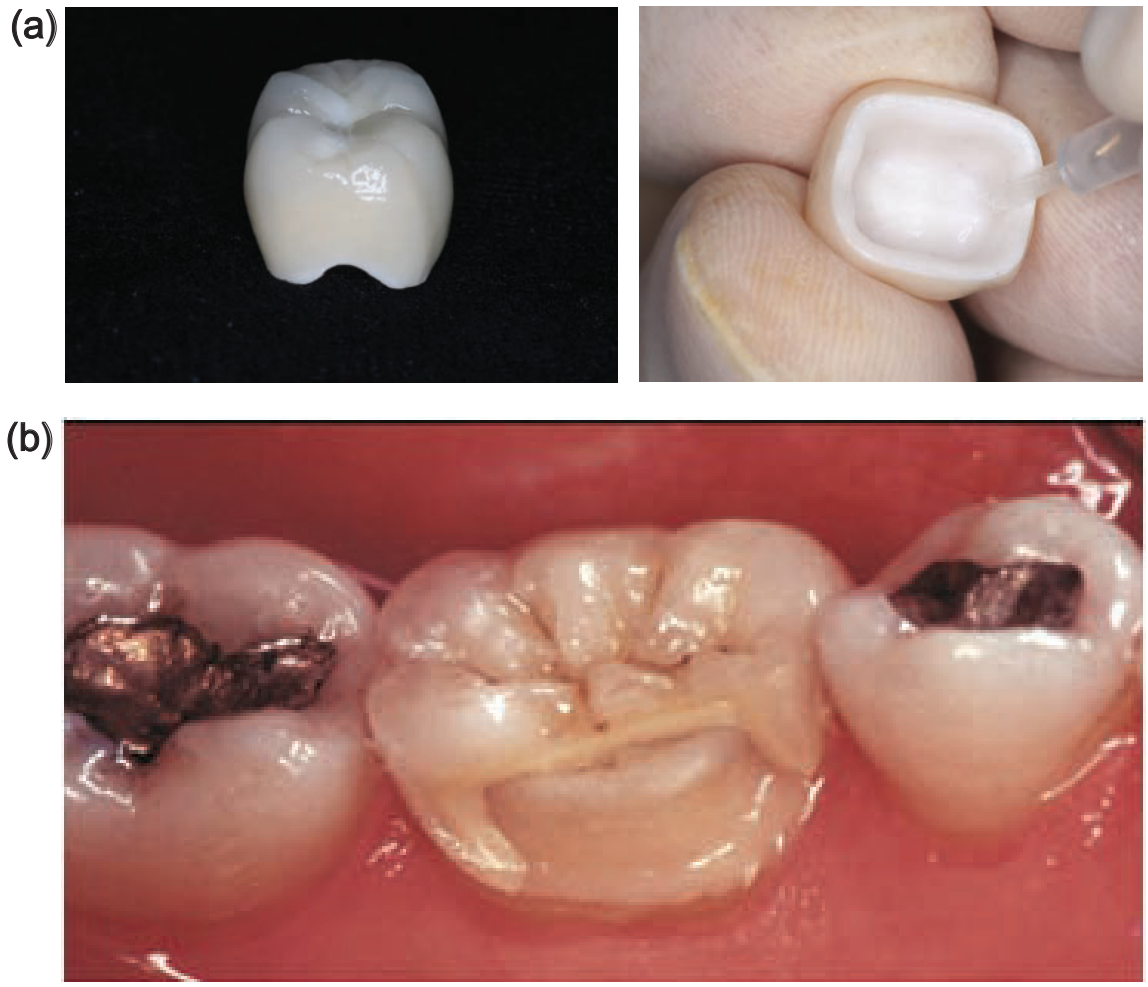

Figure 2.1 Dental crowns; (a) Veneered zirconia crown, with cement application, prior to bonding to supporting structure (Courtesy P. Coehlo). (b) Failed all-ceramic (Alumina) crown, with veneer, core and tooth structure clearly visible (Courtesy Kenneth Malament).

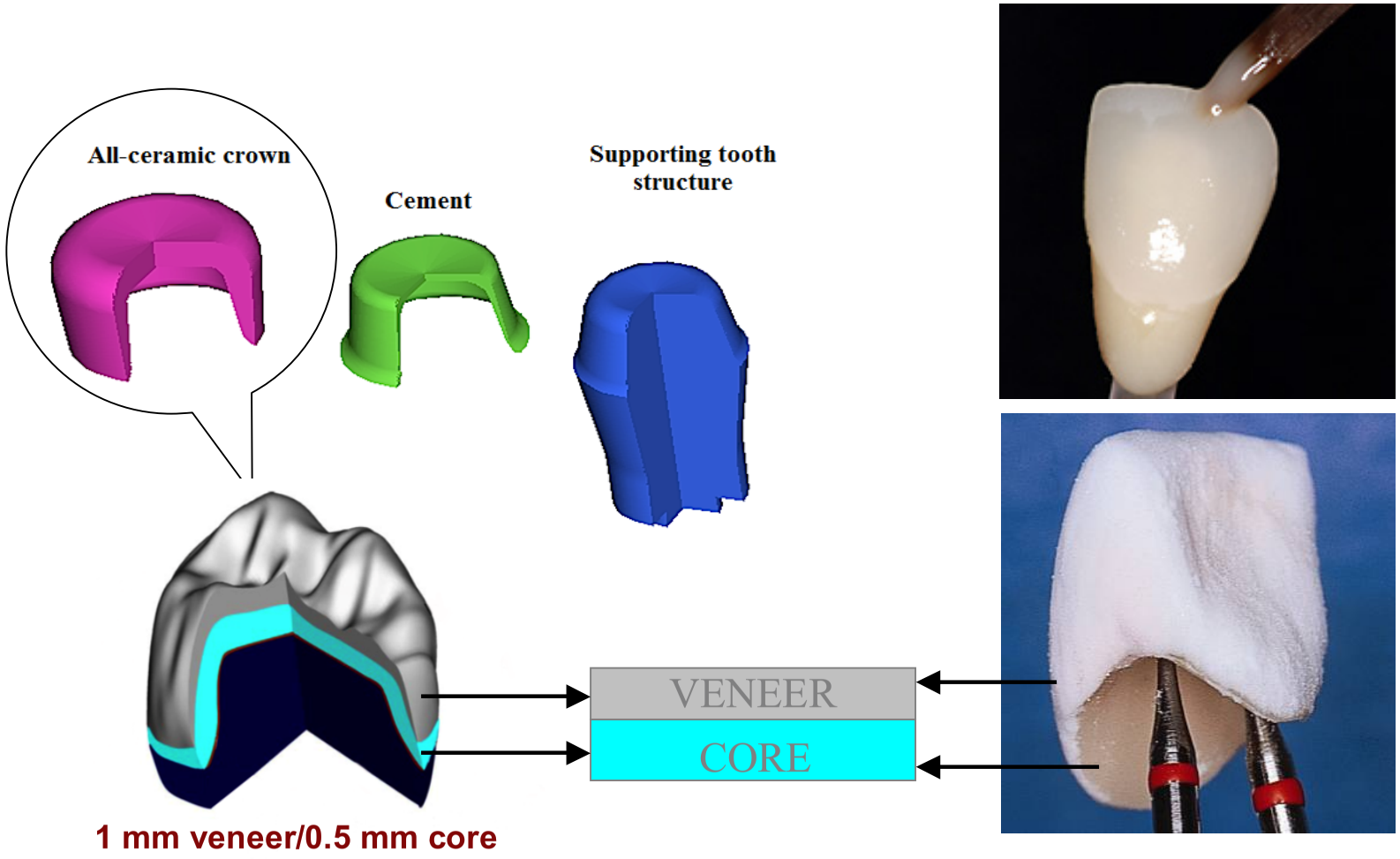

Figure 2.2 Traditional methods of making dental ceramic restorations (courtesy G. Zhang, E.D. Rekow, V.P. Thompson and Y. Wang)

For alumina we used matching NobelRondo™ Press alumina porcelain (Nobel BioCare AB, Stockholm, Sweden), and for zirconia Sagkura Interaction porcelain (Elephant Dental, The Netherlands). To make the porcelain, water-based slurries of the porcelain were poured into a mold, vibration was used to settle the porcelain and excess water was blotted off in successive layers. Then, the porcelain was dried and fired at the manufactures' recommended temperatures, as outlined in Fig. 2.3. Porcelain surfaces were then also ground and polished flat and parallel to 1 μm finish using diamond paste.

Core and veneer properties relevant to our glass composition and properties include CTE of both core and veneer materials, and T_g and T_s (transition and softening temperature of the veneer materials). T_s is the temperature at which a veneer can deform under its own weight. This would cause slumping and shape loss of the veneer, which must be avoided in dental restorations. Table 2.1 lists properties of veneer and core materials.

2.3.2 Choice of glass compositions

Initial investigations were performed on commercially-available lead-free industrial glass powders obtained commercially (Schott Electronic Packaging, Landshut, Germany and Ferro, Cleveland, OH). The 9 glasses investigated comprised glass-to-metal sealants and electronic and pharmaceutical packaging glasses, listed in Tables 2.2 and 2.3. Their compositions varied from alumino-borosilicates (high working temperature) and bismuth-based (low working temperatures, T_w). Unfortunately, the industrial glasses proved to be inadequate for a

number of reasons that will be discussed later. The need for developing laboratory-made glasses tailored to our needs thus became imperative.

First, the glass properties critical to our dental sealant application were identified. As mentioned previously, our aim was to produce a glassy chemical bond for solid freeform fabricated, or robocast separate veneer and core layers.

Accordingly, our approach was to fabricate tailored in-house glass compositions to provide CTE matching to our selected alumina- and zirconia-based bilayer systems. We used base glass compositions for which CTE properties have been determined from the glass seal literature [7], along with rule of mixture formulae to adjust individual glass components. These rules involve a empirical linear additivity relations in terms of concentrations and mol% "factors", from which CTE can be calculated.

The results of such calculations for specific glass compositions, are shown in Table 2.4 for factors from Winkelmann and Schott [24-26], and in Table 2.5 using factors from Appen [27-29]. In addition, empirical tabulations from Fluegel [35,36] were used to estimate viscosities at working temperature (800 C), along with glass transition, softening and melting temperatures (T_g, T_s, and T_m), and Young's modulus. Table 2.6 shows the results for the compositions in Table 2.5.

It will be noted that the laboratory glasses compositions listed in Tables 2.4 to 2.6 contain no toxic elements like lead. While the present study is meant simply to establish feasibility of the methodology, toxicity is still of interest.

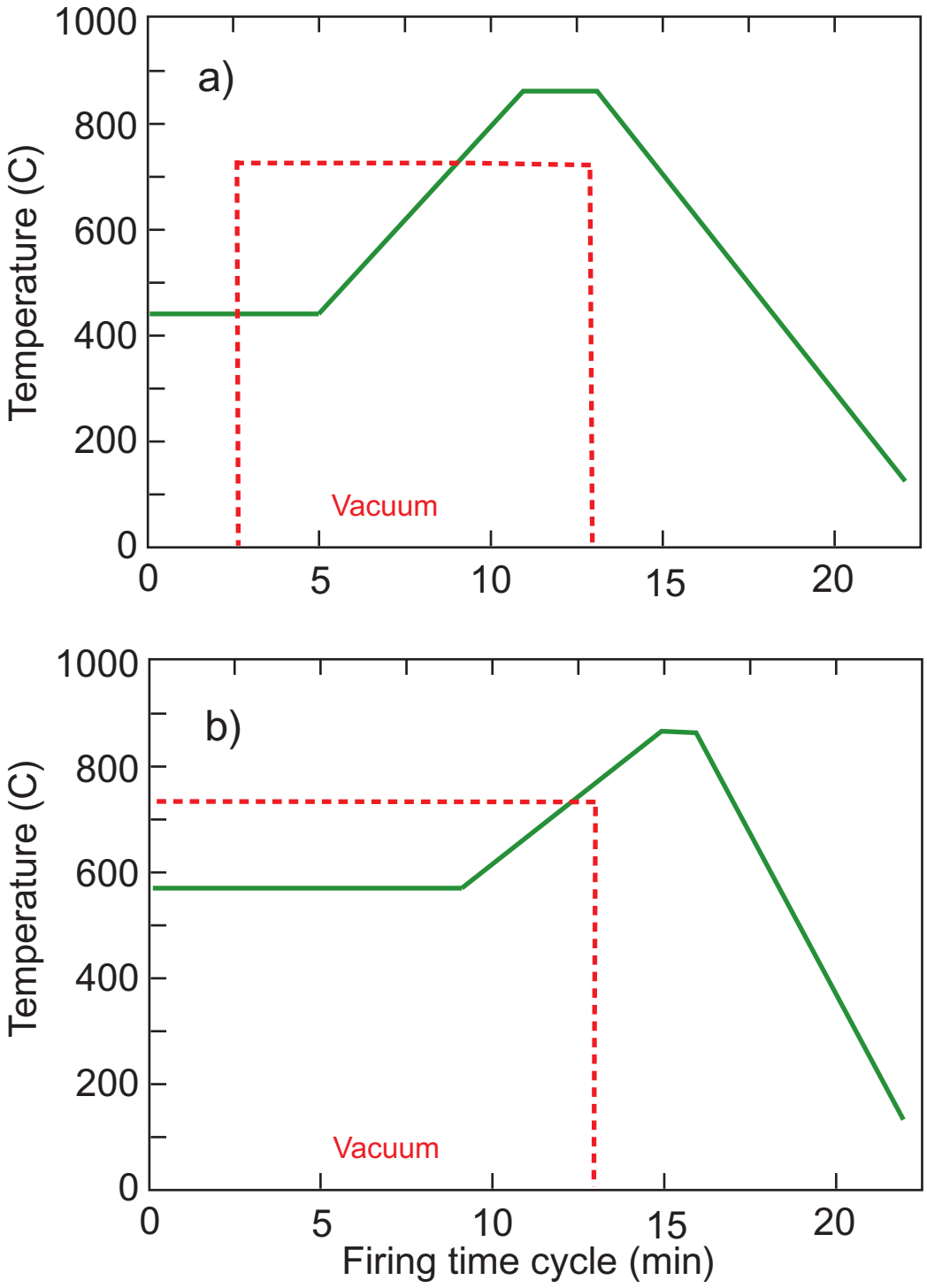

Figure 2.3 Manufacturer recomended firing cycles for a) Nobel Rondo alumina-veneering porcelain, and b) Sakura Interaction zirconia veneering porcelain.

Table 2.1 Properties of veneer and core materials

Alumina system materials

Name	Function	Supplier	*CTE 20-500 °C, x 10 $^{-6}$/C*	Flexural Strength, MPa	Elastic Modulus E, GPa	Fracture Toughness, MPa.m$^{-1/2}$	T_g °C	T_s/T_m °C
Procera	Core	Nobel Biocare	***7.0-7.3***	600-687	370	4.48	NA	***>2,000***
Rondo	Veneer	Nobel Biocare	***7.20***	120	~ 65	1.0	620	***>890***
AD999	Core	Coors	***8.0***	500	406	3.9	NA	NA

Zirconia system materials

Name	Function	Supplier	*CTE 20-500 °C, x 10 $^{-6}$/C*	Flexural Strength, MPa	Elastic Modulus E, GPa	Fracture Toughness, MPa.m$^{-1/2}$	T_g °C	T_s/T_m °C
Biozyram	Core	Cyrtina Dental	***10.5***	1,000	205	8.5	NA	***>2,600***
Sakura Interaction	Veneer	Elephant Dental	***9.9***	>50	~ 65	1.0	485	***>890***

Table 2.2 Properties and compositions of Schott industrial lead-free aluminoborosilicate and bismuth glasses

Glass No.	Function	Composition	CTE x10^{-6} C^{-1}	T_g C	T_w C (logη=4)	Modulus E, GPa	Poisson's ratio
8415	Illax®, amber tubing glass for pharmaceutical packaging	75% SiO_2, 8–12% B_2O_3, up to 5% alkaline earths and Al_2O_3 ,	7.8	535	1050	74	0.21
8421	Sealing glass for seals with NiFe45 (DIN 17745) and compression seals	No Information available	9.7	525	1000	74	0.22
8422	Sealing glass for seals with NiFe47 or 49 (DIN 17745) and compression seals	No Information available	8.7	540	1010	76	0.21
G018-193	Sinter glass ceramic for LTCC application	10-50% SiO_2 10–50% B_2O_3 1-10% Al_2O_3 , 10-50% CaF_2 1-10% ZnO 1-10% ZrO_2 1-70% alkaline earths	10	580	830	70-80	~ 0.22
G018-249	Low melting Lead-free Solder Glass	1-10% B_2O_3 0.1-2% Al_2O_3 , 1-10% SiO_2 10-50% ZnO >50% Bi_2O_3	10.11	365	380-500	70-80	~ 0.22
G018-250	Low melting Lead-free Solder Glass for CTE range 7-8	1-10% Li_2O 1-10% B_2O_3 1-10% Al_2O_3 , 1-10% SiO_2 1-10% ZnO >50% Bi_2O_3	7	380	350-540	70-80	~ 0.22

Table 2.3 Properties and compositions of Ferro industrial lead-free bismuth glasses

Glass No.	Function	Composition	CTE x10^{-6} C^{-1}	T_g C	T_w C (logη=4)	Modulus E, GPa	Poisson's ratio
EG2914	Lead-free sealing glass	Bi_2O_3 ZnO B_2O_3 SiO_2 R_2O *	10.25	430	465-525	70-80	~ 0.22
EG2964	Lead-free bonding and sealing glass	Bi_2O_3 ZnO B_2O_3	8.45	480	520-560	70-80	~ 0.22
EG2998	Lead-free lamp sealing glass	Bi_2O_3 ZnO B_2O_3	9.80	405	440-500	70-80	~ 0.22

* R = alkali metal ion

2.4 Preliminary Tests Using Industrial Glasses

As indicated above, we originally set out to investigate the possibility of effecting glass joins using the commercially available glass powders listed in Tables 2.2 and 2.3. In these cases, we mixed the powders into a thick aqueous slurry and painted the mixture as layers up to 200 μm thick onto the alumina and zirconia plates. The plates were then fired at manufacturer-recommended times and working temperatures (T_w in Tables 2.2 and 2.3). The fired plates were then examined in an optical microscope.

In short, no combinations of firing temperature could produce quality coatings on for the industrial glasses on any of the core materials. Several problems were encountered, as depicted in Fig. 2.4. These included, (a) porosity, (b) poor wetting, (c) discoloration and poor aesthetics and (d) crazing. Consequently, we turned our attention to laboratory fabricated glasses, where we had better control of the properties.

2.5 Glass Preparation by Sol-Gel Processing

2.5.1 Sol-gel wet mixing

In order to prepare the large number of experimental compositions, small batches of glass were made using sol-gel processing. We adopted the wet mixing methodology proposed by Yoldas et al. [37,38]. Silicon tetraethoxide (TEOS),

$Si(OC_2H_5)_4$, an alkoxysilane, was combined with aqueous solutions of metal nitrates in accordance with composition calculations. As TEOS is immiscible with water, it was first dissolved in 200 proof ethanol, and a small amount of water added.

Soluble nitrates were dissolved in de-ionized water then in ethanol, which was maintained as the solvent medium for the first few hours of reaction. The nitrate solution was then added to the TEOS solution, and the mixture stirred on a hot-plate at 60-70 C, where the following reactions took place:

$$\text{Si-OR} + H_2O \Rightarrow \text{Si-OH} + \text{ROH} \qquad \text{(hydrolysis)} \qquad (1)$$

$$\text{Si-OR} + \text{HO-Si} \Rightarrow \text{Si-O-Si} + \text{ROH} \qquad \text{(re-esterification)} \qquad (2)$$

$$\text{Si-OH} + \text{HO-Si} \Rightarrow \text{Si-O-Si} + H_2O \qquad \text{(alcoholysis)} \qquad (3)$$

All three reactions are concurrent throughout the sol, forming a silicate polymeric network. The sol is then allowed to cool, setting to a translucent gel as water and excess alcohol evaporate. Modifier metal ions remain within the network, and as the gel dries, cause structural variations that modify properties of resultant polymers [21]. The effect of these variations extends to the glasses obtained from the gels, and can even modify the glass's high temperature properties, including sintering, crystallization, and viscosity [22,39]. The resulting gels were then applied in their wet state onto alumina disks, dried, and fired at different temperatures in a dental furnace (Vita Vacuumat 2500, Vita Zahnfabrik, Bad Sackingen, Germany). This resulted in foaming of the gel due to water and organics trapped in the glass precursor at higher temperatures.

Table 2.4 Compositions of Winkelmann and Schott Factor-formulated lab glasses for bonding electronic alumina substrates

Glass Notation (CTE $\times 10^{-6}$/° C)	SiO_2 mol %	Al_2O_3 mol %	CaO mol %	Na_2O mol %	BaO mol %	B_2O_3 mol %
7.60	60.00	3.00	5.00	10.00	13.00	9.00
8.00	60.00	3.00	8.00	10.00	12.00	7.00
8.30	60.00	5.00	8.00	10.00	12.00	5.00
8.56	60.00	2.73	8.18	11.82	11.82	5.45
8.70	60.00	2.67	8.00	12.44	11.56	5.33
8.71	60.00	3.36	10.08	12.28	7.56	6.72
8.81	60.00	3.47	10.40	12.64	6.56	6.93
8.90	60.00	3.57	10.71	13.02	5.56	7.14
8.92	60.00	4.29	12.87	12.86	1.40	8.58
9.02	60.00	3.24	9.70	12.66	10.38	4.04
9.14	60.00	3.28	9.83	14.14	6.20	6.55
9.24	60.00	3.13	9.40	14.64	6.56	6.27

Table 2.5 Compositions of Appen Factor-formulated lab-tailored alumina-compatible and zirconia-compatible glasses

Alumina system materials

Glass Notation (CTE $\times 10^{-6}$/° C)	SiO_2 mol %	Al_2O_3 mol %	CaO mol %	Na_2O mol %	BaO mol %	B_2O_3 mol %
6.00	60	3.32	9.20	5.54	2.22	19.72
6.50	60	3.29	8.22	5.48	5.48	17.53
7.00	60	3.03	8.37	6.41	6.05	16.14
7.50	60	3.07	8.39	7.16	7.06	14.32
8.00	60	2.87	8.61	8.61	6.51	13.40

Zirconia system materials

Glass Notation (CTE $\times 10^{-6}$/° C)	SiO_2 mol %	Al_2O_3 mol %	CaO mol %	Na_2O mol %	BaO mol %	B_2O_3 mol %
9.80	60	3.36	10.09	12.27	7.56	6.72
10.20	60	3.28	9.83	14.14	6.20	6.55
10.40	60	3.13	9.40	14.64	6.56	6.27

Table 2.6 Calculated properties of selected join Appen glass compositions

Alumina system materials

Glass Notation	CTE (by Appen) $\times 10^{-6}$ °C^{-1}	$\log_{10}$ (viscosity Pa·s) at 800 °C	*T_g, °C	*T_s, °C	*T_m, °C	Young's Modulus GPa,
AP0600	6.00	3.9	586	607	1,281	73
AP0650	6.50	4.6	595	622	1,265	74
AP0700	7.00	4.9	586	613	1,201	74
AP0750	7.50	4.8	585	615	1,171	77

Zirconia system materials

Glass Notation	CTE (by Appen) $\times 10^{-6}$ °C^{-1}	$\log_{10}$ (viscosity Pa·s) at 780 °C	*T_g, °C	*T_s, °C	*T_m, °C	Young's Modulus GPa,
AP0980	9.80	4.8	573	608	1,171	78
AP1020	10.20	4.6	567	600	1,169	77
AL1040	10.40	4.6	563	597	1,162	77

* T_g °C (log η in Pa.s =12): glass transition T; T_s °C (log η in Pa.s =9): glass flow T; T_m °C (log η in Pa.s =1.5): glass melting T.

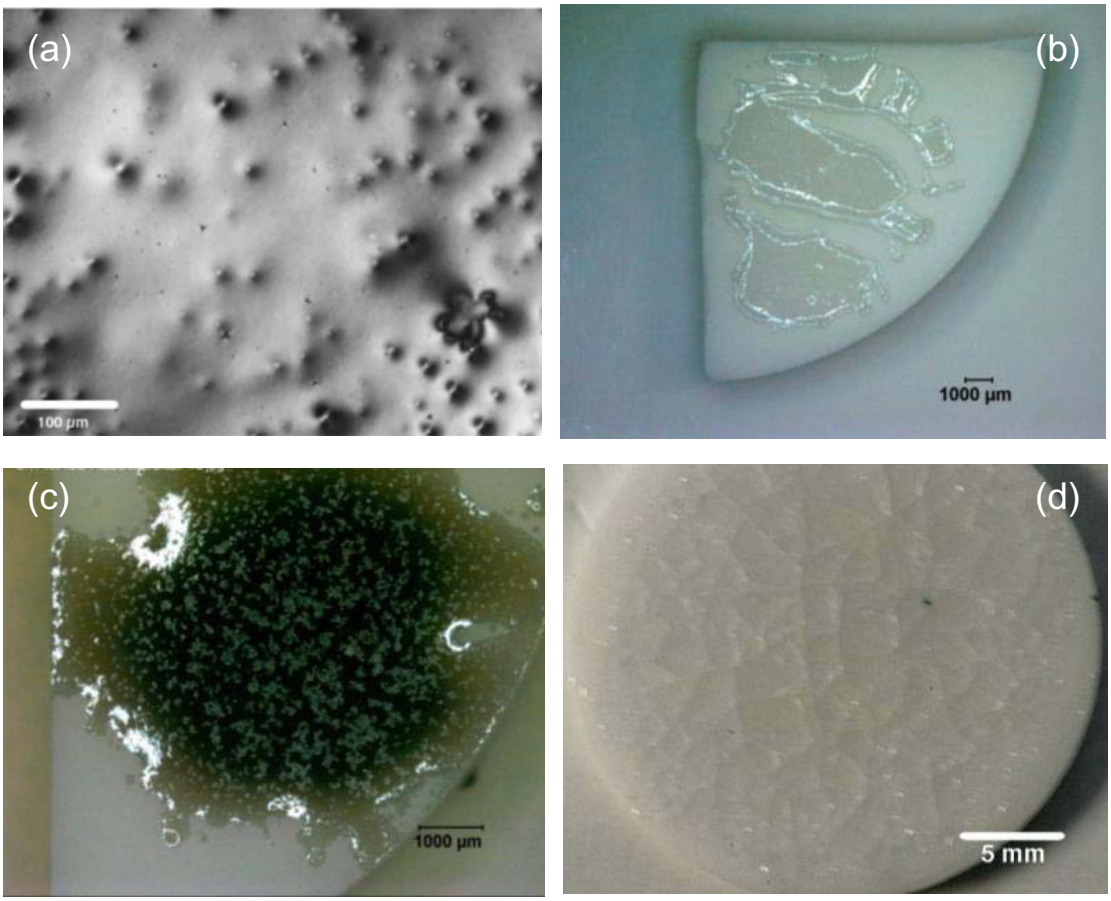

Figure 2.4 Lead-free commercially available glasses from Schott (Bad Sackingen, Germany and Ferro, USA). (a) Schott glass No. 8415, CTE $7.8 \times 10^{-6} C^{-1}$ on electronic alumina (EA) sintered at 800 C, showing pitting; (b) Ferro EG2964 CTE $8.5 \times 10^{-6} C^{-1}$ on alumina, showing poor wetting; (c) Schott G01-8249 CTE $10.1 \times 10^{-6} C^{-1}$ on zirconia, showing discoloration; (d) Schott G01-8421 CTE $9.7 \times 10^{-6} C^{-1}$ fired at 1000C on alumina, showing improved melting but crazing.

We subsequently decided that it would be best to heat the dried gel at a temperature high enough to remove these organics (but low enough to avoid melting, i.e. calcine them), then to grind the resultant powders and reapply them to the alumina disks. This alternative route is indicated in the flow diagram in Fig. 2.5. Melting tests were then conducted to determine appropriate firing temperatures. Two problems nevertheless persisted with this alternative route. First, in some of the mixtures, precipitation occurred when the TEOS and modifier salt solutions were combined. This meant that the glass was inhomogeneous on a molecular level, which could result in phase transformations during melting, and a highly unpredictable join behavior. The second problem was that some foaming of the powder still occurred between 600 and 1000 C, leading to some porosity. This was taken as evidence that some residual organics must have remained even after calcining.

Both these latter problems were tackled concurrently. Precipitation is common in alkoxysilane gels and has been documented elsewhere [37,38]. We first tackled this problem by using a more soluble barium salt, in the acetate form. The resultant gels were inconsistent in terms of precipitation. We then mixed the solutions with a higher ethanol component. The slow evaporation of the ensuing sol resulted in a gel that was completely homogenous to the eye, and therefore acceptable for our needs.

As to the second problem, calcining of the gels at 600 C for up to 15 hours resulted in powders that still foamed during firing on alumina disks. We ran a series of tests in which the specimens were heated in intervals of 50 C between 650 C and 1200 C. For this, the calcined powders were placed onto an alumina substrate before

heat treatment. Specimens were examined after each temperature interval. We observed some foaming in our melts up to about 850 C, and complete absence at 1200 C. Separate thermogravimetric analysis (TGA) was carried out in a Shimadzu TGA 50 at a heating rate of 10 C/ min to 1000 C, to check removal of organic volatiles. TGA profiles are shown in Fig. 2.6, for several gel compositions (Table 2.5). Weight loss is substantial up to 150 C, with subsequent gradual falloff, to a plateau at about 850 C, i.e. at the point where foaming ceases.

To reduce porosity (cf. Fig. 2.4a), we subsequently decided to run a second heating cycle up to 800 C. This succeeded in removing most of the pores. However, some minor crazing persisted in some specimens (cf. Fig. 2.4d), and some specimens showed evidence of poor wetting (cf. Fig. 2.4b). Another problem that arose, especially in those systems that used a higher content of ethanol to reduce precipitation was discoloration—in these cases, the calcined gels tended to turn to a dark grey or black powder (cf. Fig. 2.4c), presumably due to the entrapment of larger amounts of carbonized organics.

2.5.2 Melt and quench process

In an attempt to eliminate the problems outlined at the end of Sect. 2.5.1, we decided to augment the processing route with an addition melt and quench stage. The calcined gel powder was melted and fined at 1200 C for 3 hr, before quenching into an ice/water bath. This caused the glass melts to fragment into dense shards. The fragments were then broken down by grinding into powder using a corundum mortar and pestle, and sieved to a maximum 38 μm frit. This route is illustrated in Fig. 2.7.

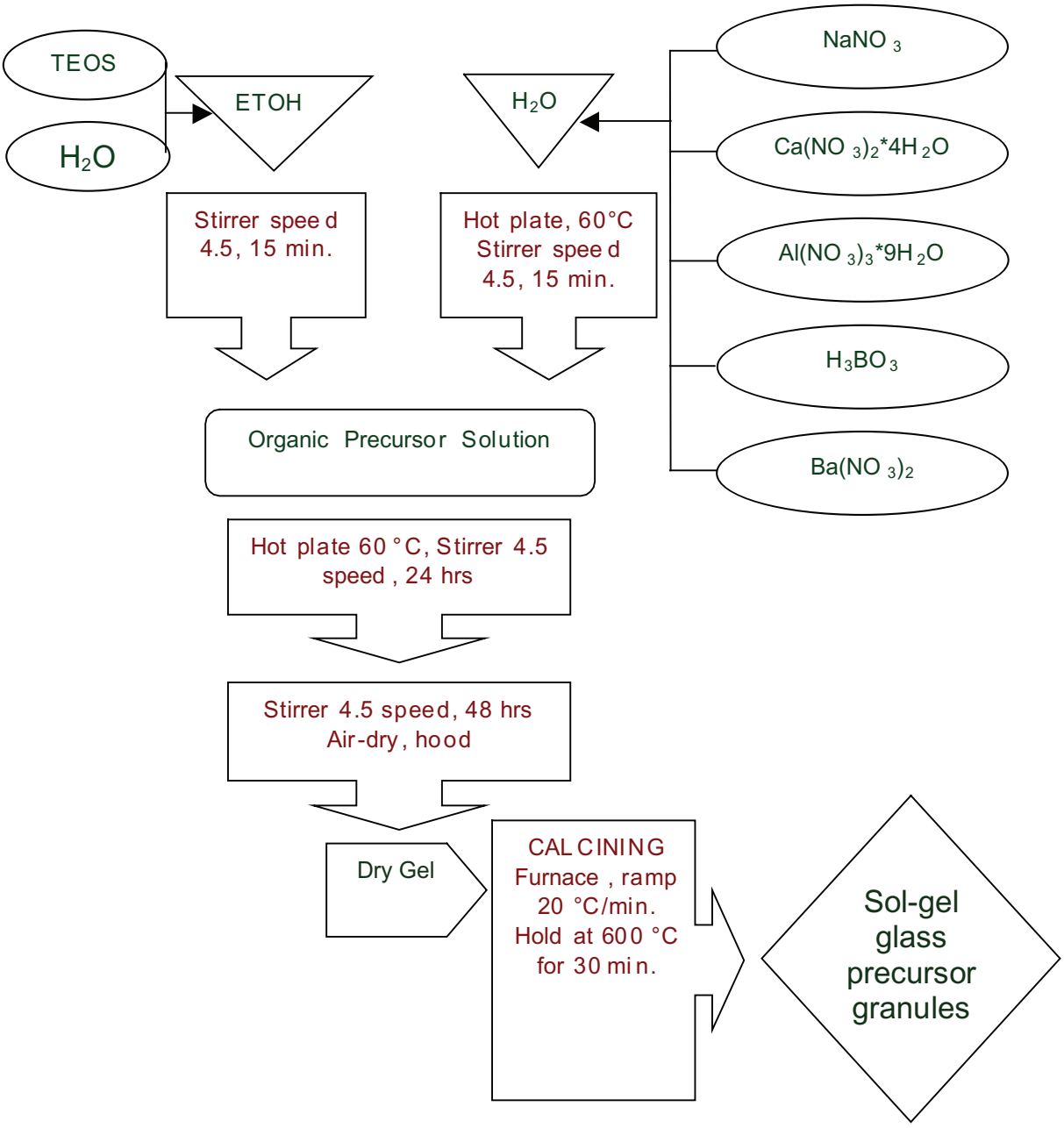

Figure 2.5 Sol-gel/wet mixing glass precursor preparation process diagram

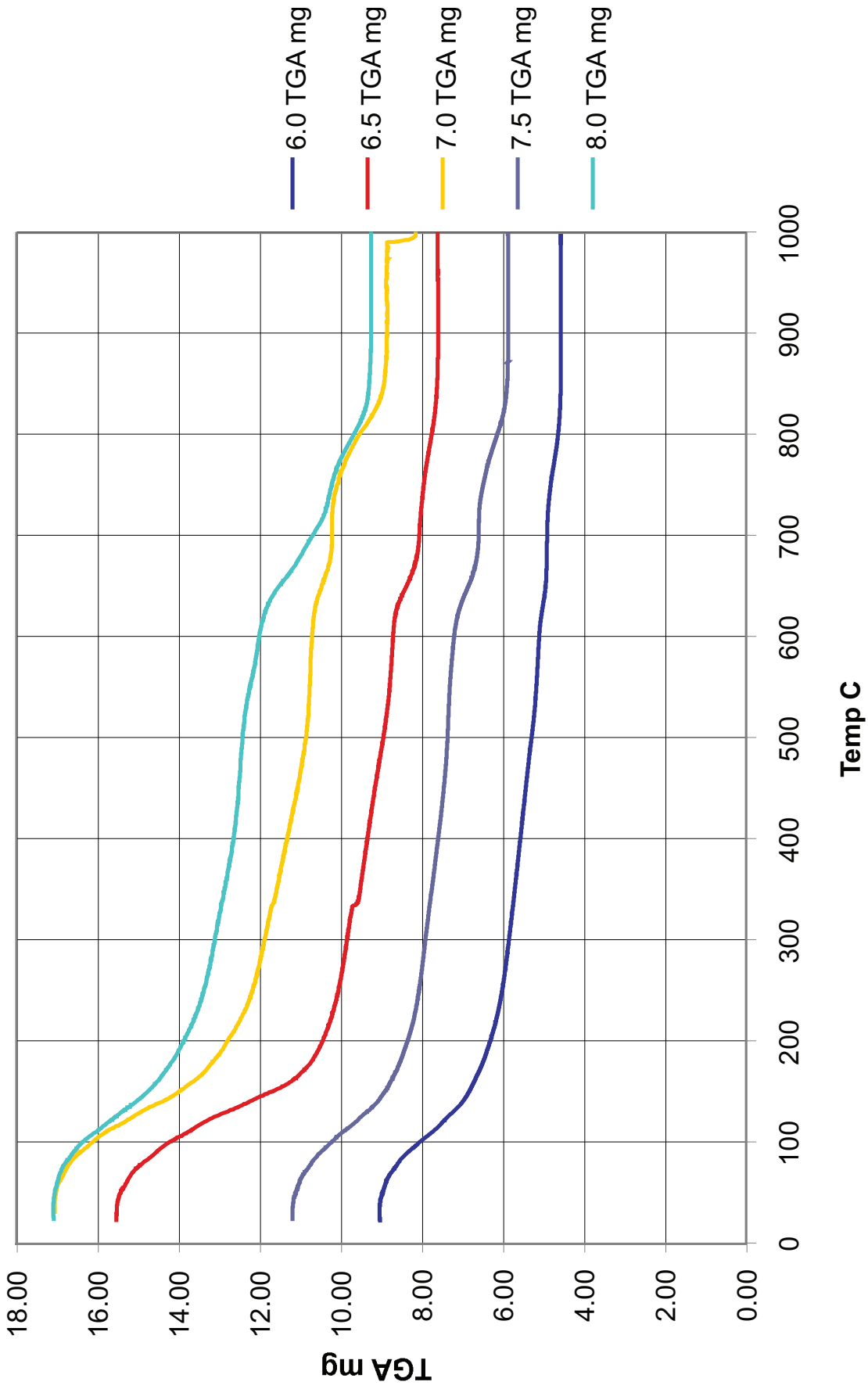

Figure 2.6 TGA of gels to assess minimum temperature for complete removal of volatiles

The frits were then mixed into aqueous slurries. At first, 0.5 wt% polyvinyl alcohol was tried as a binding agent, in order to enable smooth application of the slurry mixture onto the core ceramic substrates with a paint brush. However, even at the slowest drying rates available with our furnace, some discoloration occurred, from encapsulation of carbon particulates [40]. We then tried a solution of 50 vol% ethanol and water mixture. This was a little more inconvenient, because it required painting on of several layers of the slurry. However, the end result was a significant improvement, with no detectable porosity, good wetting, good aesthetics and no crazing. A typical example is shown in Fig. 2.8, for an Appen-formulated glass on a dental alumina substrate.

2.6 Material Characterization

Characterization tests were run on the core, veneer and final glass compositions, (AP700 for alumina systems, and AP 1040 for zirconia systems) material components to measure pertinent properties. These included thermomechanical analysis (TMA) primarily to confirm calculated CTE values. Additional dilatometry tests were run on just the glasses, to obtain additional information on the glass working temperatures.

After the melting and fining process, some of the glass melts were poured into preheated graphite bar molds and then annealed 580 °C for 1 hour. The glasses were then allowed to cool to room temperature, emptied from the molds, and cut into plates 7 mm on each side and 1 mm thick. Specimens of similar size were also prepared for

the dental alumina and zirconia core materials, as well as for the corresponding porcelain veneers. These were placed in the TMA furnace (IPC TM-650, Northbrook, IL) and heated to 500 C at a rate 25 C/min. Measured relative expansion is plotted as a function of temperature for each material in the alumina and zirconia systems in Figs. 2.9 and 2.10, respectively. Data are shown only within the range 100 C to 500 C, because the specimens take some time to 'settle in' on initial heating (hence the relative displacement of the curves along the expansion axis). The key observation is a common curve-fit slope (inclined lines) within $1x10^{-6}$ C^{-1}, representing the CTE for the 3 materials in each plot. This indicates good thermal matching in the critical temperature range with respect to mismatch stresses.

Additional tests were run using a dilatometer (Orton dilatometer DIL 2016 STD, Westerville, OH) on just the glass materials. These were conducted on larger bar specimens, 25 long and 3 mm square cross section. These tests enabled us to expand the temperature range up to 625 C, thus allowing for determination of working temperatures. For these tests, the heating rate was much slower, 3 C/min, eliminating much of the settling-in problem observed in the TMA. Figures 2.11 and 2.12 contain results from these tests, again for the selected glasses used in the alumina and zirconia systems. Results are shown as the curves, with the lines representing calculated CTE values from Table 2.5. These values compare favorably (within $1x10^{-6}$ C^{-1}) with the fitted lines from the TMA data in Figs. 2.9 and 2.10.

Also indicated in Figs. 2.11 and 2.12 are the glass transition temperatures T_g and dilatometry softening temperature T_s. These values also compare favorably with those calculated in Table 2.6.

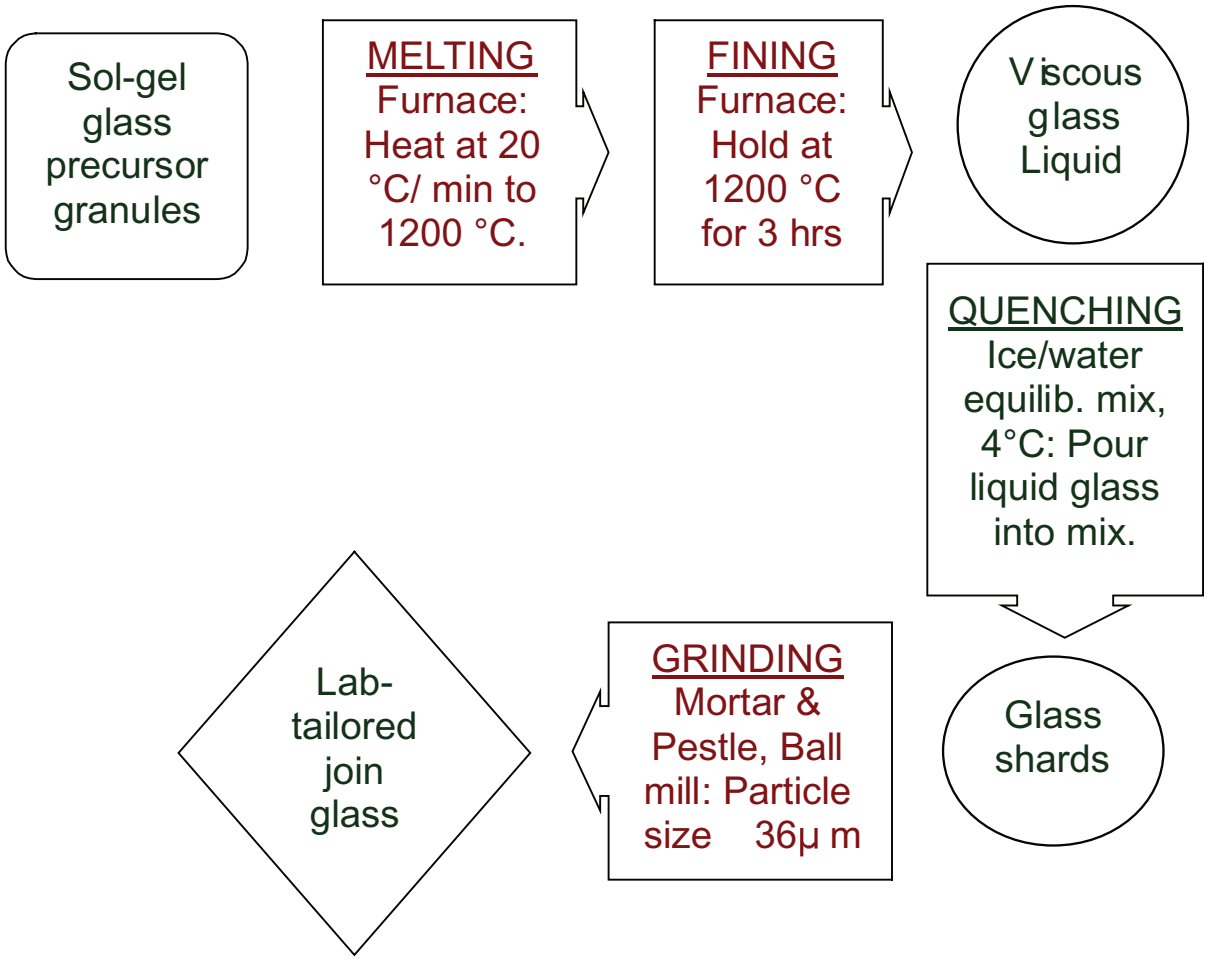

Fig. 2.7 Diagram of glass preparation from sol-gel precursors

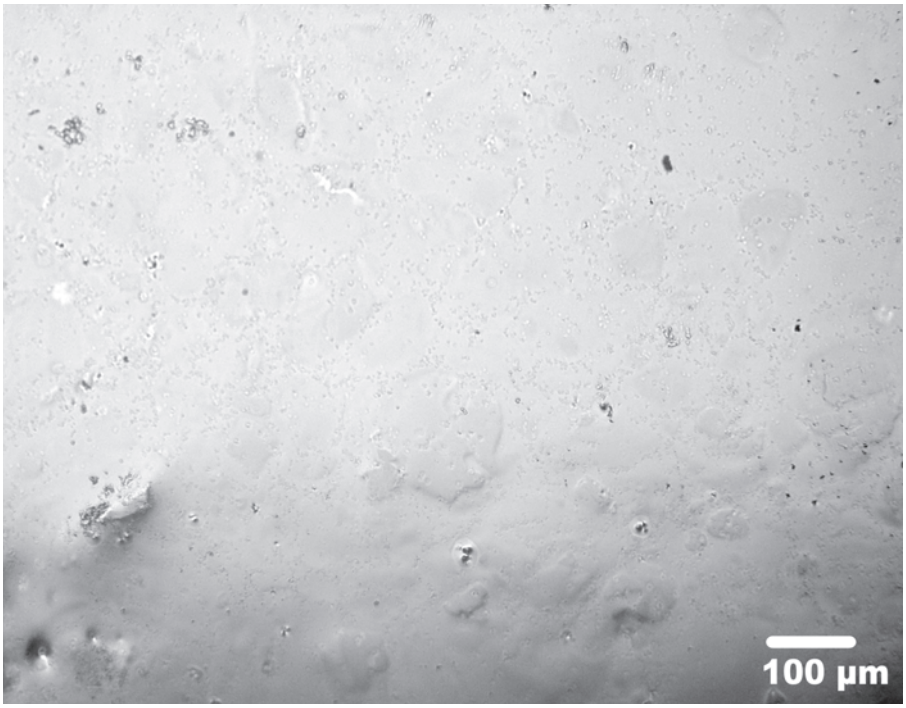

Figure 2.8 Crazing in Appen-formulated glass, AP650 (CTE = 6.5 x 10^{-6} C^{-1}) fired at 800 ºC for 10 mins on Procera alumina substrate. No crazing, porosity is visible, and wetting is good. Matt finish is due to surface roughness.

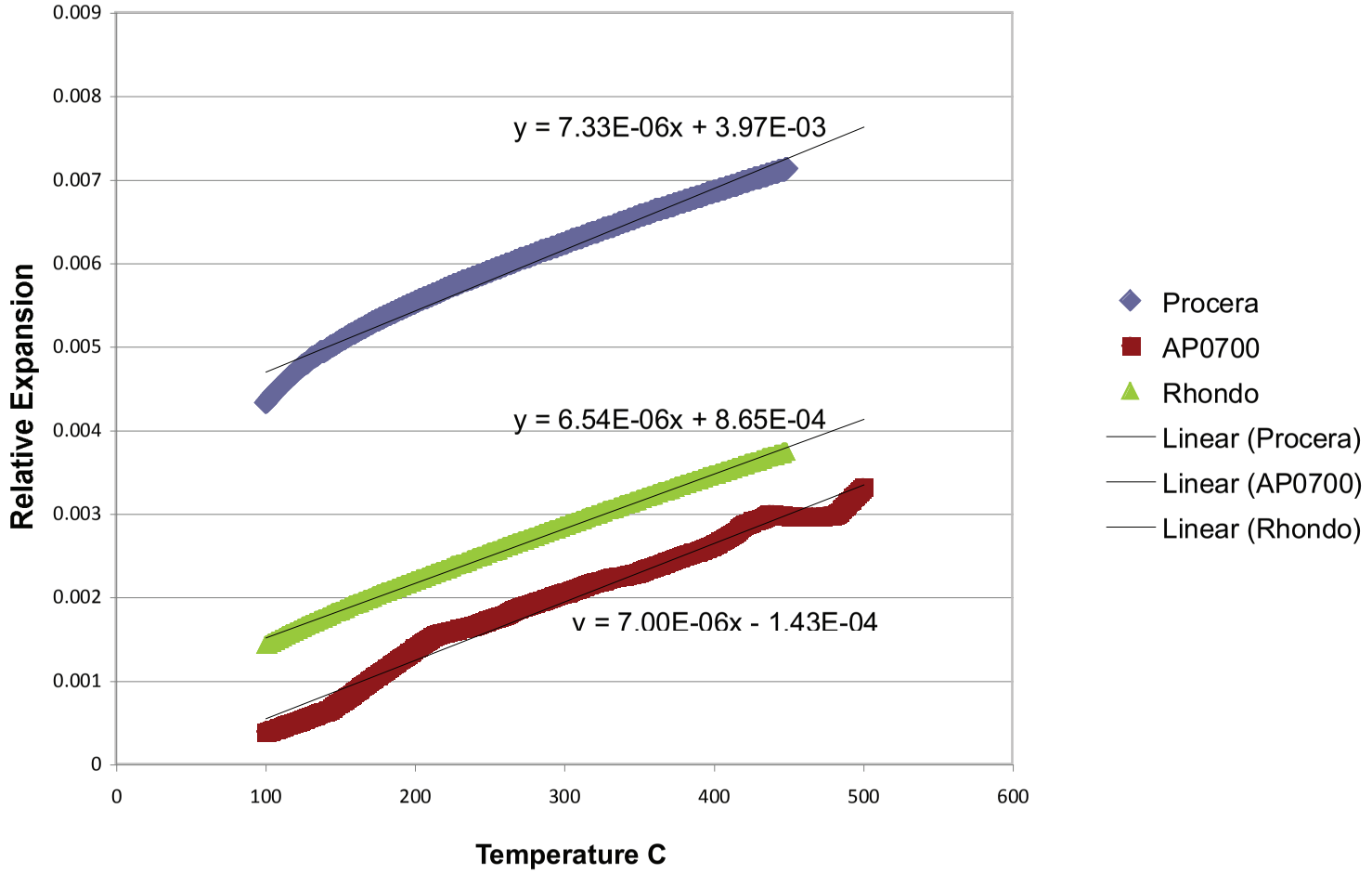

Figure 2.9 Thermomechanical Analysis (TMA) of alumina system with data of tailored glasses overlaid. The matching CTEs over the sintering temperature range are represented by the slopes of the graphs. Procera is the alumina core material, AP0700 is the glass join, and Rondo is the veneering porcelain.

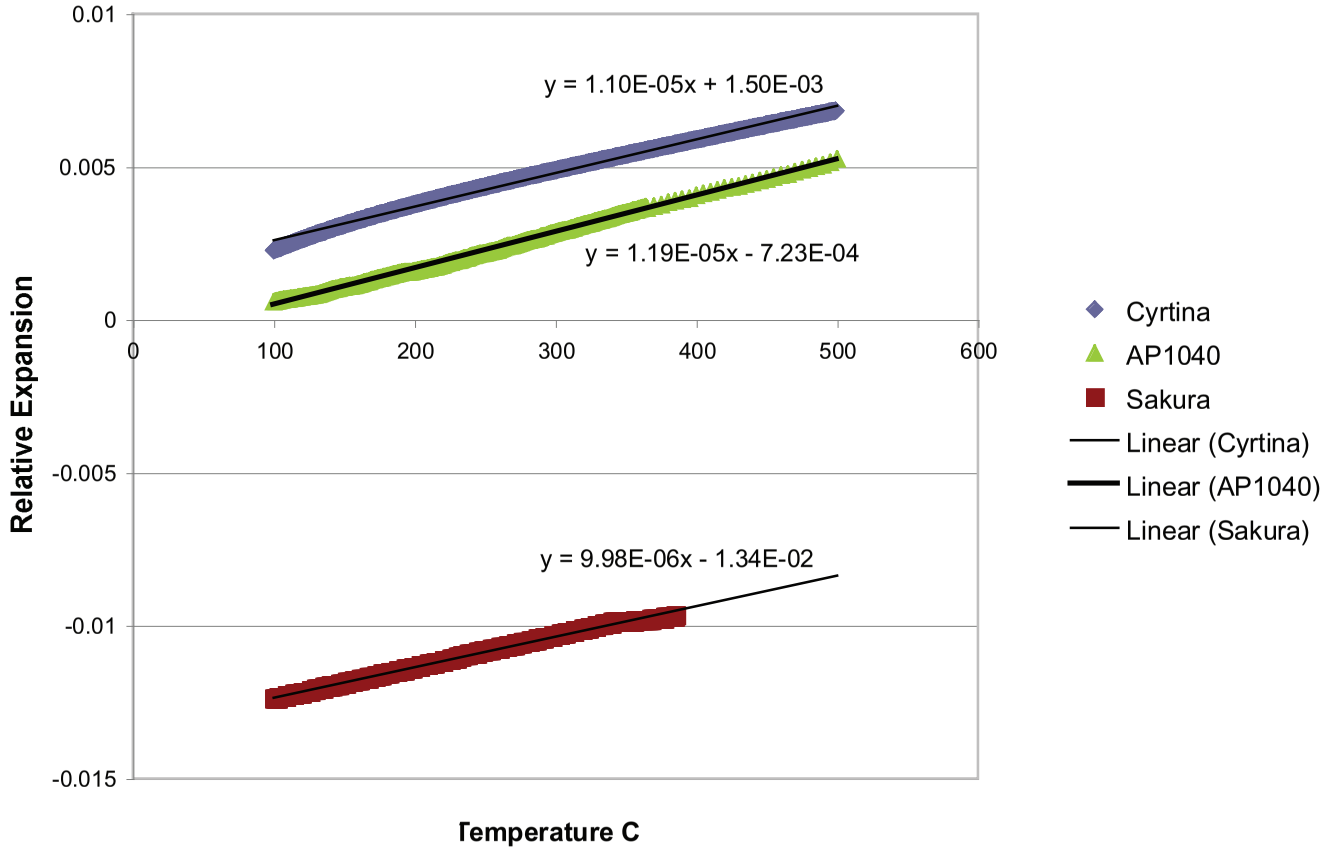

Figure 2.10 Thermomechanical Analysis (TMA) of zirconia systems with data of tailored glasses overlaid. The matching CTEs over the sintering temperature range are represented by the slopes of the graphs. Cyrtina is the zirconia core material, AP1040 is the glass join, and Sakura is the veneering porcelain.

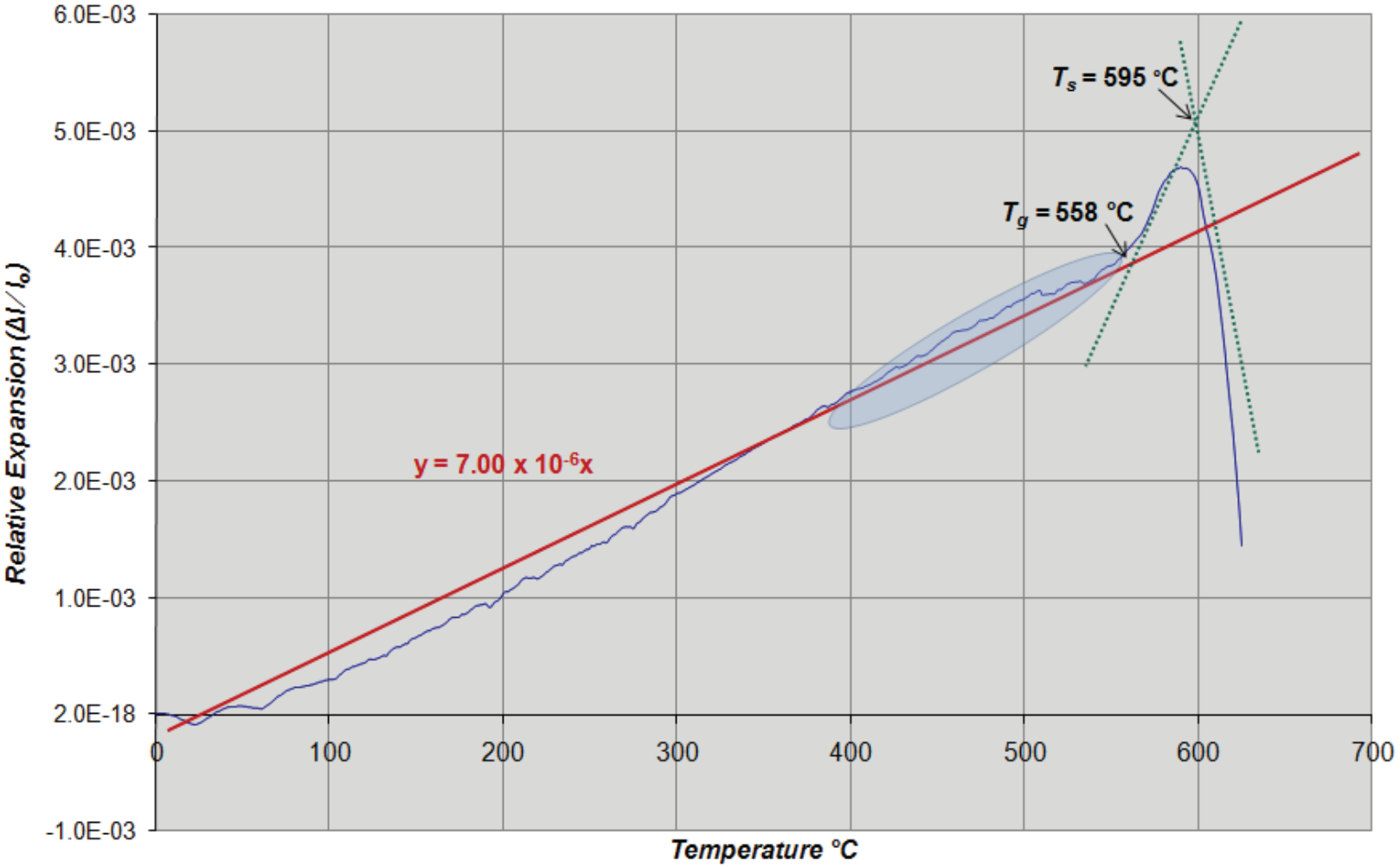

Figure 2.11 Dilatometry of AP700 alumina systems joining glass. The red line represents a slope of y = mx, where m represents the coefficient of thermal expansion at the denoted temperature range and is calculated as 7.00 x 10^{-6} C^{-1} for this glass. T_g and T_s (transition and softening temperatures respectively) areare denoted by the intersection of the green dotted lines representing change in slope, or transition of expansion behavior. The blue shaded ellipse identifies the area where calculated and measured thermal expansion behaviors match.

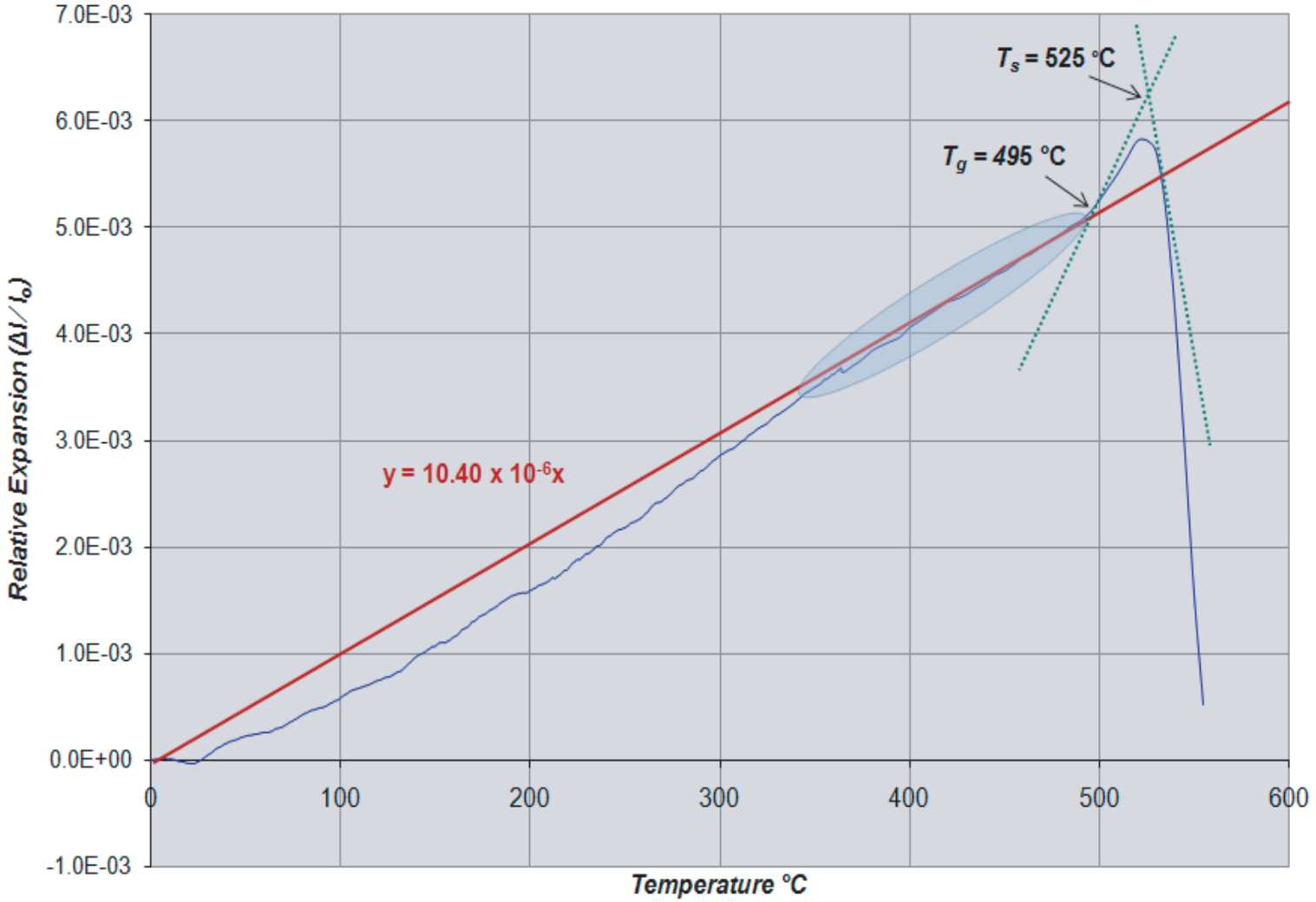

Figure 2.12 Dilatometry of AP1040 zirconia systems joining glass. The red line represents a slope of y = mx, where m represents the coefficient of thermal expansion at the denoted temperature range and is calculated as 10.40 x 10^{-6} C^{-1} for this glass. T_g and T_s (transition and softening temperatures respectively) are denoted by the intersection of the green dotted lines representing change in slope, or transition of expansion behavior. The blue shaded ellipse identifies the area where calculated and measured thermal expansion behaviors match.

2.7 Discussion

We have set out to select glasses for the subsequent bonding of porcelain veneers to dental alumina and zirconia substrates. Detailed melting experiments of selected glass frits onto alumina and zirconia substrates have been carried out, to determine which compositions will provide good wetting and bonding without porosity or crazing, without discoloration, and with a sufficiently low melting temperature. Various processing routes were investigated, from sol gel to wet chemistry to melting and quenching. We discovered that obtaining suitable glasses to match both veneer and core ceramics, yet provide good wetting and bonding, was not straightforward. Several early failures, followed by experimental design modification finally led us to glasses that appeared to meet the need.

Apart from the need to choose glasses that wet well and yet show no porosity or crazing, other criteria had to be met. These included biocompatibility, with zero toxicity. Of particular concern was the need to avoid any lead (or bismuth) in the compositions. Only a small range of glasses met all these conditions. Our first attempts to use commercially available glasses failed because of our lack of control over their critical properties such as CTE matching. This forced us to expand our scope to include glass compositions fabricated in-house. Many early attempts at such fabrication also failed, and much effort was expended before we were able to manufacture fully compatible glass joining compositions.

The next stage was then to use these glasses to join the veneers to the corresponding core ceramics. This forms the subject of the next chapter.

Chapter 3: Fused Joins: Laminar Ceramic Structures and Glass-Ceramic Interface Chemistry

3.1 Introduction

Once glass compositions that match specific porcelain/core combinations have been obtained, it is necessary to join the two layers into a bilayer. It has been indicated that dental crowns are laminar structures, with generally complex geometries. Since we are concerned only with the joining process in this thesis, experiments will be conducted here on flat layers, always mindful that the techniques will need to be applicable to more general geometrical shapes. Traditionally, porcelains are painted on to a core material layer by layer, a time consuming and expensive process. One alternative fabrication route is free-form fabrication, in which each layer is shaped individually (e.g. by robocasting) and then integrated with a glass join, as in Fig. 3.1. Such techniques are currently being investigated by materials processors, and hold the promise of new-generation crown fabrication [41-43].

The integrity of the glass-ceramic interface is crucial to success of our approach. First and foremost, a strong bond is required, so that delamination failure does not occur before any other failure modes. In order to maintain this integrity, it is also required to avoid thermal expansion mismatch stresses and to ensure high

resistance to degradation in an aqueous environment, particularly over time.

This demands characterization of the interface chemistry. It will be necessary to determine interdiffusion characteristics either side of the nominal interface, with particular attention to ionic diffusion and elucidation of new phases. Such changes will be evident as gradients in chemical composition.

This chapter will describe ways to effect glass joins between CTE-matched porcelains and alumina or zirconia cores. For this, it is necessary to heat the bilayer combination to an elevated temperature, sufficiently high to make the glass flow and wet each component, but not so high to cause deformation of the porcelain (typically 950^{o}C). At this stage, the test that adequate CTE matching has been achieved through the heating and cooling cycle will simply be that the bilayer remains intact during preparation and subsequent handling. On the other hand, evaluations of the integrity of the resulting interfaces, using electron microscopy and microprobe methods, will form an important part of the characterization. It will be recalled that we have chosen materials to minimize residual stresses from thermal expansion mismatch (Chapter 2). Confirmation of the absence of any such residual stresses in our structures will be deferred to the next chapter.

Methods employed to carry out characterization of the interface chemistry will be outlined in this chapter. This will be done by first using conventional optical microscopy to determine geometrical elements, e.g. interfacial roughness. Then SEM (scanning electron microscopy) and SEM microprobe analysis will be used to map out the grain structures in the core and veneer layers, and the width and composition of the resulting interdiffusion layer (IDL). Diffusion kinetics will be determined by

observing changes in the compositional maps over time. The coefficient of thermal expansion is also a crucial factor in these applications, but we will proceed on the assumption that we have achieved good matching between components (Chapter 2), and return later to confirm that the level of any residual stresses from such mismatch is negligibly small (Chapter 4).

3.2 Background

3.2.1 Glass as a seal

Historically, glass has been used as a ceramic/glass seal in clay-based ceramic pottery, to negate the weakness and porosity of the fired ceramic. Clearly, this ancient technology was developed by trial and error. Functionally, glazing promoted waterproof capability and prevented bacterial infestation in clay vessels, while also allowing decorative artistic expression to be preserved on the surface. For this, we owe our ancestors a debt of gratitude, in the name of culture as well as technology.

More recently, a similar method has been developed to form bioactive glass coatings on medical ceramic devices, such as alumina hip replacements. Further functional grading is required, however, to prevent leaching of alumina into the bioactive glass at the high temperature of glazing, as well as to prevent thermal mismatch between the bioactive glass-ceramic and the alumina component. Such mismatch has been mitigated by the addition of an intermediate glass layer to improve CTE match and further protect the bioactive glass from alumina leaching [44].

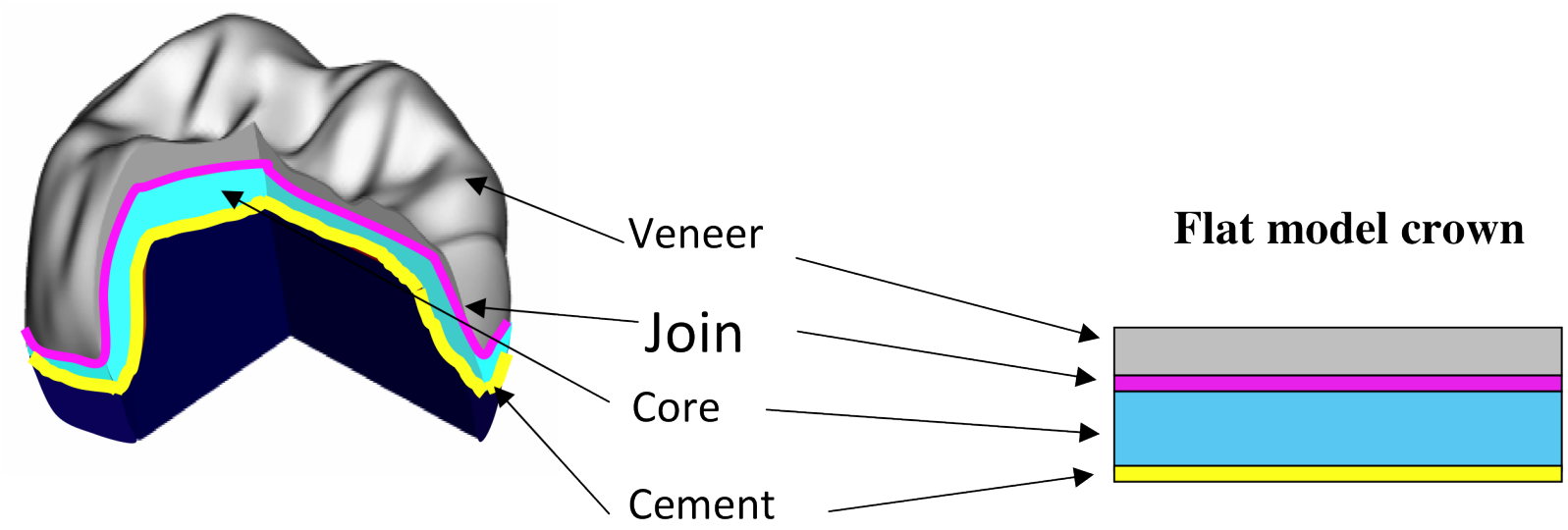

Figure 3.1 All-ceramic crown with join interlayer translated to a flat model crown

In other medical applications, such as dental crowns, the notion of a glassy interface has special appeal, because of its bioinertness. Unlike metallic components, glass is not susceptible to electrochemical interaction with the oral environment. The issue of toxicity is also avoided, provided certain elements (especially lead, and possibly also bismuth) are not present.

3.2.2 Traditional applications in glass/ceramic joining

Although the use of glass to join layers is a new approach in dentistry, it is a method widely used in lighting [7], fuel cells [9] as well as electronic packaging [17], which require hermetic seals. When glass is used to join materials together, it is often applied at viscosities between 10^3–10^5 Pa.s ($kg \cdot m^{-1} \cdot s^{-1}$), in order to promote flow and wetting of the separate layers [36]. In silicate glasses, these viscosities are attained at temperatures in the range 600–1200 ºC. During the joining process at these temperatures, interdiffusion or atomic mixing occurs between the layers. While, some interdiffusion is critical to wetting and good bonding between layers, intuition and ceramic processing science indicates that too much interdiffusion is likely to be detrimental. The amount of interdiffusion that occurs depends on the relative component compositions, the temperature and time required for joining.

Glass has long been used in industry to provide seals for metals [7]. As always, the secret to success has been matching of CTE between the glass and metal. This rich history in materials technology gives credence to our proposition that glasses could be used as veneer/core joining agents in dental crown systems. In modern technology, glass sealants are in use for their low electrical conductivity in

electronic packaging [17]. Glass joins are in common usage in solid oxide fuel cells (SOFC) [9,18,45,46], where resistance to thermal cycling is an issue.

Glass joining is also a highly developed field in electronics packaging applications. Some groups [17] have carried out similar research involving sealing glass for silicon carbide electronic packages. Glasses have been selected for low dielectric loss, high service temperature and high insulation, and then assessed for reactivity with silicon carbide. Wetting behavior, mass transport across interfaces, and formation of new phases have been investigated to create and maintain the best hermetic seal. Thermal expansion matching was found to be important, since a 5% difference in CTE could result in cohesive or adhesive failure, compromising the component. Sealed cross sections have been examined for chemical reaction and structural integrity using electron microscopy. Reaction kinetics were linked to reactant transport across the interface, leading to an optimum glass and interdiffusion layer. The end result has been a successful means of interlayer joining in these systems, setting a precedent for our study.

3.2.3 Dental all-ceramic restorations

As indicated, all-ceramic crowns are currently fabricated by painstaking sequential processing, in which thin layers of porcelain are painted on step by step. This stepwise procedure is needed to avoid buildup of residual stresses, as well as to control aesthetic appearance. We have repeatedly mentioned that such stresses can lead to catastrophic failure of the component, most likely during the preparation itself but also subsequently in service, from buildup of damage within one or other layer. Most all-ceramic crowns use alumina or zirconia as a core material, for strong support

of an otherwise weak porcelain veneer. The tendency is more toward zirconia these days, because of its superior strength and lifetime, but alumina remains a useful material for baseline comparison [47-49].

To avoid the problem of residual stress, two methods of fabrication have been considered. One simply uses a single ceramic for the entire crown, thus avoiding the mismatch issue altogether. Glass-ceramics have been used in the field for this purpose [50]. The problem is that those ceramics which provide pleasing aesthetics are invariably weak, and do not last acceptably long in the mouth. This is because the same enamel-like particulates within the glassy matrix that provide the tooth-like aesthetics also weaken the microstructure. The second method of fabrication of this kind is to join a porcelain veneer to a strong ceramic core, as advocated in this study, but using a polymeric adhesive that can be cured at room temperature. This approach has in fact been investigated by others in our laboratory [2,3]. While avoiding CTE stresses, adhesive joining is limited by a relatively weak veneer/core interface, which is susceptible to degradation over time in harsh oral conditions. The use of glass as a sealing agent as proposed here represents a compromise approach, with processing temperatures low enough to keep residual stresses low but high enough to produce a strong chemical bond. The higher modulus of the glass also diminishes flexural modes in the veneer distortion during mastication, thereby reducing the possibility of porcelain fracture (Chapter 4) [3]. Of course, other issues now present themselves, such as the role of interdiffusion gradients at the interface, and these will be part of our investigation.

3.3 Experimental Methods

In all the joining applications described in 3.2 above, including the dental systems of interest here, the integrity of the bond is influenced by the properties of the interface diffusion layer (IDL). These layers tend to be small, of the order μm, with large gradients in chemical composition. A feature that plays an important role in the integrity of the join is the existence of residual stresses, so a great deal of attention is paid to minimization of thermal expansion mismatch, typically to less than $1x10^{-6}$ C^{-1}. In the case of dental ceramics of interest here, there are virtually no comparative data on the chemical properties of IDLs. This deficiency provides a principal motivation for the present chapter. In what follows, we will outline how the joins are made, and then describe how the interfaces are characterized.

3.3.1 Preparation of bilayer specimens

Flat alumina and zirconia layers were prepared as outlined in the previous chapter, along with their matching porcelains. A thin layer ~ 50–100 μm of the appropriate glass slurry was placed onto the surfaces of each of the core ceramics and their matching porcelains, ensuring coverage over the entire surfaces to be bonded. Biscuit firing was conducted for each specimen layer at a rate of 30 C/min to 700–750 C for 5 min, as shown for alumina (Fig. 3.2a) and zirconia (Fig. 3.3a), to bind the glass particles onto the surface and begin wetting. The specimens were then slowly cooled within the furnace and removed for examination.

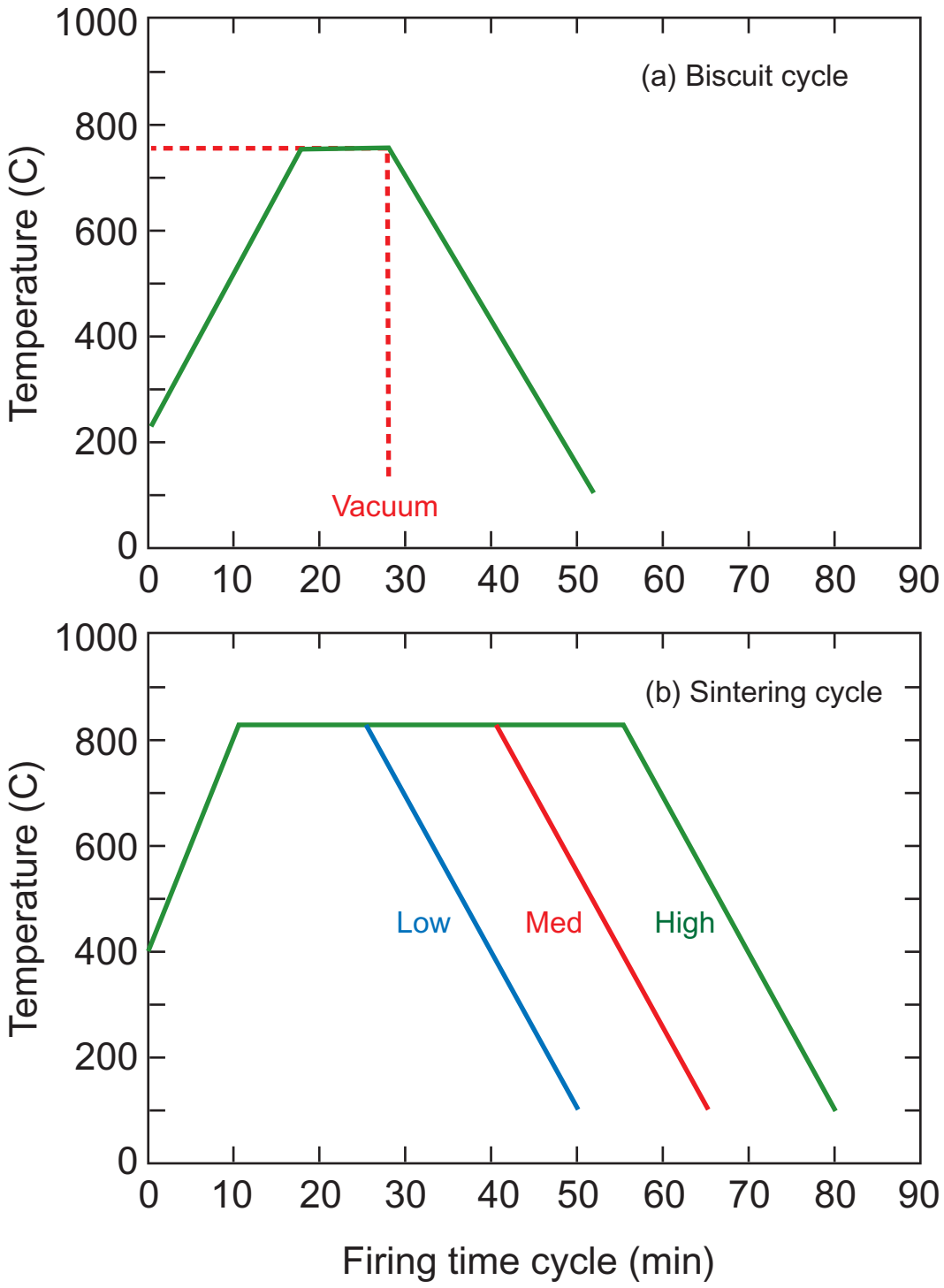

Figure 3.2 Firing cycles for alumina systems. a) Glass slurry was applied to both veneer and core layers, then biscuit-fired at 750 C (to promote adhesion of the glass to the substrates). b) Veneer and core blocks were then sintered at 830 C (to complete the join).

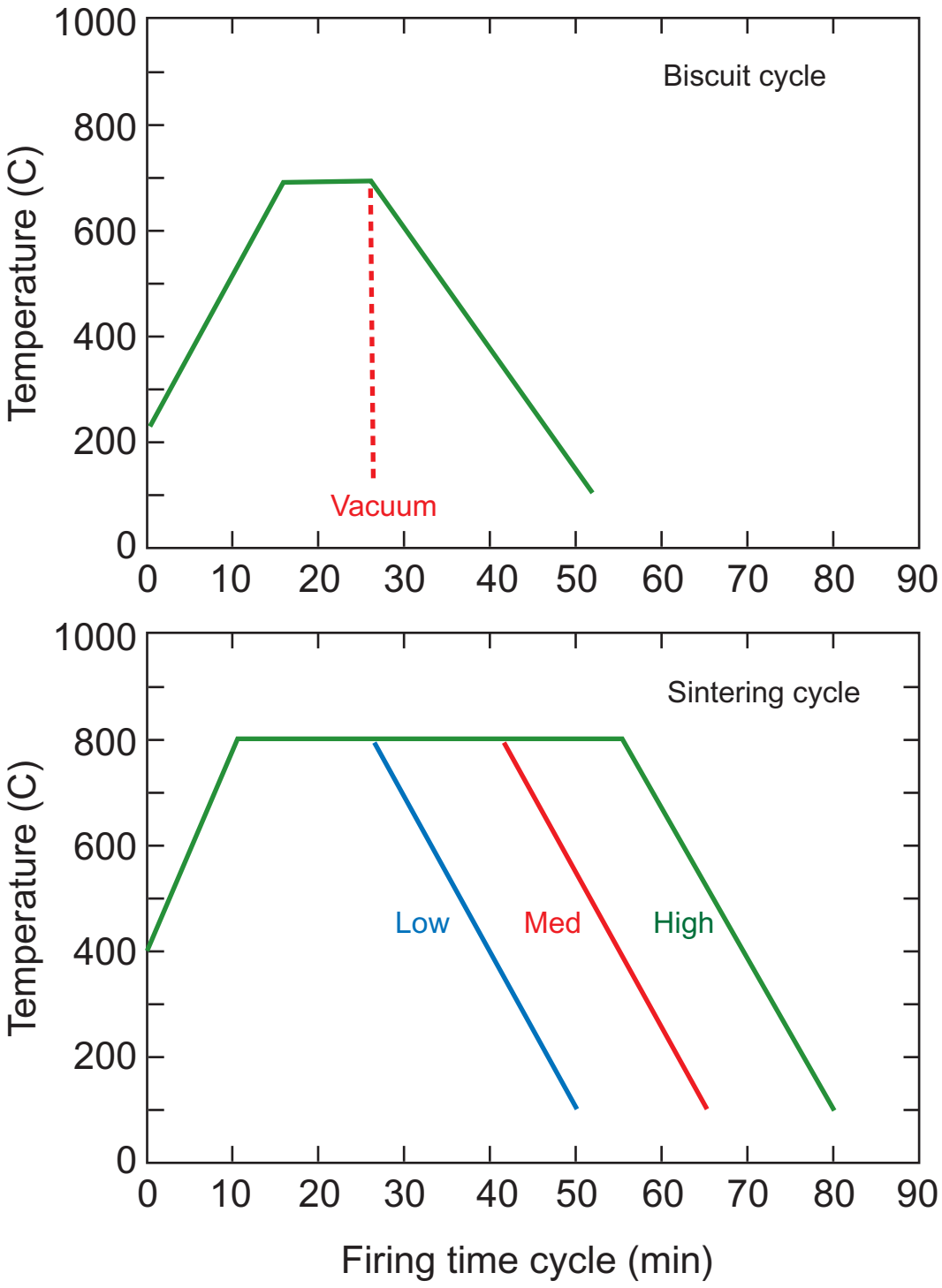

Figure 3.3 Firing cycles for zirconia systems. a) Glass slurry was applied to both veneer and core layers, then biscuit-fired at 700 C (to promote adhesion of the glass to the substrates). b) Veneer and core blocks were then sintered at 800 C (to complete the join).

The fired porcelain biscuits were then placed on top of their respective cores, alumina (Fig. 3.2b) and zirconia (Fig. 3.3b), and heated at a rate of 40 C/min under dead weight (4.4 g refractory ceramic) to 800–830 C. This was well below the firing temperature of the veneer recommended by most manufacturers, and was chosen in order to avoid "slumping" or loss of veneer shape. The specimens were held for prescribed hold times of 15 min (low), 30 min (medium) and 45 min (high) to fuse the surfaces together. These times were chosen to investigate appropriate levels of interdiffusion.

After cool-down, the sandwich specimens were sectioned perpendicular to the interface using a low-speed diamond saw blade, bonded with resin onto aluminum specimen holders. The surfaces were polished down to 1 μm for optical microscopy, SEM and microprobe analysis.

3.3.2 Characterization of layer interfaces

The fired bilayer sections were subjected to several tests, to establish the integrity of the joins. The first set of these were simple tests of specimen survival from preparation. To begin, the newly fabricated bilayers were subjected to interfacial shearing by hand, the so-called "finger test". Although crude, this test usefully eliminates the weakest interfaces in the population tail. The second such test of survival was a "cutting test", in which specimens were sectioned with a diamond saw, followed by surface grinding and polishing down to 1 μm finish (Sect. 3.3.1). Those that broke during the cutting and polishing operation were also eliminated—a kind of proof test.

Those specimens that survived intact were then examined by various forms of microscopy. First, reflection optical microscopy was used. The interfaces could be readily resolved by this method. The quality of the observed joins, uniformity of thickness and lack of porosity, were taken as first indicators of a "good" interface. Some specimens were also examined by scanning electron microscopy.

Wavelength dispersive spectroscopy (JEOL JXA-8900 SuperProbe, Japan Electron Optics, Tokyo, Japan) was used to examine any diffusion of ions between the bonding glass and the ceramic sandwich layers. Across the ceramic layers, a 1 μm-wide electron beam was scanned across the join, with readings taken every 1.5–2.8 μm. Results were plotted as intensity versus location across the interface.

3.4 Results

3.4.1 Screening tests

Tables 3.1 and 3.2 shows results of the finger and cutting screening tests for specimen integrity, for glasses of different CTEs and for different firing temperatures. Table 3.1 contains data from the initial finger tests. This table lists the pass (P) and fail (F) results for electronic alumina (EA) and dental alumina (DA), and for dental zirconia (DZ). Some specimens failed during preparation before even getting to the finger test (FP). The pass rate for EA specimens was 5/13, for DA specimens was 5/6, and for DZ specimens 3/3. The pass rate using Winkelmann–Schott (WS) glasses was only 5/12, and for Appen (AA) glasses was 7/9. The survivors were then passed on to the sectional cutting and polishing phase. Results for pass and fail rates

during this phase are shown in Table 3.2. The pass rates for surviving EA specimens was 3/5, for DA was 5/5, and for DZ was 3/3. The pass rate using Winkelmann–Schott (WS) glasses was only 3/5, and for Appen (AA) glasses was 7/7.

From these results, it was concluded that good bonds could be formed for DA and DZ interfaces only. By contrast, EA specimens responded poorly, and were excluded from further consideration. AA glasses gave better pass rates in both the finger and cutting tests. With these results we chose as conditions for further study those bilayers with the lowest firing temperature and yet survived the screening tests. For the DA bilayers, this meant a glass CTE of 7.0×10^{-6} C^{-1} and a firing temperature of 830 C; for the DZ bilayers, a CTE of 10.4×10^{-6} C^{-1} and a firing temperature of 800 C.

3.4.2 Optical microscopy

The selected sectioned and polished specimens were then examined by microscopy for structural integrity. Interfaces for porcelain/glass/alumina structures in Fig. 3.4 and porcelain/glass/zirconia structures are shown in Fig. 3.5. Typical width of the glass layer in these specimens was 20–70 μm. In Fig. 3.4, the porcelain was Rondo and the alumina was Procera (Table 2.1). The glasses used were Appen (a) AP600 with frit size < 100 μm and (b) AP700 with frit size < 38 μm (Table 2.6), applied in slurry of water/ethanol slip suspension in both cases. The porosity evident in the glass in Fig. 3.4a is due to the large grit size (Chapter 2). In Fig. 3.5, the porcelain was Sakura and the zirconia was Cyrtina (Table 2.1).

Table 3.1 Finger test, to determine 'pass' (P) or 'fail' (F) for bonded alumina- and zirconia-based specimens bonded with Winkleman–Schott (WS) and Appen (AA) glasses. Premature failures during prep indicated as FP

Glass (WS)	**7.60**	**8.00**	**8.30**	**8.56**	**8.70**	**8.71**	**8.81**	**8.90**	**9.14**	**8.92**	**9.02**	**9.24**
Fire temp C	1000	1000	950	850	850	950	900	850	950	900	900	750
Substrate	EA	EA	EA	EA	EA	EA	EA	EA DA	EA	EA	EA	EA
Pass rate	F	F	F	P	P	P	P	P	F	F	F	F

Glass (AA)	**9.15**	**8.00**	**7.50**	**7.00**	**6.50**	**6.00**	**9.80**	**10.20**	**10.40**
Fire temp C	850	850	850	830	850	850	850	800	800
Substrate	EA	DA	DA	DA	DA	DA	DZ	DZ	DZ
Pass rate	FP	FP	P	P	P	P	P	P	P

EA: electronic alumina, DA: dental alumina, DZ: dental zirconia

Table 3.2 Cutting test, to determine 'pass' (P) or 'fail' (F) for bonded alumina- and zirconia-based specimens bonded with Winkleman–Schott (WS) and Appen (AA) glasses.

Glass (WS)	**8.56**	**8.70**	**8.71**	**8.81**	**8.90**
Fire temp C	850	850	950	900	850
Substrate	EA	EA	EA	EA	EA DA
Pass rate	P	F	P	F	P

Glass (AA)	**7.50**	**7.00**	**6.50**	**6.00**	**9.80**	**10.20**	**10.40**
Fire temp C	850	830	850	800	850	800	800
Substrate	DA	DA	DA	DA	DZ	DZ	DZ
Pass rate	P	P	P	P	P	P	P

EA: electronic alumina, DA: dental alumina, DZ: dental zirconia

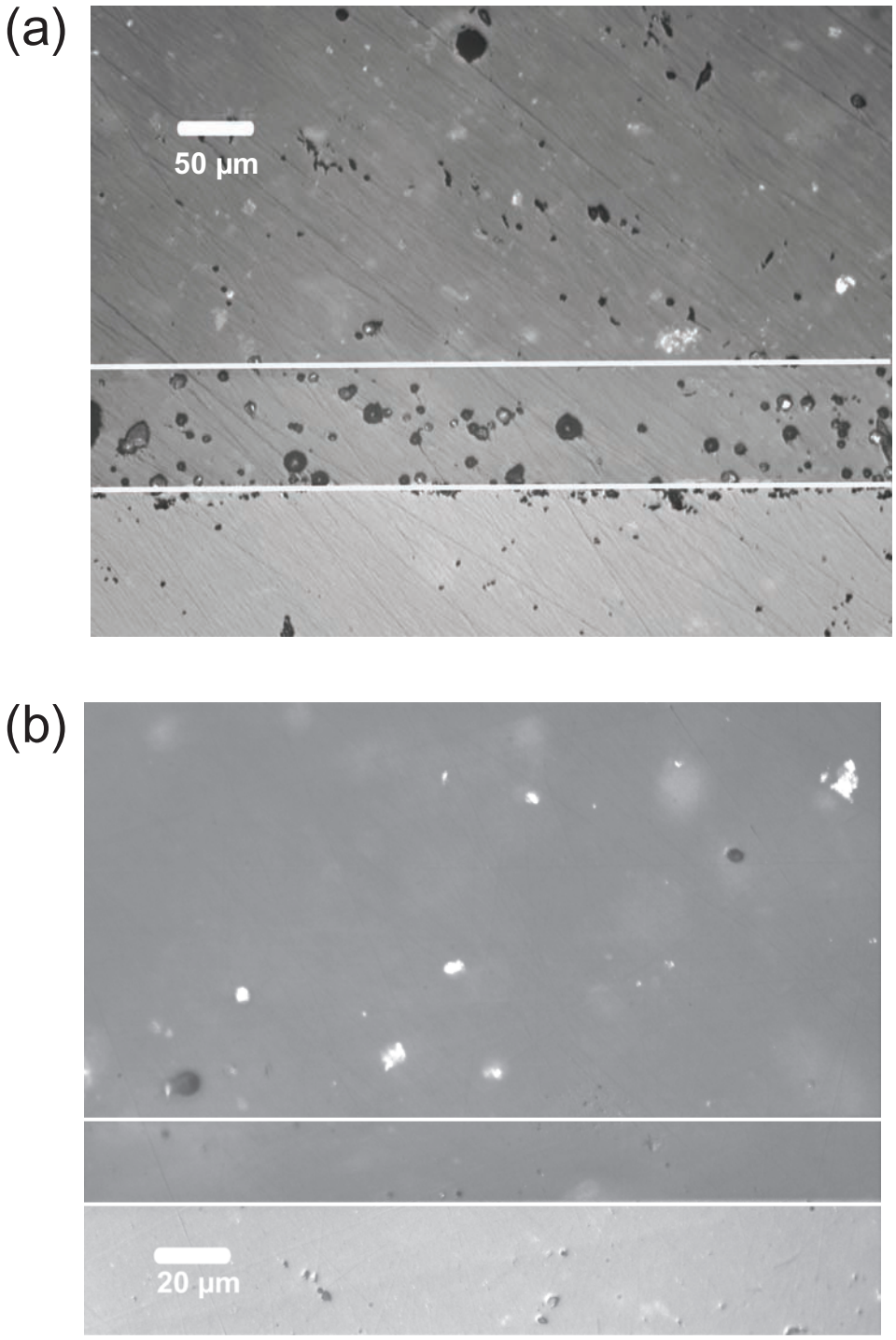

Figure 3.4 Showing joins in glass-bonded Rondo porcelain and Procera alumina bi-layer. Glass in (a) AP600, in (b) AP700. White horizontal lines are used to highlight the veneer/glass junction. Some porosity is evident in (a).

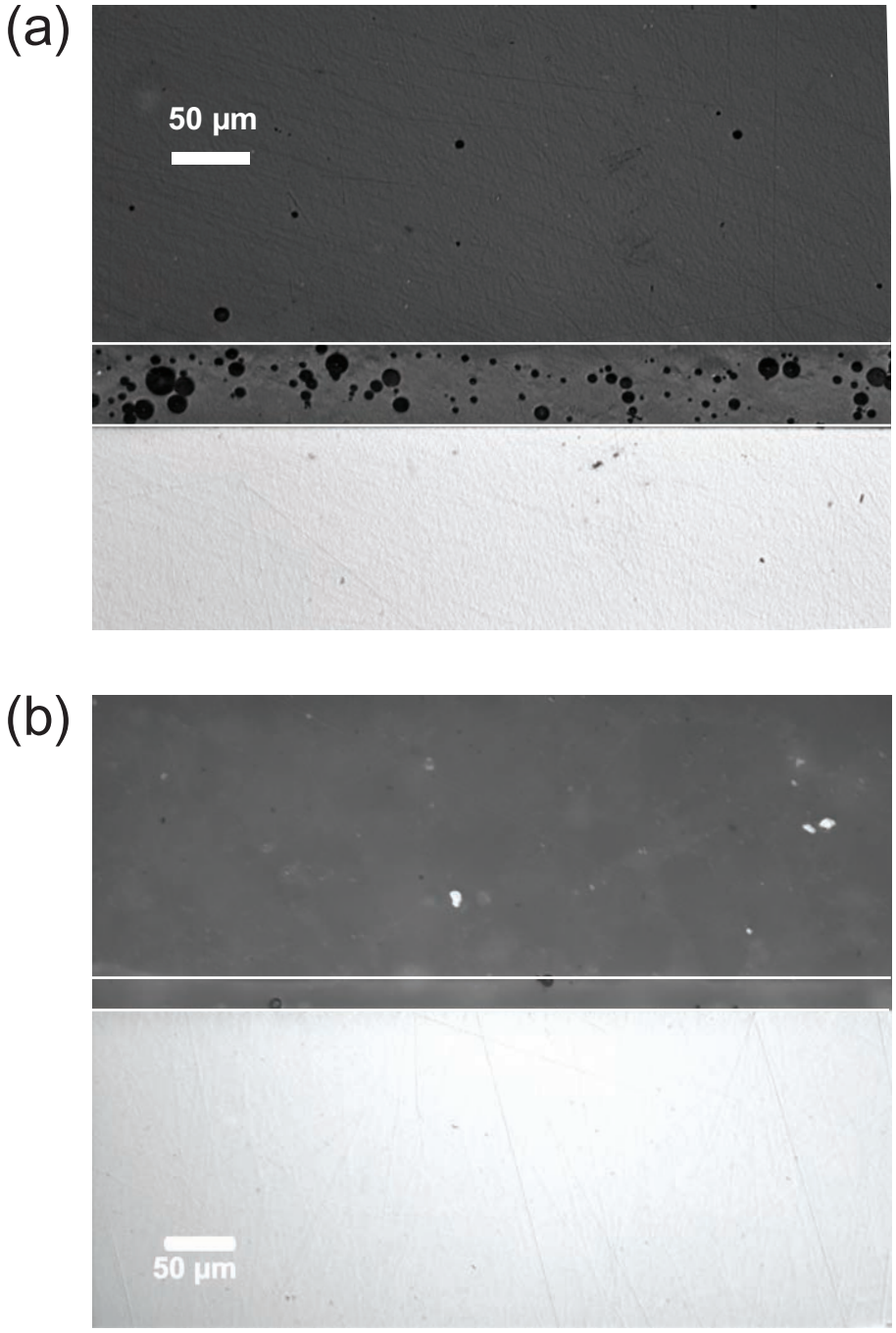

Figure 3.5 Showing joins in glass-bonded Sakura porcelain and Cyrtina zirconia bi-layer. Glass in (a) AP600, in (b) AP700. White horizontal lines are used to highlight the veneer/glass junction. Some porosity is evident in (a).

The glasses used were (a) AP1020 with frit size < 38 μ and (b) AP1040 with frit size < 38 μm) (Table 2.6), applied with PVA binder in water solution in first case and water/ethanol slip suspension in second. In this case, the porosity evident in Fig. 3.5a was due to the PVA binder (Chapter 2). Hence we chose smaller grit sizes and avoided PVA binders in our glass slurry preparations.

Note that the specimens in Figs. 3.4 and 3.5 all passed the screening tests for integrity indicated above. Clearly, such tests are insufficient to determine ultimate interface integrity. We leave this to Ch. 4.

3.4.3 Electron microprobe analysis

Electron microprobe analyses with backscattered electron microscopy were conducted on the samples to determine compositional gradients across the glass-bonded interfaces. Results are shown in Figs. 3.6 to 3.7.

In these figures the veneer, glass and core zones are delineated, and the various ionic species indicated in the legend. Specifically, these plots enable the quantification of interdiffusion layers (IDLs) at the veneer/glass (V/G) and glass/core (G/C) interfaces. Widths of IDLs are shown as the vertical colored bands, as the distance over which ion concentrations have undergone significant change, although this distance is difficult to quantify. Of special interest here is the diffusion of the network-modifier ions, i.e. Na^{+}, K^{+}, Ca^{++} and Ba^{++}, across the boundaries.

The first set of plots shows gradients across interfaces in alumina-core systems fired at 830 C (Fig. 3.6) and zirconia-core systems fired at 800 C (Fig. 3.7), for (a) low (15 min), (b) intermediate (30 min) and (c) high (45 min) anneal cycles, as

depicted earlier in Figs. 3.2 and 3.3. Note the considerable scatter in intensity for some ions within the glass bond, indicating some fluctuation in composition. For the alumina-based system in Fig. 3.6, the IDL extends over 10–15 μm, increasing with anneal time. The levels of Na^{+}, K^{+} and Ca^{++} and Ba^{++} show signs of diffusion across the V/G interface, Ca^{++} and Ba^{++} from the glass into the veneer and K^{+} and Na^{+} in the opposite direction. The curve for K^{+} is most interesting. As all the glass joins were formulated with no K^{+} in the glass, the presence of this ion indicates interdiffusion from the porcelain. For this particular ion, the diffusion has extended well beyond the shaded V/G band in Fig. 3.6, and is shown more clearly in Figs 3.8a. There is not much evidence of a large diffusion of ions across the G/C boundary into the core, consistent with the higher density and crystallinity of the core material. On the other hand, there is indication of some diffusion of Al^{+++} into the glass from the core in the more highly annealed system in Fig. 3.6c. Ba^{++} and Ca^{++} ions vary throughout the IDL width, with anneal time, as can be seen in Figs 3.8b and 3.8c for alumina. A plot of Si at the V/G interface and Al at the G/C interface mapping of major components at the veneer and core interfaces, highlights core interdiffusion in Fig 3.8d

The behavior of the zirconia-based system in Fig. 3.7 is similar in the Na^{+}, K^{+} and Ca^{++} and Ba^{++} diffusion, but there are some minor differences too. The IDL at the V/G interface appears to extend over a similar distance, i.e. 10–15 μm, again increasing with anneal time. However, the behavior at the G/C interface shows higher diffusivity of the Zr^{++++} (also detailed in Fig 3.9d) and Y^{+++} ions than their Al^{+++} counterpoints, commensurate with normal diffusion behavior.

As indicated above, the diffusion of network modifier ions, Na^{+}, K^{+} and Ca^{++}

and Ba^{++}, is of special interest. Detailed intercomparison of diffusion profiles for these ions is difficult to ascertain from the plots in Figs. 3.6 and 3.7, because of the compressed intensity scales, but plots of K^{+}, (Fig. 3.9a), Ca^{++} (Fig. 3.9b) and (Ba^{++} Fig. 3.9c) show similar behavior for as for alumina systems, particularly in the case of K^{+}.

It is particularly difficult to compare numbers for the different anneal cycles in (a), (b) and (c) of those figures. Therefore, individual plots for each of these ionic species is given with expanded scales in Figs. 3.8 and 3.9, comparing low, intermediate and high anneal cycles on each plot. Composition fluctuations in the glass are magnified in these plots and the IDL zone is generally clearer. Systematic variation between the different anneal cycles is not strongly apparent, especially given the data scatter, suggesting that longer anneals above some optimal level are only marginally beneficial. Basically, an anneal that thoroughly melts the glass frits is enough to produce a strong bond.

3.5 Discussion and Summary

In this chapter the aim has been to bond porcelain to either alumina or zirconia using glass seals. The methodology required to do this has been laid out. We have described an optimal procedure for selecting the right materials and fusing conditions to produce joins of apparent structural integrity. A principal stipulation was that the various components, veneer, glass and core, should have close CTE matching.

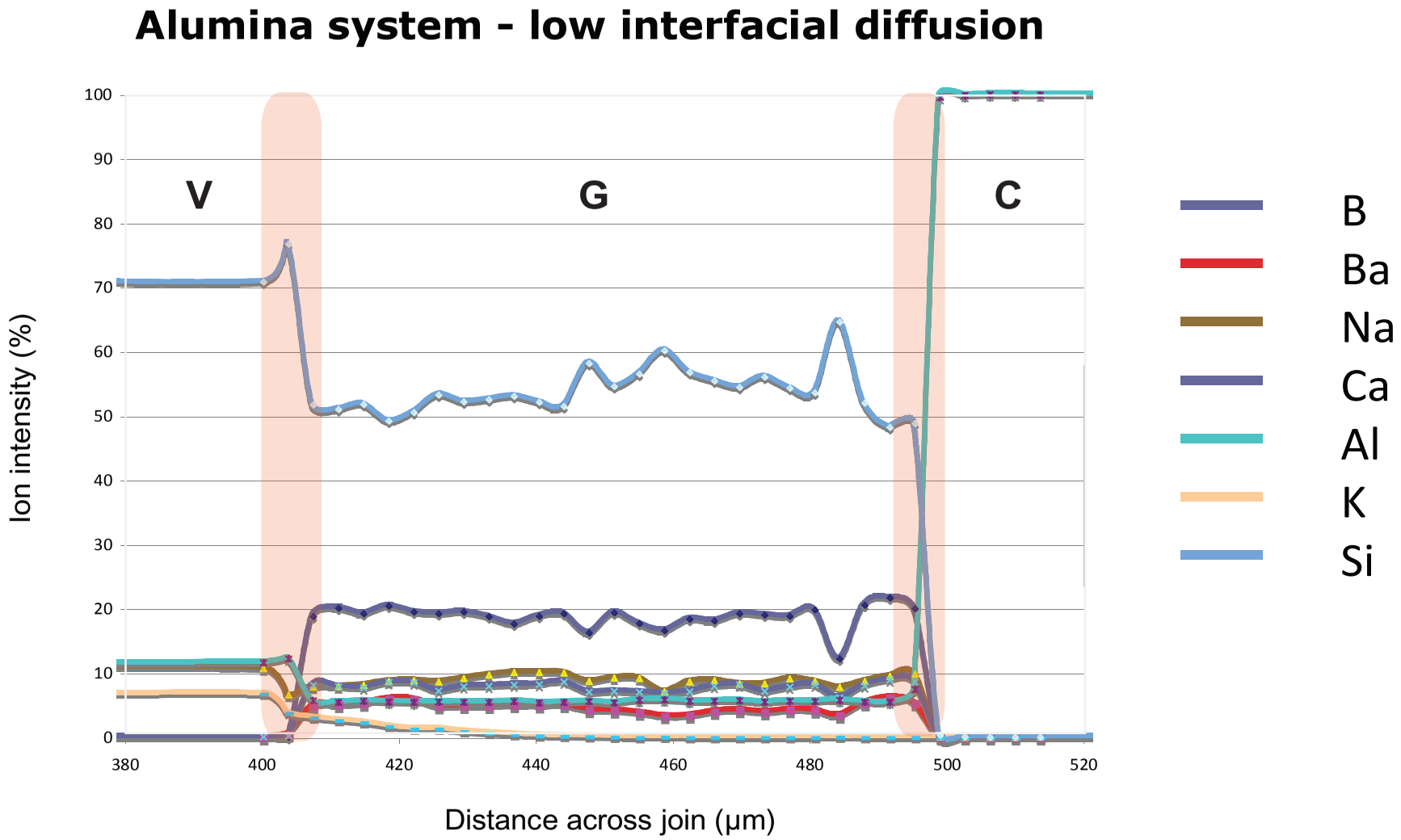

Figure 3.6a Microprobe scans of ion concentration across glass-bond interface for alumina-core system, for low anneal cycle. Colored bands indicate interdiffusion layers. Veneer (V), glass (G) and core (C) zones indicated.

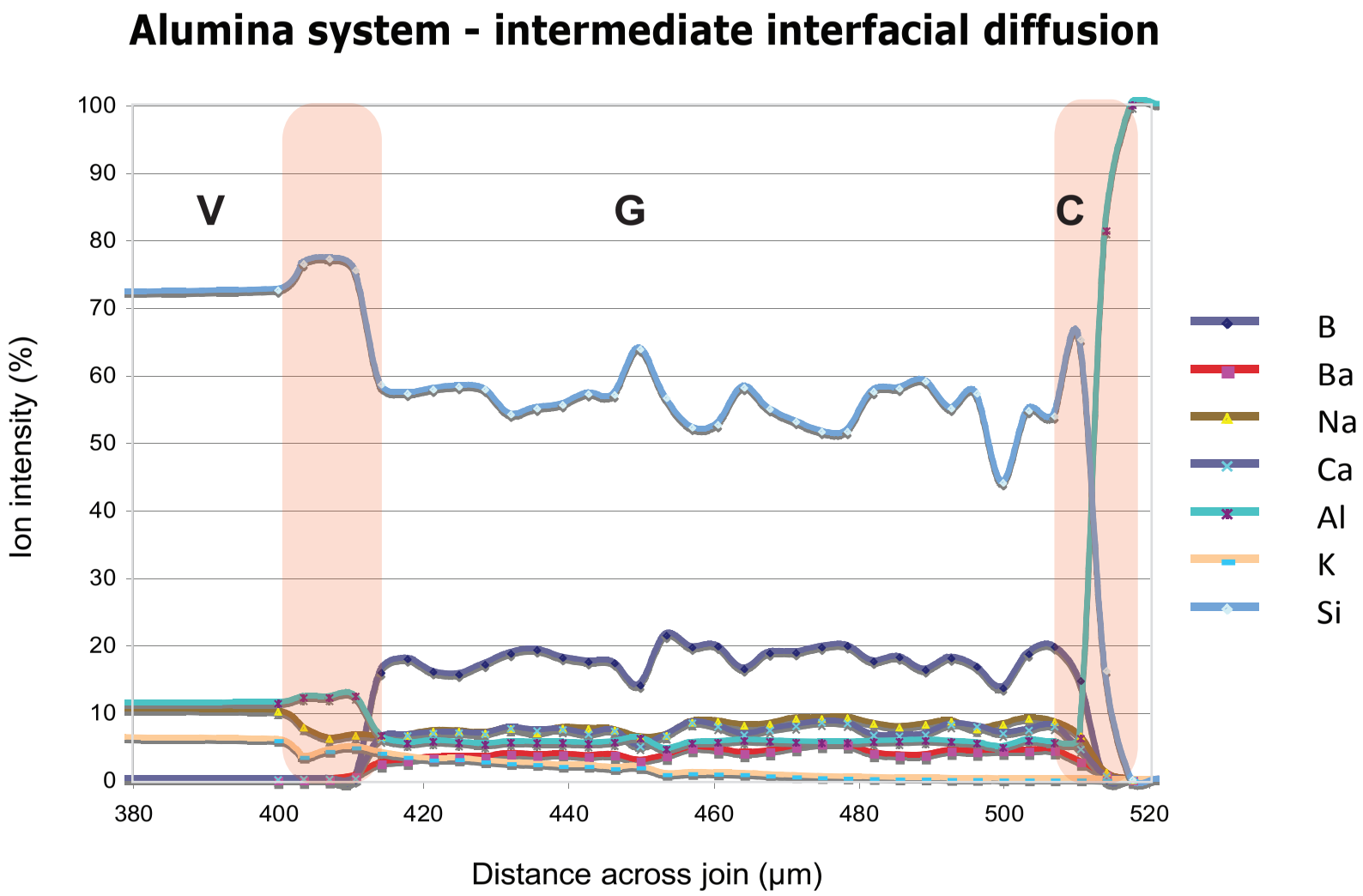

Figure 3.6b Microprobe scans of ion concentration across glass-bond interface for alumina-core system, for intermediate anneal cycle. Colored bands indicate interdiffusion layers. Veneer (V), glass (G) and core (C) zones indicated.

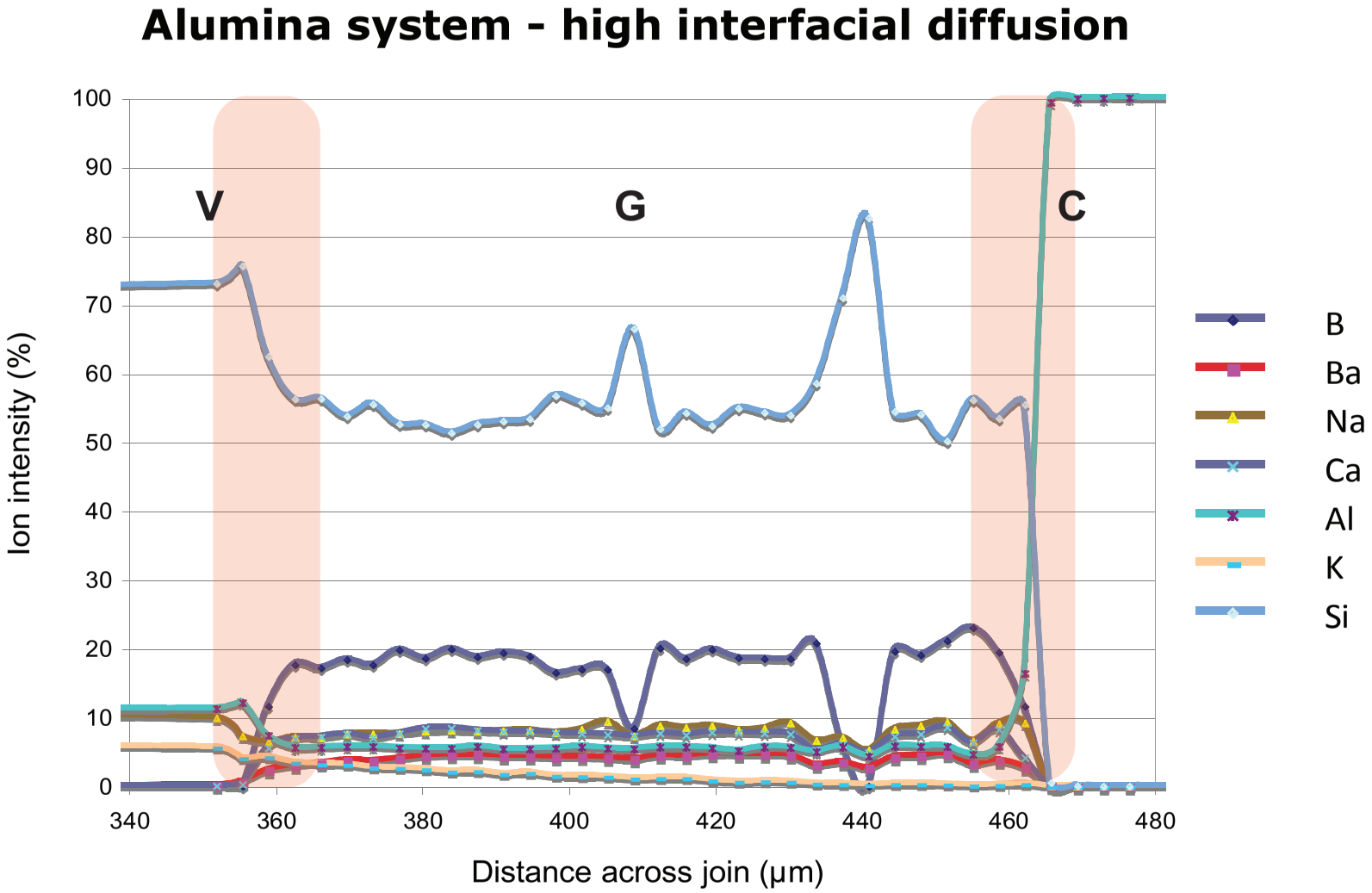

Figure 3.6c Microprobe scans of ion concentration across glass-bond interface for alumina-core system, for high anneal cycle. Colored bands indicate interdiffusion layers. Veneer (V), glass (G) and core (C) zones indicated.

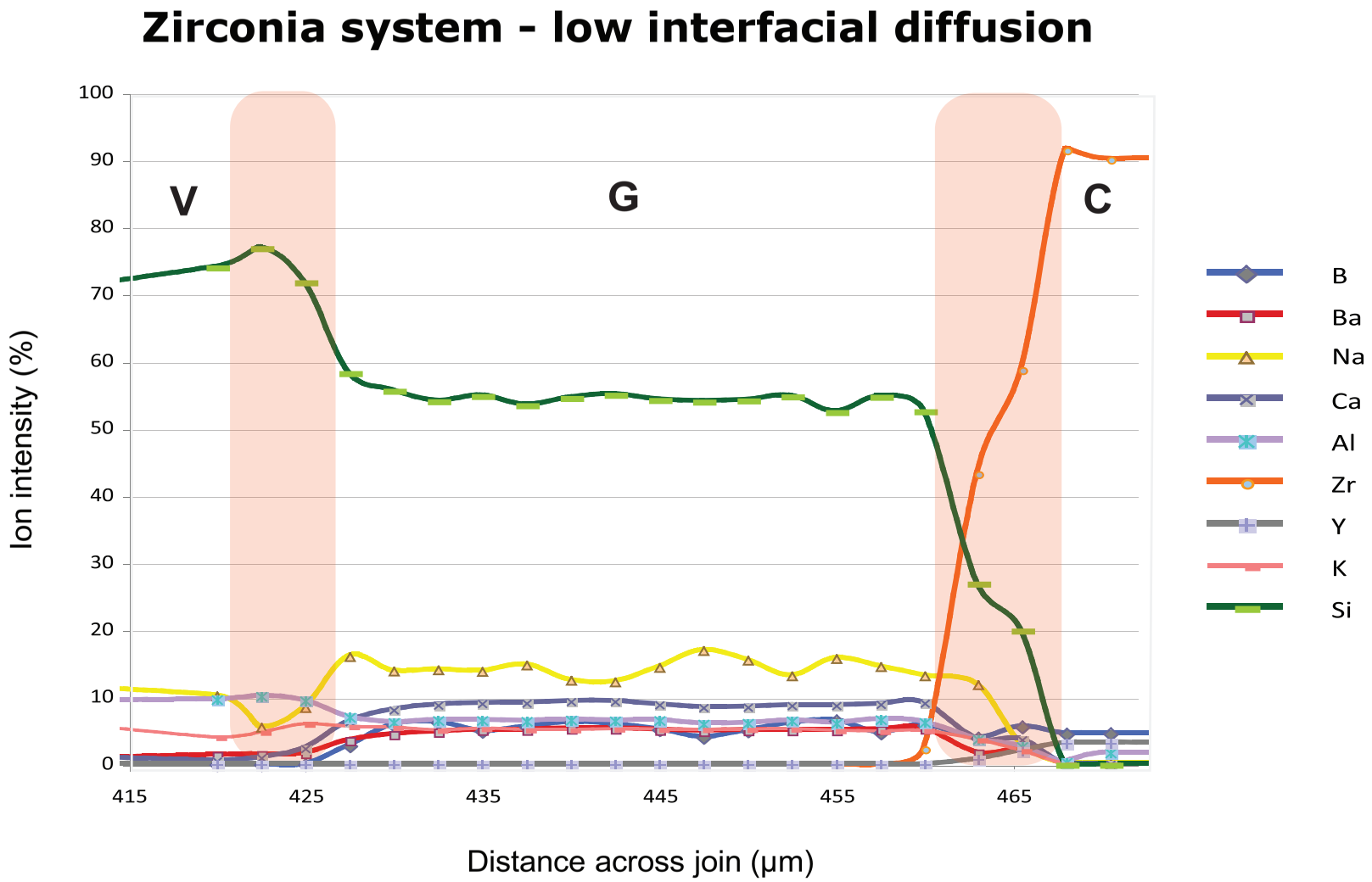

Figure 3.7a Microprobe scans of ion concentration across glass-bond interface for zirconia-core system, for low anneal cycle. Colored bands indicate interdiffusion layers. Veneer (V), glass (G) and core (C) zones indicated.

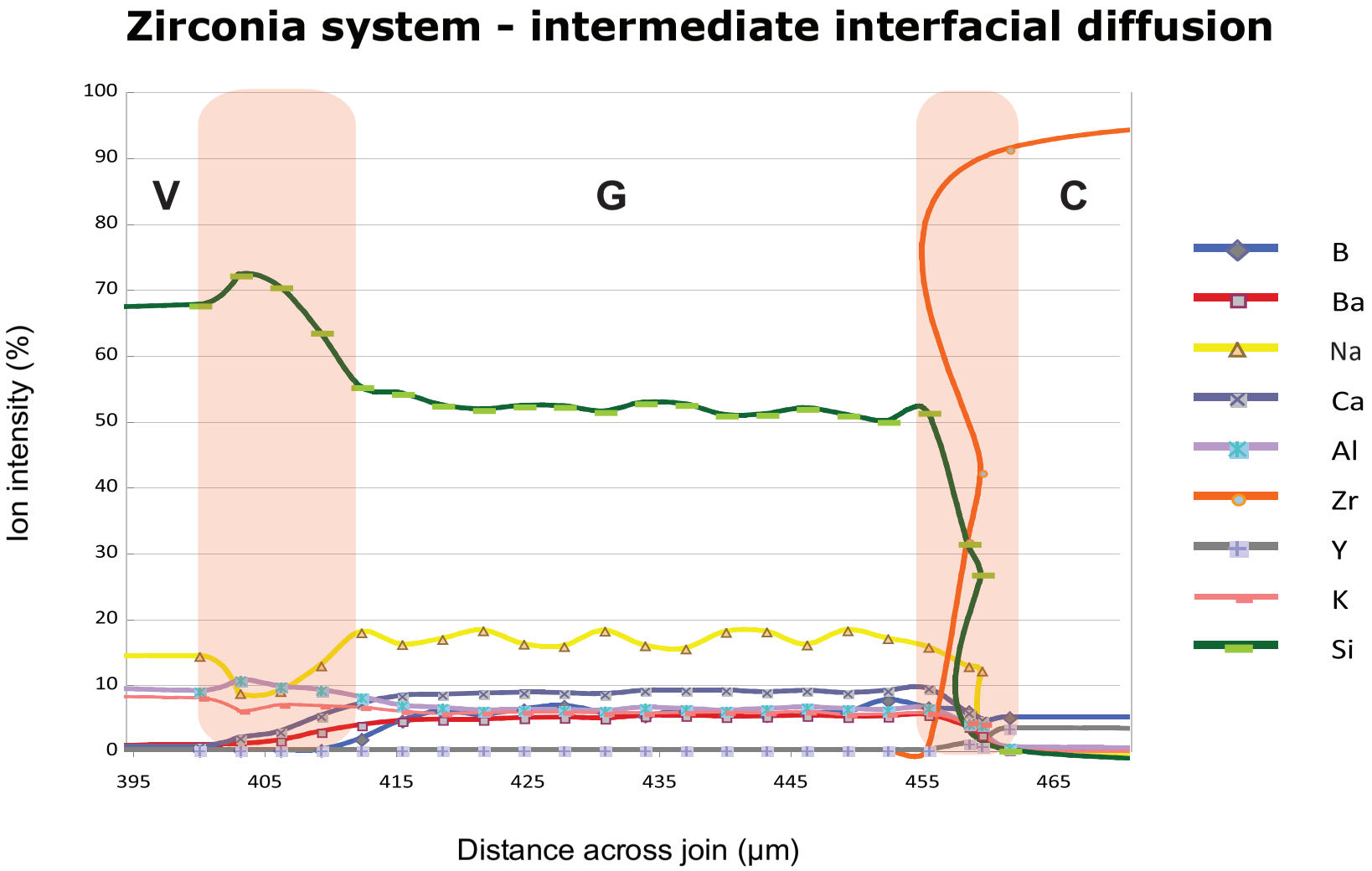

Figure 3.7b Microprobe scans of ion concentration across glass-bond interface for zirconia-core system, for intermediate anneal cycle. Colored bands indicate interdiffusion layers. Veneer (V), glass (G) and core (C) zones indicated.

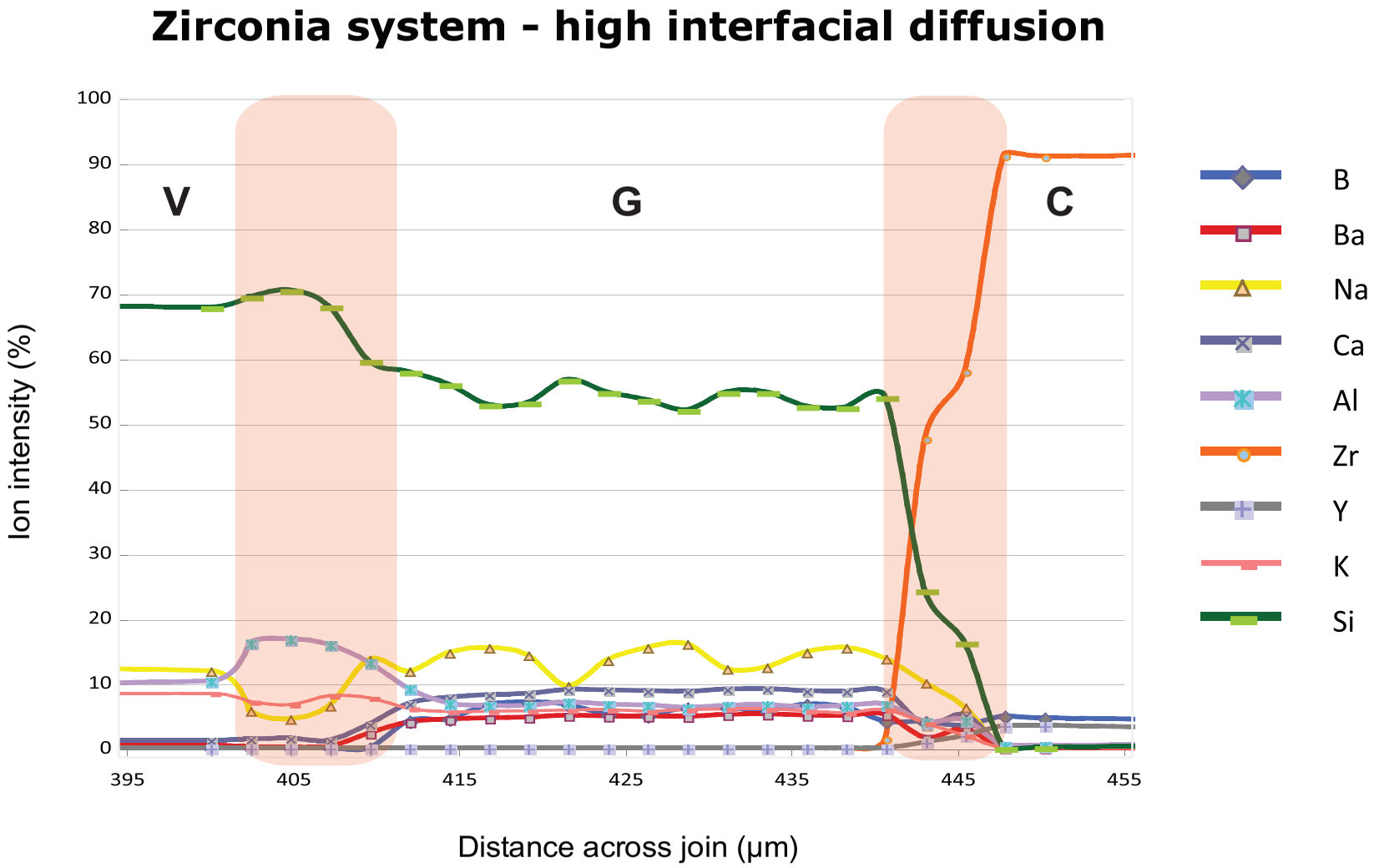

Figure 3.7c Microprobe scans of ion concentration across glass-bond interface for zirconia core system, for high anneal cycle. Colored bands indicate interdiffusion layers. Veneer (V), glass (G) and core (C) zones indicated.

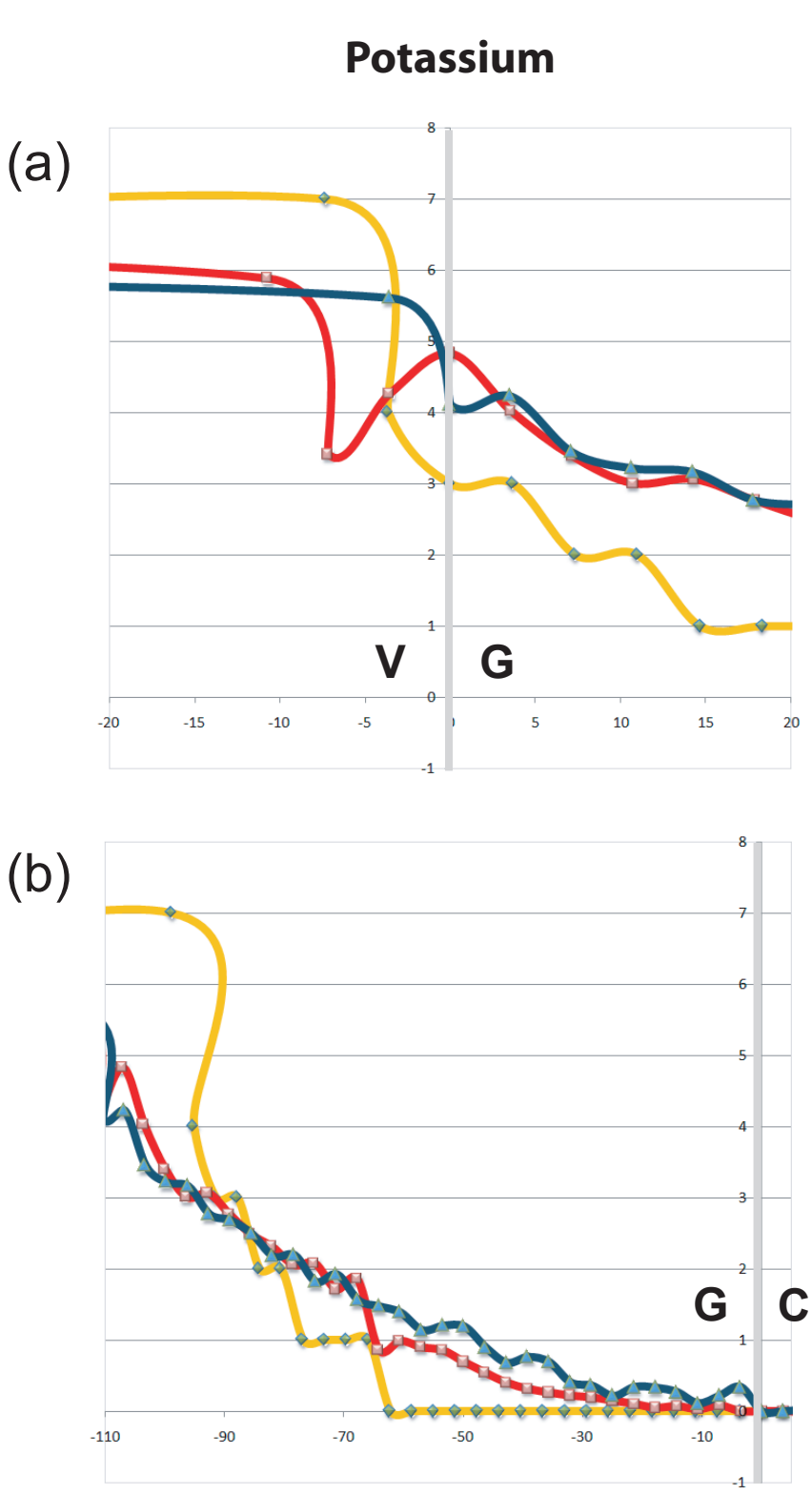

Figure 3.8a Potassium diffusion in alumina systems, a) veneer/glass (V/G) join interface, b) glass/core (G/C) interface For low (yellow ◇), intermediate (red □) and high (blue △) anneal times. The vertical axis is vertical intensity, and the horizontal axis is distance (μm).

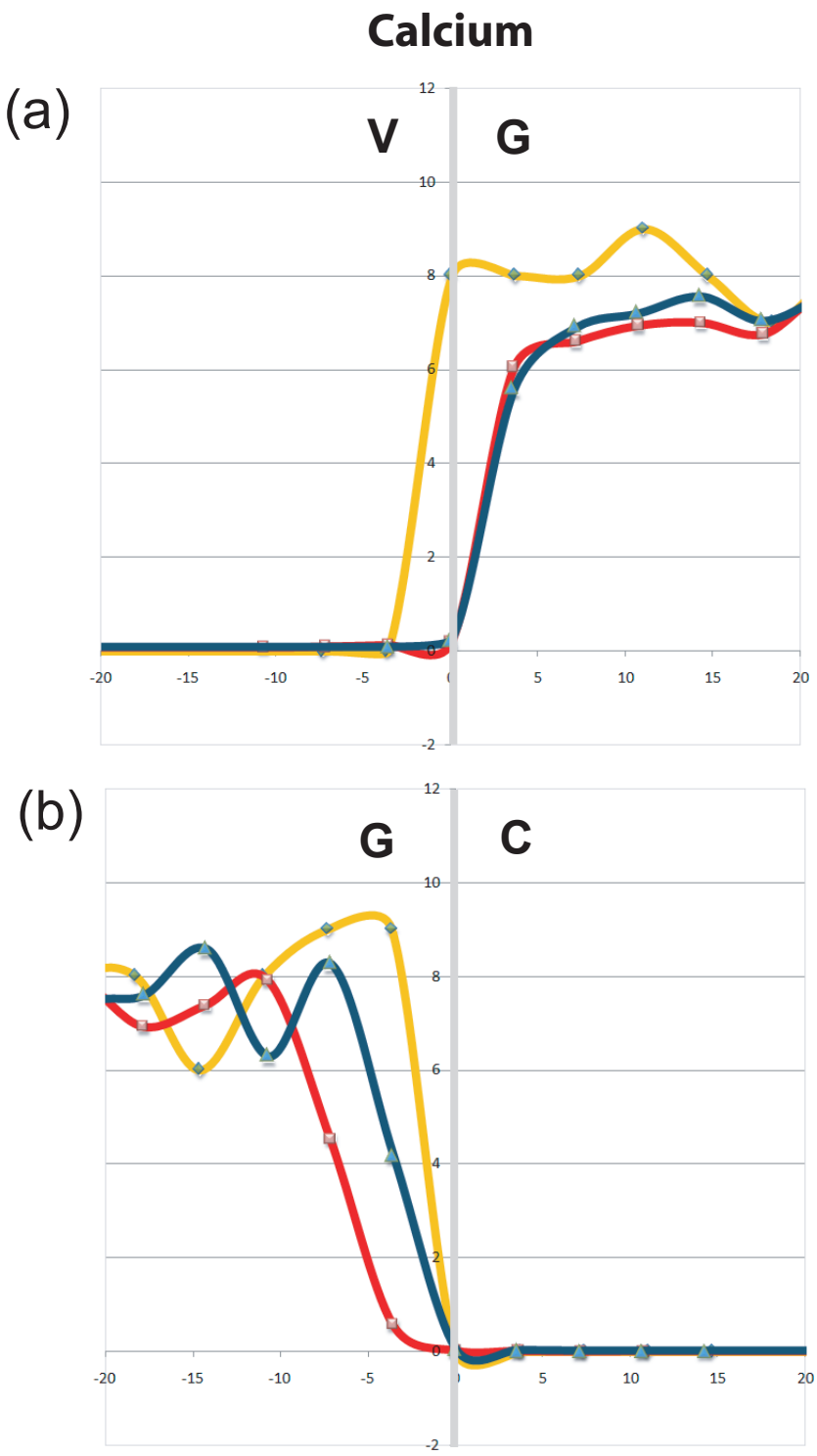

Figure 3.8b Calcium diffusion in alumina systems, a) veneer/glass (V/G) join interface, b) glass/core (G/C) interface For low (yellow ◇), intermediate (red □) and high (blue △) anneal times. The vertical axis is relative intensity, and the horizontal axis is distance (μm).

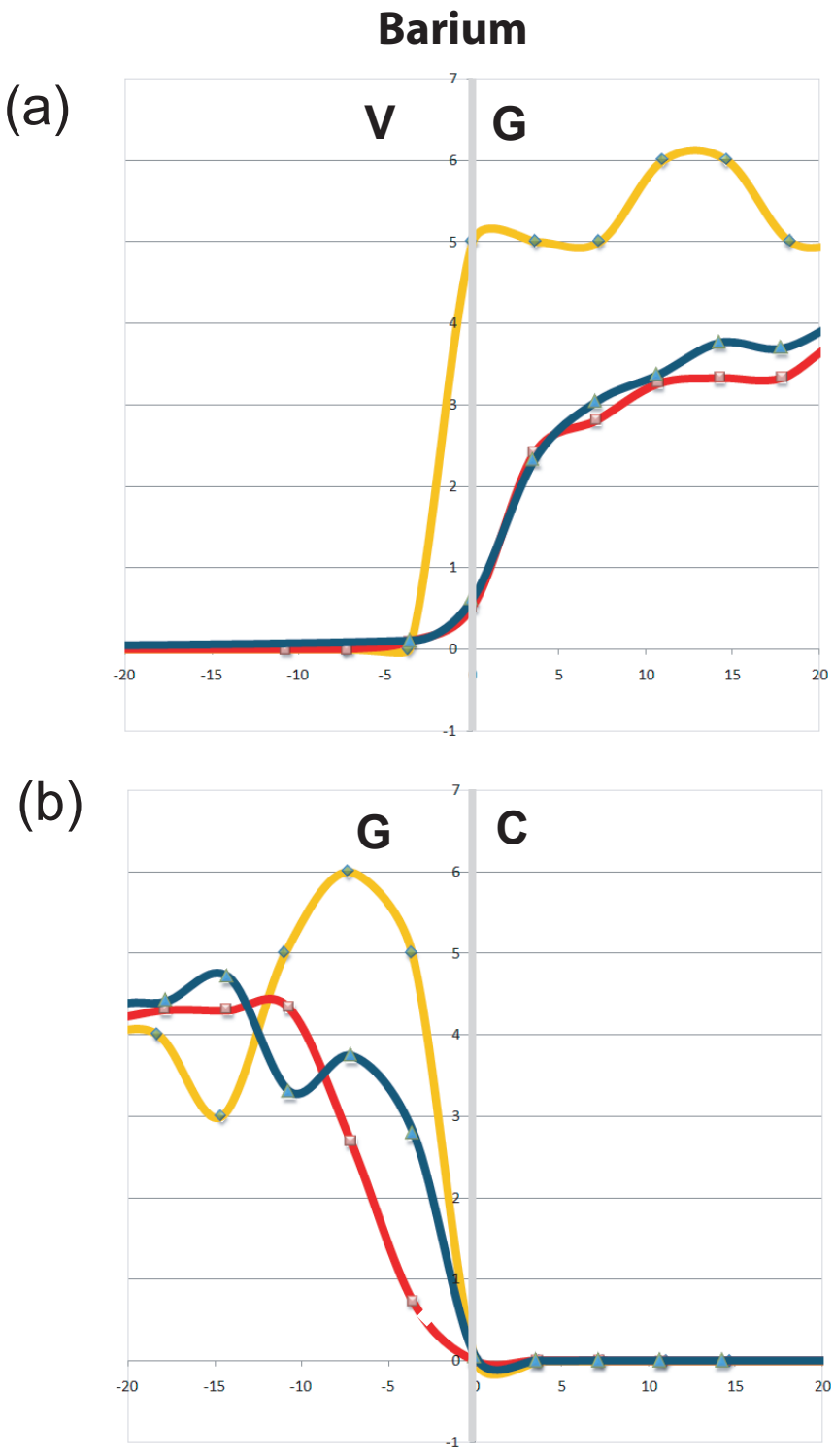

Figure 3.8c Barium diffusion in alumina systems, a) veneer/glass (V/G) join interface, b) glass/core (G/C) interface For low (yellow ◇), intermediate (red □) and high (blue △) anneal times. The vertical axis is relative intensity, and the horizontal axis is distance (μm).

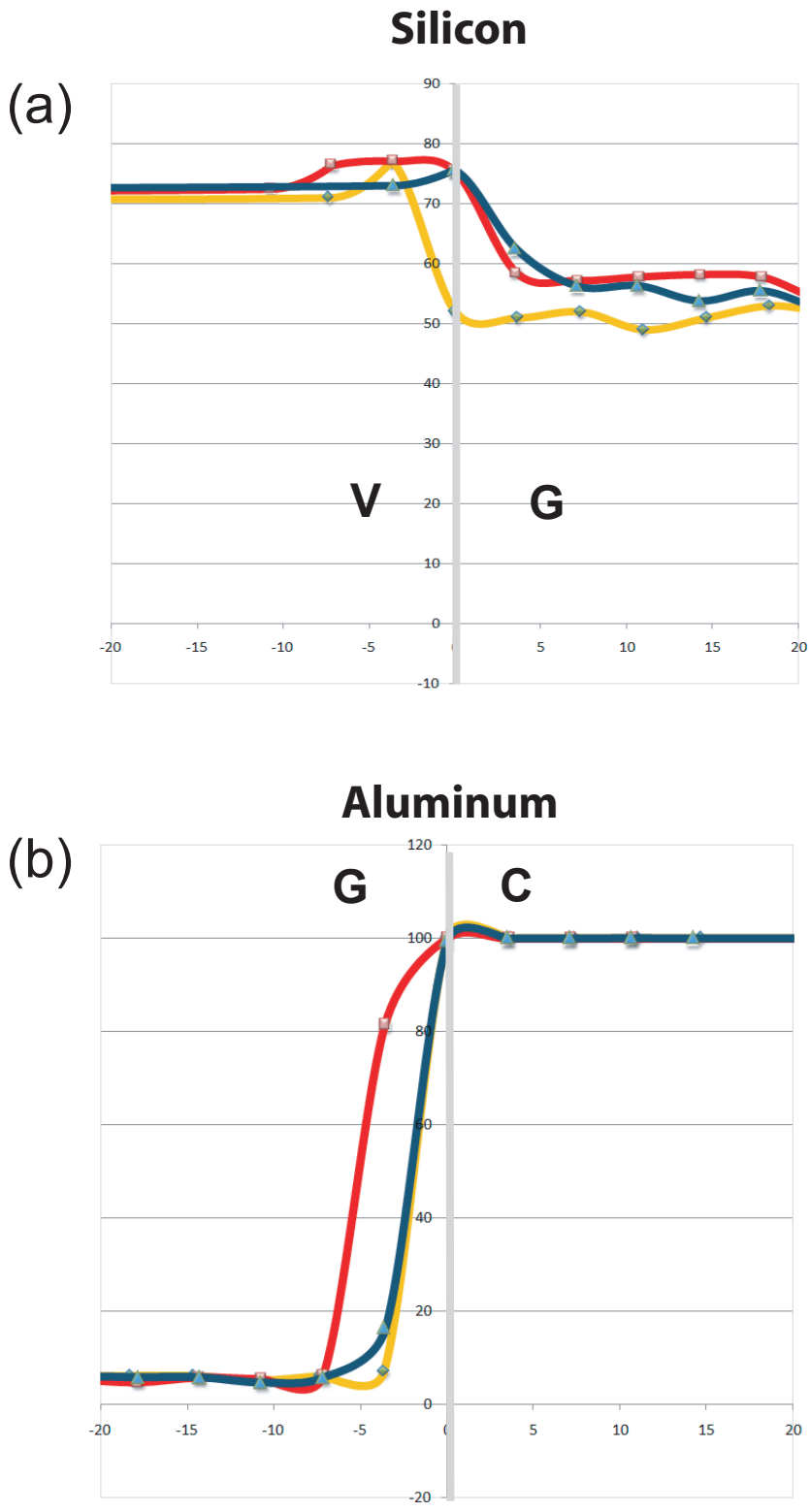

Figure 3.8d Diffusion in alumina systems, a) silicon at veneer/glass (V/G) join interface, b) aluminum at glass/core (G/C) interface. For low (yellow), inter-mediate (red) and high (blue) anneal times. The vertical axis is intensity, and the horizontal access is distance (mm).

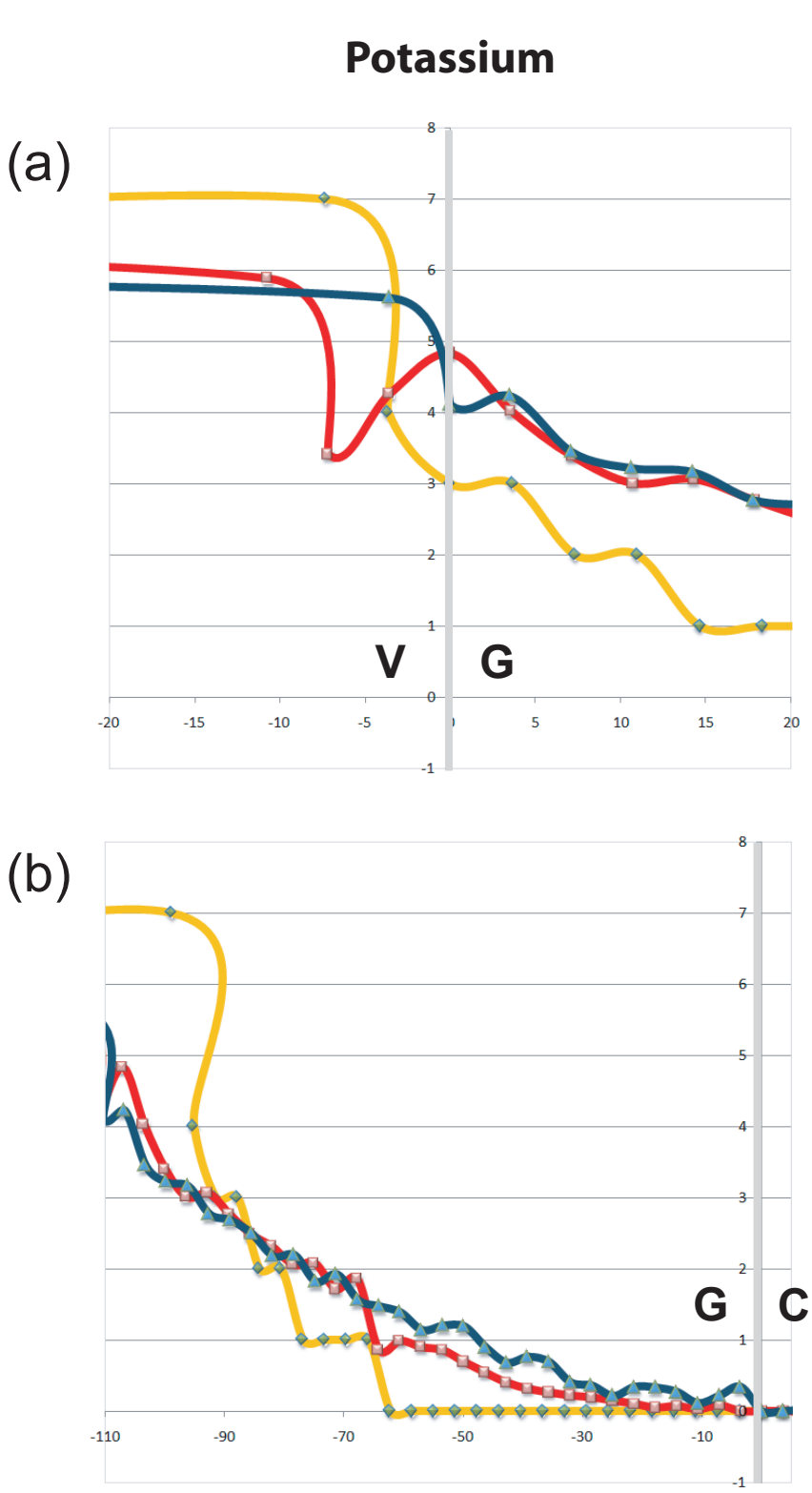

Figure 3.9a Potassium diffusion in zirconia systems, a) veneer/glass (V/G) join interface, b) glass/core (G/C) interface For low (yellow ◇), intermediate (red □) and high (blue △) anneal times. The vertical axis is relative intensity, and the horizontal axis is distance (μm).

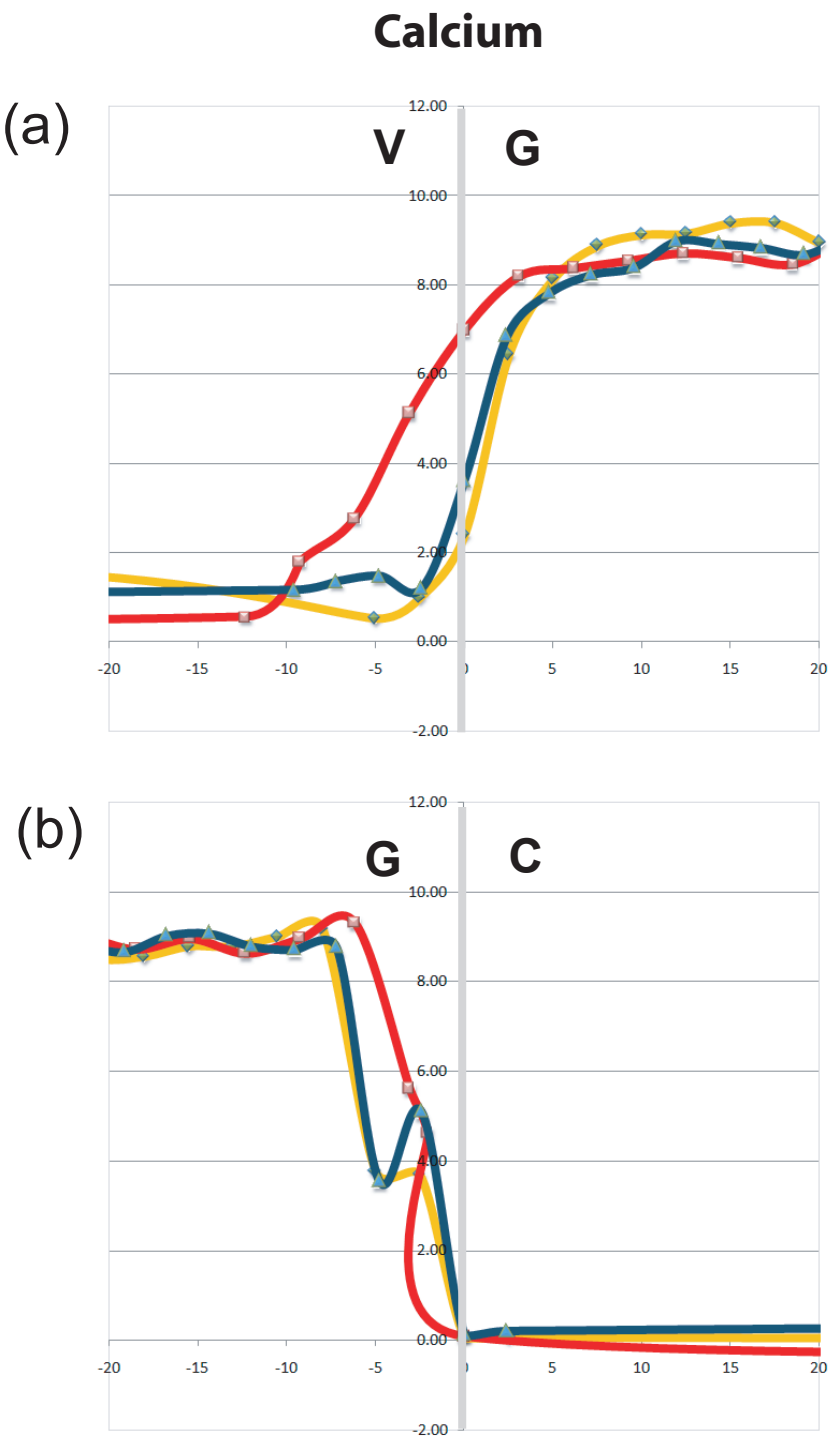

Figure 3.9b Calcium diffusion in zirconia systems, a) veneer/glass (V/G) join interface, b) glass/core (G/C) interface For low (yellow ◇), intermediate (red □) and high (blue △) anneal times. The vertical axis is relative intensity, and the horizontal axis is distance (μm).

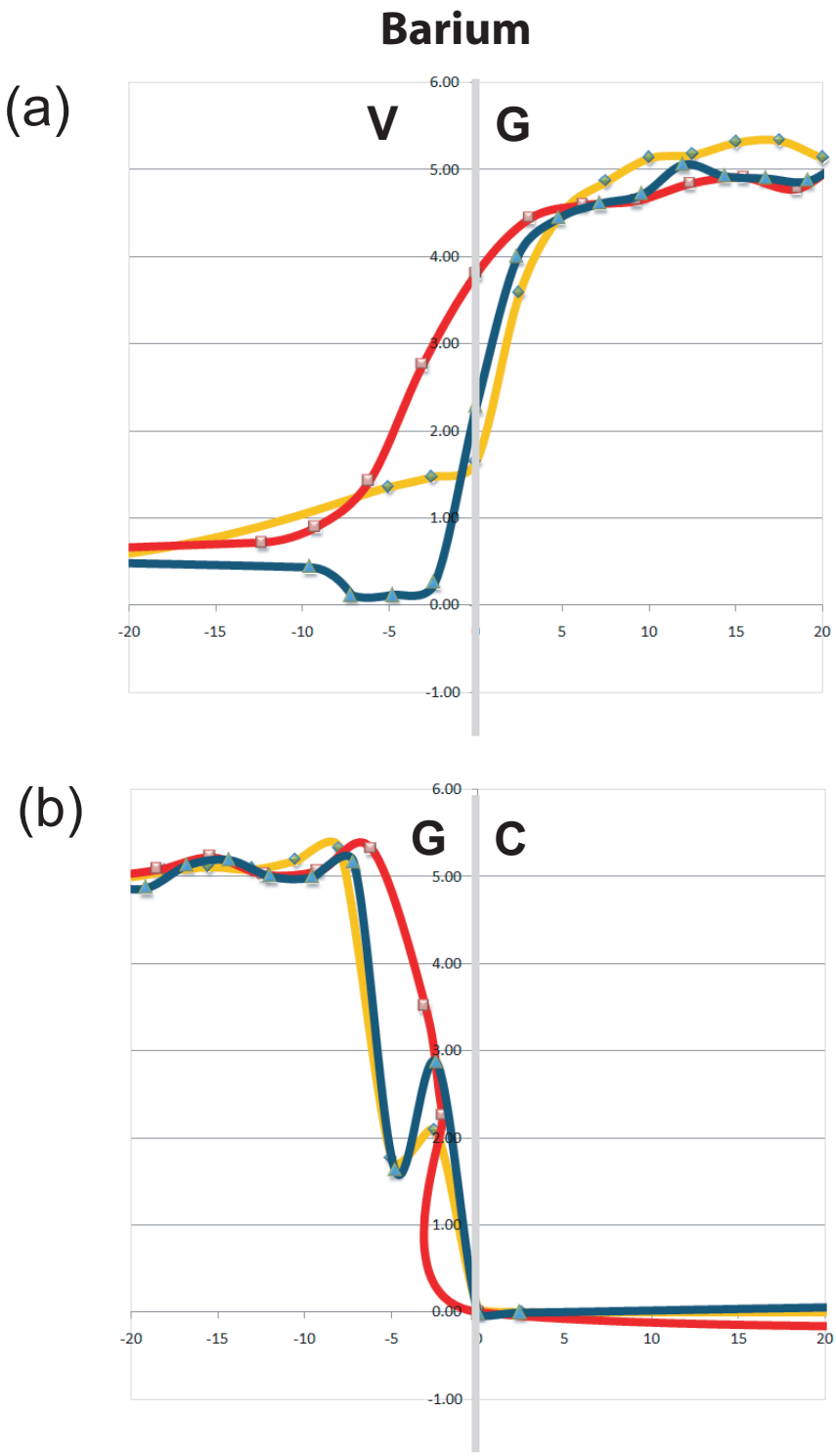

Figure 3.9c Barium diffusion in zirconia systems, a) veneer/glass (V/G) join interface, b) glass/core (G/C) interface For low (yellow ◇), intermediate (red □) and high (blue △) anneal times. The vertical axis is relative intensity, and the horizontal axis is distance (μm).

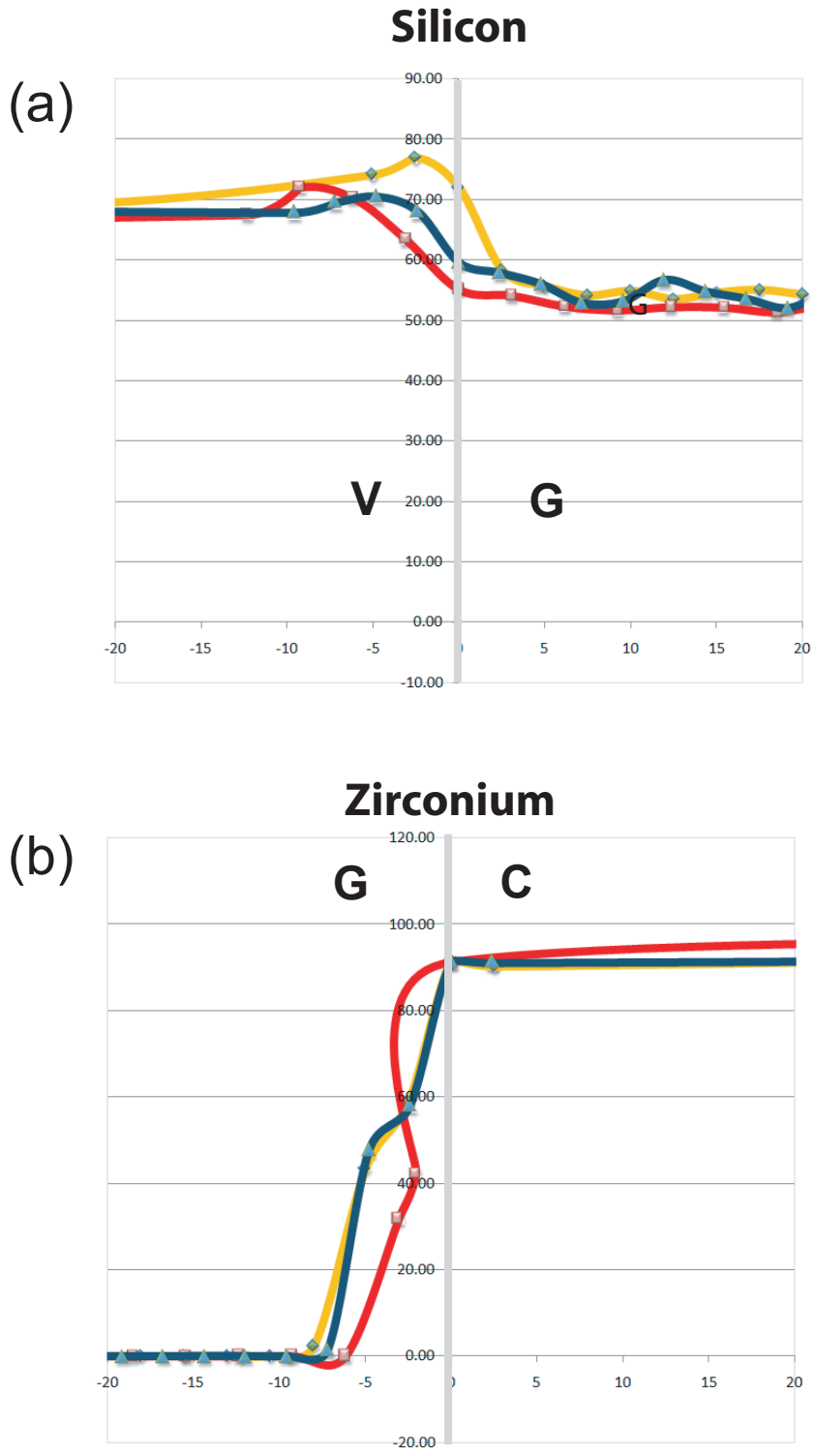

Figure 3.9d Diffusion in zirconia systems, a) silicon at veneer/glass (V/G) join interface, b) zirconium at glass/core (G/C) interface For low (yellow ◇), intermediate (red□) and high (blue △) anneal times. The vertical axis is relative intensity, and the horizontal axis is distance (μm).

The higher passrate for AA glasses indicated that Appen-formulated compositions were a better fit with respect to CTE matching. This is due to the improved capacity of the Appen approach to better predict the coefficient of expansion of our glasses. Detailed attention to glass frit preparation and subsequent join firing conditions was then found to be necessary. As indicated in Chapter 2, it is crucial to choose the right conditions, to avoid non-wetting, crazing and porosity in the glass join itself. Finer frits produced the best joins. To determine optimum fusion conditions, specimens were produced over a range of firing temperatures. Those that survived the firing were then passed on to simple, preliminary screening for mechanical integrity, by means of a 'finger' bend test. The survivors were then subjected in turn to a 'cutting' screen test, in which specimens were cut into shape using a diamond saw.

Optical microscopy was used to examine section of the intact fused interlayers, so as to help select the conditions for the best joins, i.e. uniformity of interlayer thickness and free of porosity or cracking. Those joins that showed clean interfaces and also survived the mechanical screening test were then selected for further examination.

Electron microprobe analysis was then used to examine diffusion of network modifier species in the glass join, quantified by measurement of an interdiffusion layer (IDL). Extensive testing was carried out on this aspect of the work. For this part of the work, 3 firing (anneal) times at the optimal firing temperatures were examined. Basically, we found that Na^{+}, K^{+} and Ca^{++} and Ba^{++} ions moved across the veneer/glass interface, at different rates, with K+, the most mobile, moving furthest

from veneer to glass. This was expected as monovalent cations have a greater diffusivity than divalent modifiers. Some Al^{+++} and Zr^{++++} ions diffused from the core ceramics into the glass joins. At low anneal times, the IDLs of both V/G and G/C were narrow, 10–15 μm for both alumina and zirconia systems, extending somewhat in range for larger anneal times. These were all indicators of well-bonded interfaces, and demonstrate the feasibility of applying the technology to the formation of dental crown systems.

Having successfully demonstrated capacity to make these joins, it remains now to evaluate mechanical integrity more closely. This forms the subject of the next chapter.

Chapter 4: Mechanical Evaluation

4.1 Introduction

Mechanical properties are important in our application. As indicated earlier, our goal is to join two brittle layers by fusion with a chemical bond. In such a system, both veneer and core layers are vulnerable to fracture, most generally to cracks that traverse the layer thickness—'transverse' cracks. More importantly, in the context of the present work in which the bond is accomplished by glass fusion, the interlayer between the two layers is itself vulnerable. Accordingly, we need to ensure that the interface has sufficient strength or toughness to survive the stringent conditions under which dental crowns are expected to operate. Can the glass bond arrest cracks in the veneer layer from penetrating into the core, or vice-versa? Above all, can the glass interlayer prevent cracks from delaminating the interface? The last of these issues is most key to acceptable performance.

Accordingly, our aim is to conduct simple tests on fabricated layer structures to evaluate the strength of the interfacial bond that joins the veneer and core ceramic layers. For this, we use the indentation microprobe method with a Vickers diamond. This approach is simple but powerful, and is used extensively in materials research to characterize fracture and deformation properties, measure residual stresses, and, most important, evaluate the tendency for cracks to penetrate interfaces or delaminate them [51-54].

4.2 Background

As indicated above, layer systems used in all-ceramic crowns are susceptible to fracture, particularly from cracks traversing the layer thicknesses. Many studies have been made of such crack systems, particularly by the NIST group [51-55]. At issue here is how a fused interface between the veneer and core layers interacts with such cracks. In particular, does the fusion layer impede the progress of these cracks, or deflect them along the interface? If the second of these scenarios is true, then the strength of the interface is suspect.

A schematic indicating some of the more deleterious fracture modes is shown in Fig. 4.1. This system consists of an aesthetic veneer (porcelain) layer joined to a core (alumina or zirconia) support layer, with the whole cemented onto a soft and compliant substrate representing tooth dentin. The veneer/core layer system is subject to concentrated loading at the top surface, simulating an occlusal contact. The concentrated 'Hertzian' stresses can initiate a variety of cracks within the veneer, depending on the specific loading conditions [56,57]. These include two kinds of cone cracks initiated within the Hertzian elastic contact zone: elastically generated outer (O) cracks [58] and hydraulically pumped inner (I) cracks [59,60]. Such cracks are generally axisymmetrical with the geometry of truncated cones, and penetrate downward and outward into the veneer subsurface.

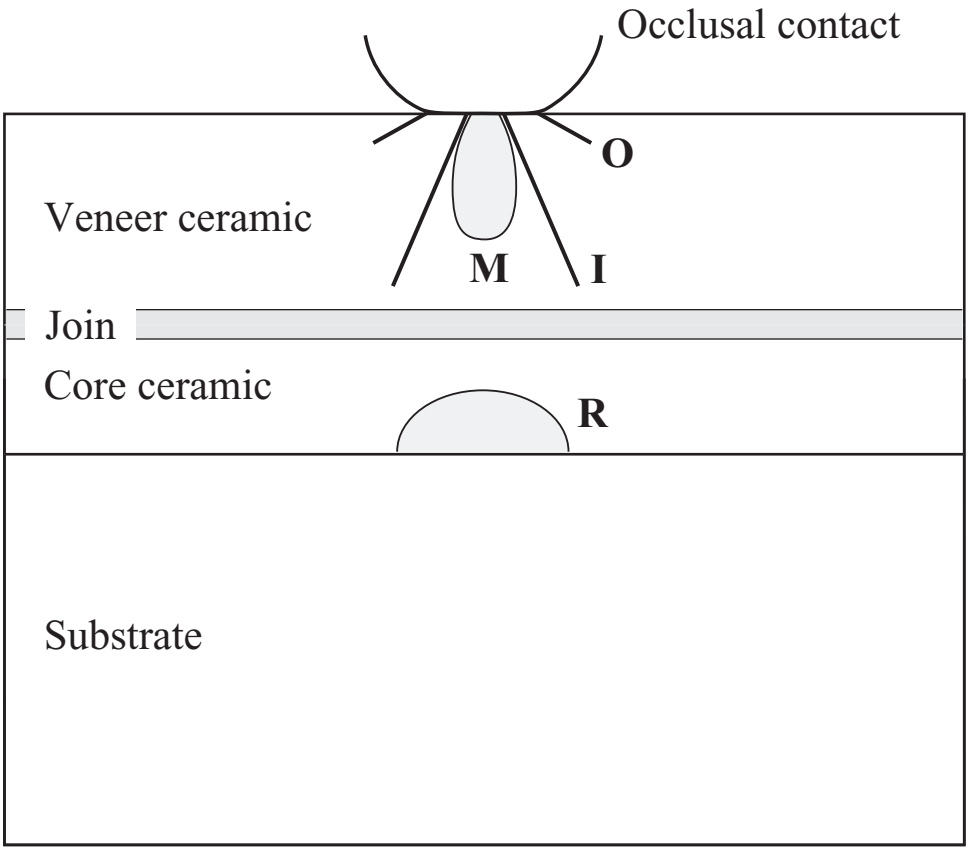

Figure 4.1 Schematic showing various cracks that can form in ceramic veneer/core layers joined by glass, and cemented onto a compliant support layer. At top surface, elastic contact can generate outer (O) and inner (I) cone cracks, and plastic contact can generate median (M) cracks. At bottom surface, flexural stresses can generate lateral cracks. All these cracks grow transversely though the layer thickness, and ultimately intersect the join interface.

In addition, in the case where some plasticity is generated beneath the contact, median (M) cracks can initiate and propagate directly downward on median planes containing the load axis [61]. These cracks are particularly evident in cyclic loading in moist environments, from fatigue effects [62-64].

Even though the supporting core layer is generally much stiffer, harder, tougher and stronger than the veneer, it too is susceptible to fracture. This comes about because the combined veneer/core system experiences some flexure beneath the concentrated surface load, placing the core undersurface in tension [52,65]. Cracks initiate from flaws at the bottom surface, and pop in to form so-called radial (R) cracks which spread upward and radially outward, again on median planes. Thus attention has to be paid to the possibility of fractures in both veneer and core layers.

The important point about all these crack systems is that they traverse the layers, from the outer surfaces toward the interface. Ideally, we would like the interface to be infinitely strong, to prevent the cracks penetrating from one layer to the next, or, more importantly, from delaminating along the interface itself. Of course, no interface is infinitely strong—in fact, most (not all) interfaces tend to be weaker than the layers they bond. Generally, from studies of interface mechanics, if the toughness of the interface is greater than one half that of the bulk material in the adjacent brittle layer, the crack will arrest and/or penetrate rather than delaminate [51]. We will explore this issue in more detail below.

As had been made clear in many places in this thesis, it is crucial also to avoid high CTE mismatch stresses in the composite layer system, because that will introduce some tension in one or both layers. The existence of such stresses in any

bilayer that survives the joining process will inevitably enhance one or other of the fracture modes depicted in Fig. 4.1.

In what follows, we will use a simple indentation test developed by researchers at NIST [53] for joined bilayers to determine the integrity of our fused interlayers and to confirm the absence of significant CTE stresses. We will follow that work closely, since that group has already outlined the basic theory behind the methodology. The major difference in the present study is the presence of the additional, intervening glass bond layer between the veneer and core layers.

4.3 Experimental Methods

Vickers indentation tests were carried out on sections of glass-joined porcelain/alumina and porcelain/zirconia layers. The sections were cut normal to the top surface with a diamond saw, ground and polished with diamond paste to 1 μm diamond finish. A final polish was made with a 0.1 μm colloidal silica suspension on a felt cloth. Figure 4.2 shows the section geometry. The thickness d of the join varied between 10 to 30 μm in these specimens.

Conventional microindentation testing was then carried out on the polished sections using a Vickers indenter in a Zwick tester (Zwick, Riverview, Michigan USA). Preliminary tests were made on each of the porcelain veneer and core materials before joining, to ensure well-formed indentations. The sizes of cracks c_1, c_2, c_3 and c_4 emanating from the indentation corners were then measured in a high power microscope, from which the fracture toughness was calculated for each material using the following relation [66]

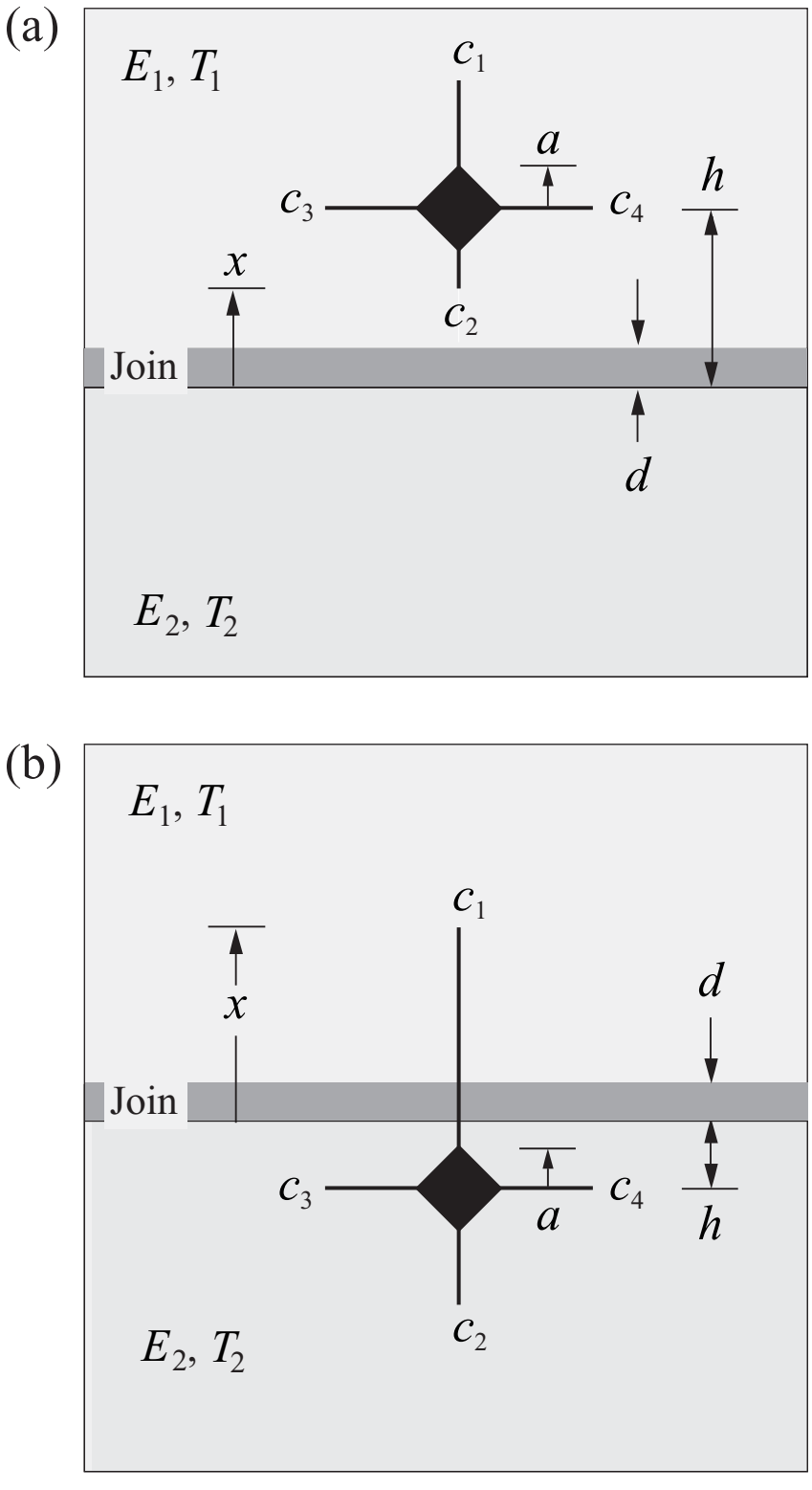

Figure 4.2 Schematic showing Vickers indentations in ceramic layers joined by glass. Coordinate system shown for measuring lengths c of crack arms at different distances h from interface (taken at boundary between core and glass), for crack in (a) veneer and (b) core layers.

$$T = \xi(E/H)^{1/2}P/c^{3/2}$$

where P is the indentation load, c is the size of the crack traveling towards the interface measured from indent center to crack tip (c_1 in the core, and c_2 in the veneer), E is Young's modulus, H is hardness, and $\xi = 0.016$ is a dimensionless coefficient. The calculated modulus of the glass is 70-78 GPa, while the measured hardness was 4-5 GPa both of which are similar to values for porcelain.

Indentations were then placed in the specimen sections at prescribed distances h from the interface between core and fused glass interface, with cracks parallel and perpendicular to interface, as depicted in Fig. 4.2. Different loads were used in each layer material, so as to maintain indentations with well-defined cracks in each case: in the porcelains, P = 10 N (higher loads tended to produce excessive chipping, disrupting the crack patterns); in the alumina, P = 10 N, whereas in the zirconia, P = 35 – 40 N (needed to initiate corner cracks). Indents far from the interface were compared with those in the dummy, unjoined specimens, to examine for the presence of any residual compression or tension CTE stresses—any such stresses would reveal themselves by shortening or lengthening the crack arms parallel or perpendicular to the interface [67]. Typically, cracks that are less than 30% longer than the average crack length in unjoined material at the same load may be considered to be indicative of the presence of an insignificant stress level, i.e. < 30 MPa [54].

The behavior of the cracks with diminishing distance h from the interface was then observed for the layered structures. In particular, observations were made as to whether perpendicular cracks arrest, deflect, bend or penetrate at the interface. From

such observations, one can evaluate minimum interface toughness values [53]. Bending of parallel cracks toward or away from the interface indicates either presence of significant residual stress or a stress field modifying effect of a lower modulus interface layer.

4.4 Results

4.4.1 Qualitative observations

Figures 4.3 and 4.4 show indentations in the veneer/glass/core-ceramic systems remote from the glass interface. In these figures, cracks are equi-sized in all directions, indicating well-behaved materials without significant CTE stresses from the join process. The crack patterns are in fact almost identical to those seen in control, separate porcelain, alumina and zirconia specimens. As an example, a CTE mismatch of $1x10^{6}$ C^{-1} corresponds to a residual stress of 30 MPa [53], which would in turn show as a difference of about 30% in crack lengths in the parallel and perpendicular [54]. We observe no measurable differences at all, certainly not more than 10%, within the scatter in data. From these observations we can conclude that the CTE stresses in either of the layers in Figs. 4.3 and 4.4 are < 10 MPa, and can therefore be neglected.

Figures 4.5 and 4.6 show indentations much closer to the glass/core interface, such that the nearest, lead corner crack intersects the interface itself.

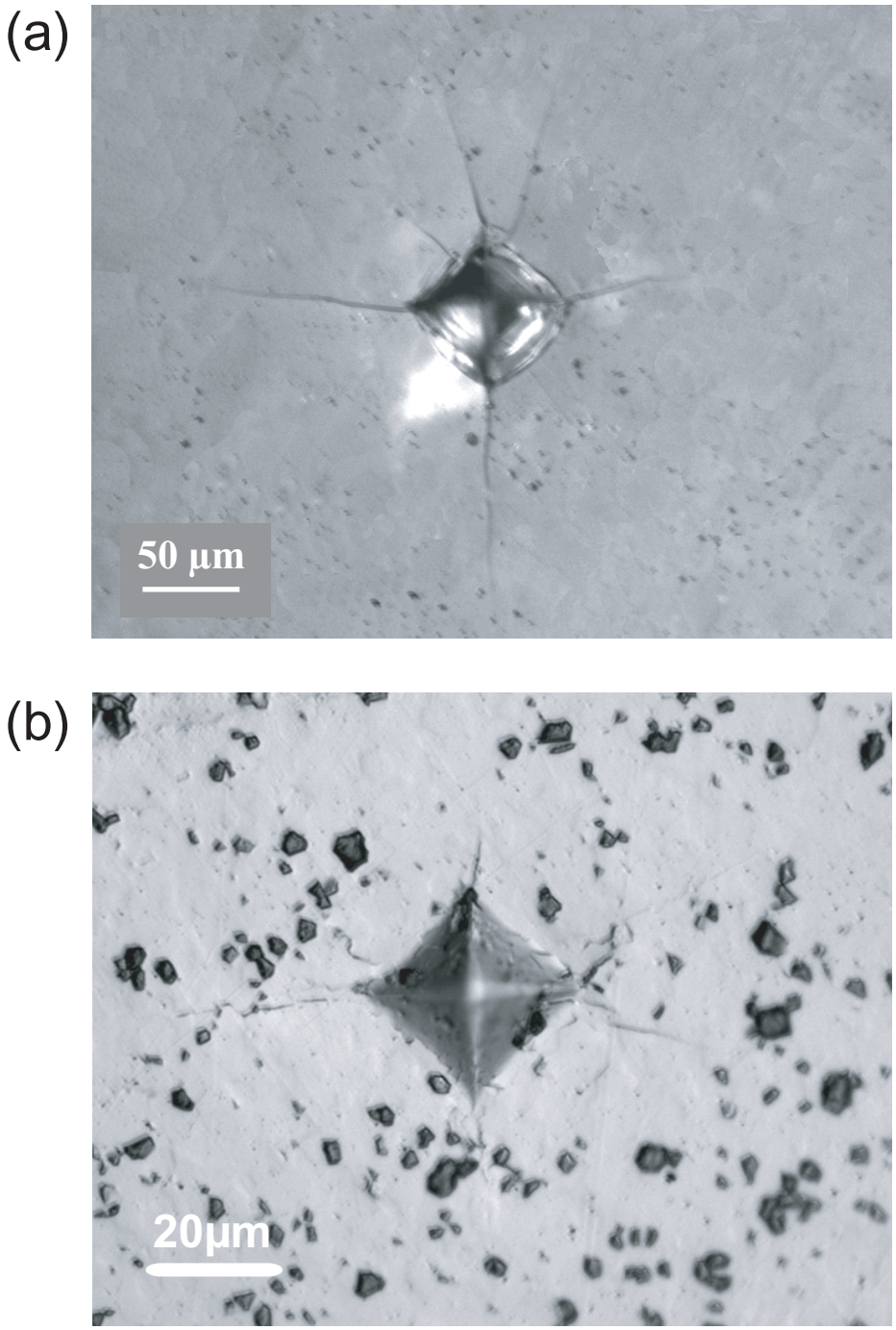

Figure 4.3 Vickers indentations in porcelain/glass/alumina layer structures, remote from bonding glass interface in (a) porcelain and (b) alumina. Note essential symmetry of corner crack patterns in both materials, indicating absence of significant residual stresses.

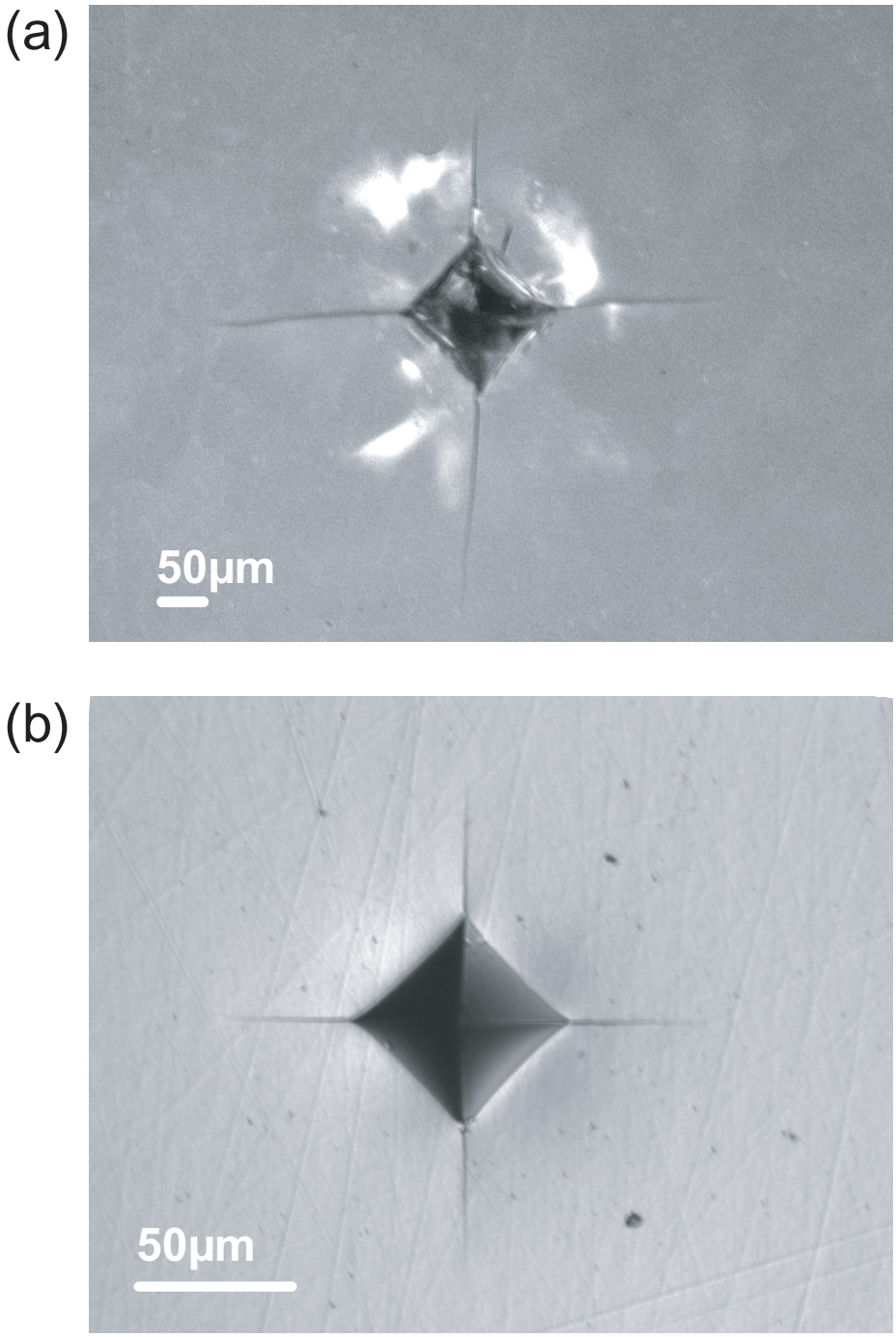

Figure 4.4 Vickers indentations in porcelain/glass/zirconia layer structures, remote from bonding glass interface in (a) porcelain and (b) zirconia. Note essential symmetry of corner crack patterns in both materials, indicating absence of significant residual stresses.

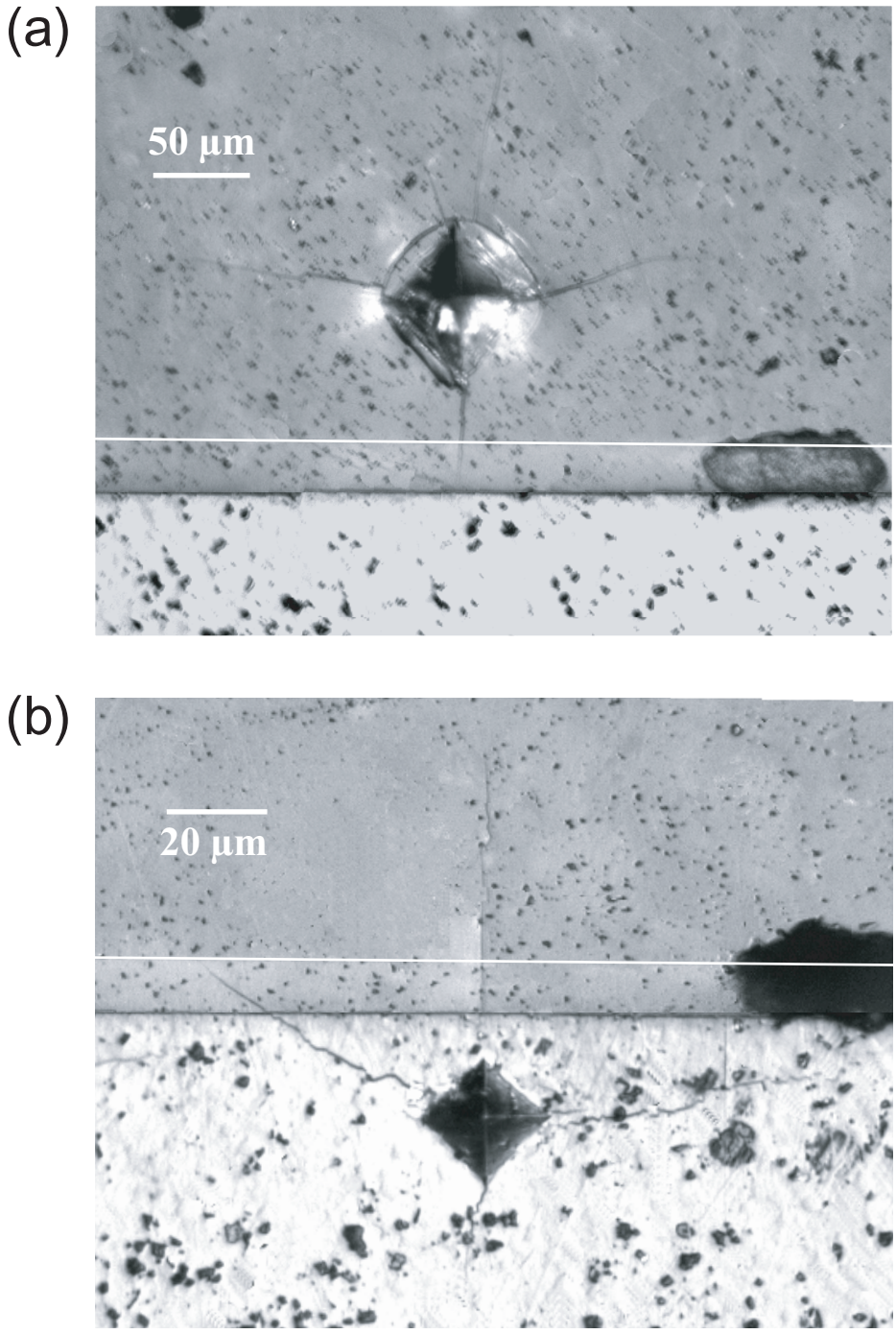

Figure 4.5 Cracks from Vickers indentation in glass-bonded porcelain/ alumina bi-layer. Indentations in a) porcelain and b) alumina. Note crack arrests at alumina traverses glass bonding layer and arrests at alumina interface in a), and penetration across glass into porcelain in b). White horizontal lines are used to highlight the veneer/glass junction.

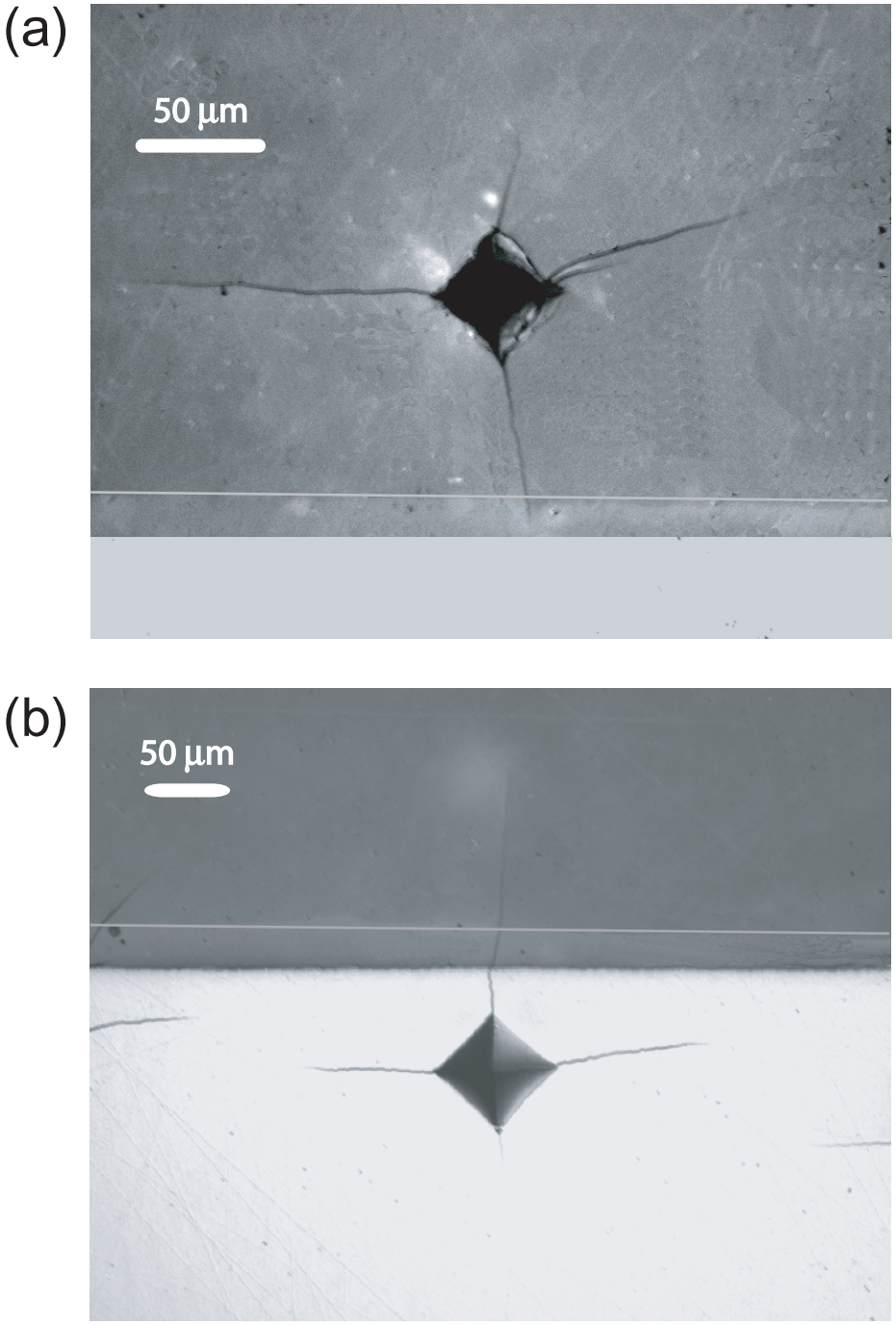

Figure 4.6 Cracks from Vickers indentation in glass-bonded porcelain/ zirconia bi-layer. Indentations in a) porcelain and b) zirconia. Note crack traverses glass bonding layer and arrests at zirconia interface in a), and penetration across glass into porcelain in b). Grey horizontal lines are used to highlight the veneer/glass junction.

For the cracks in the porcelain veneer (Figs. 4.5a and 4.6a), the lead crack arrests at the interface. (In the examples shown, the crack tip is difficult to discern, but can be seen at the interface in very high magnification.) It was difficult to place these cracks much closer to the interface without causing chipping, as reported by Kim et al. [53], then only for cracks approaching the core from the porcelain side. In no case did the cracks penetrate into the core.

For indentations in the core, on the other hand, the lead cracks appeared to be attracted to the interface, before penetrating into the veneer (Figs. 4.5b and 4.6b). This latter suggests that the interface does little to arrest upward extending fractures; but, most importantly, nor does it indicate any breakdown of the interface itself. These are robust joins. Note the bending of laterally extending corner cracks toward the interface in the case of alumina cores in Fig. 4.5. Since we have established that there are no significant residual stresses in any of the layers, this 'attraction' of the crack arms can be attributed to a modification of the local indentation stress field by an adjacent low modulus interface layer [68], especially manifest in the case of the porcelain/alumina system where the modulus mismatch is particularly large (note tables 2.1 and 2.6 for properties of ceramics and glasses respectively).

4.4.2 Quantitative analysis

To quantify these observations, we plot measured crack lengths c as a function of location h relative to the glass/core interface in Figs. 4.7 and 4.8. The subscript on the c quantities in the insets define the crack orientation (compare Fig. 4.2).

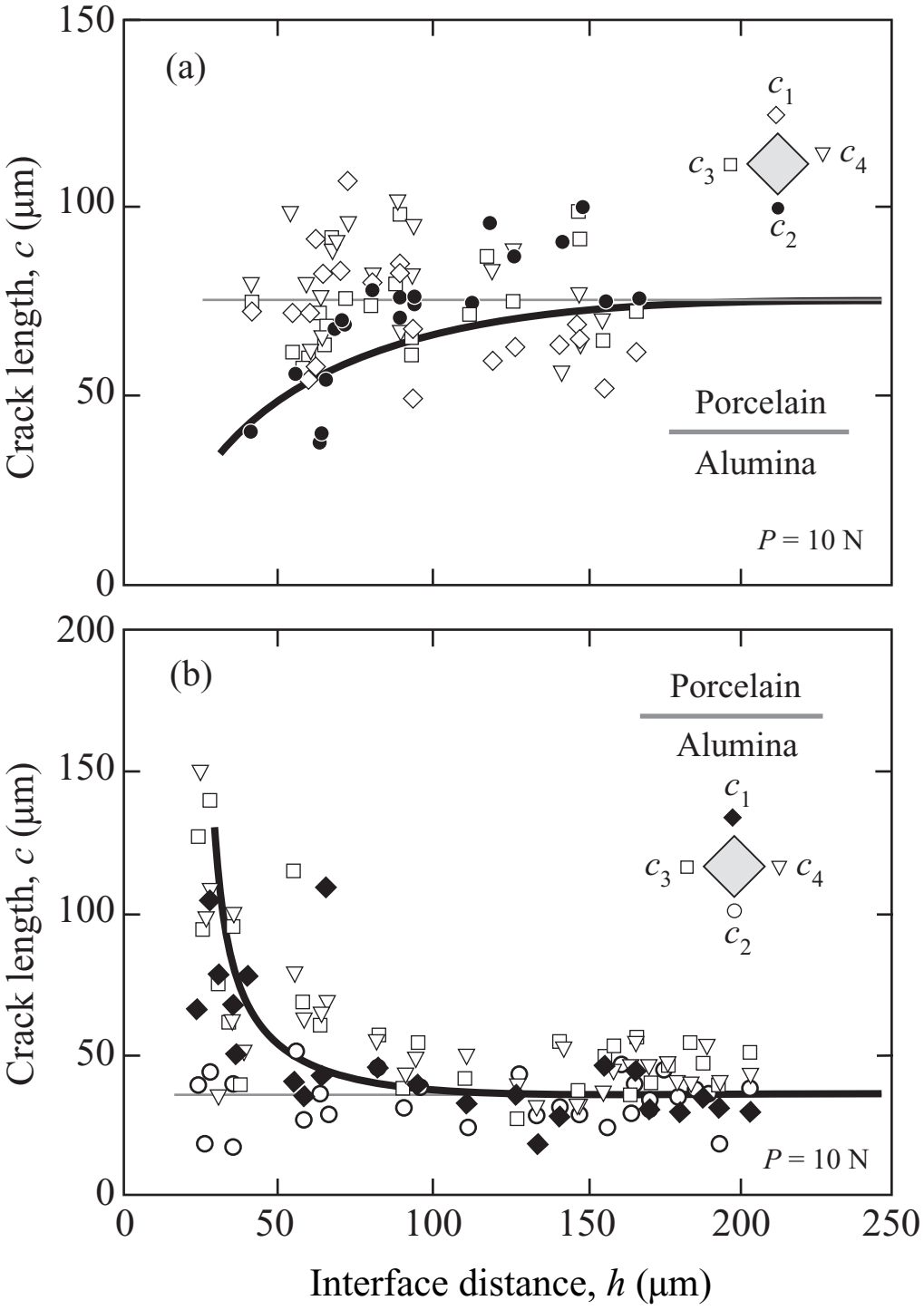

Figure 4.7 Crack sizes c_1, c_2, c_3 and c_4 *versus* distance h of indentation center to interface in glass-bonded porcelain veneer/alumina core systems. Indentations at P = 10 N in (a) porcelain and (b) alumina, orientation relative to interface indicated by inset.

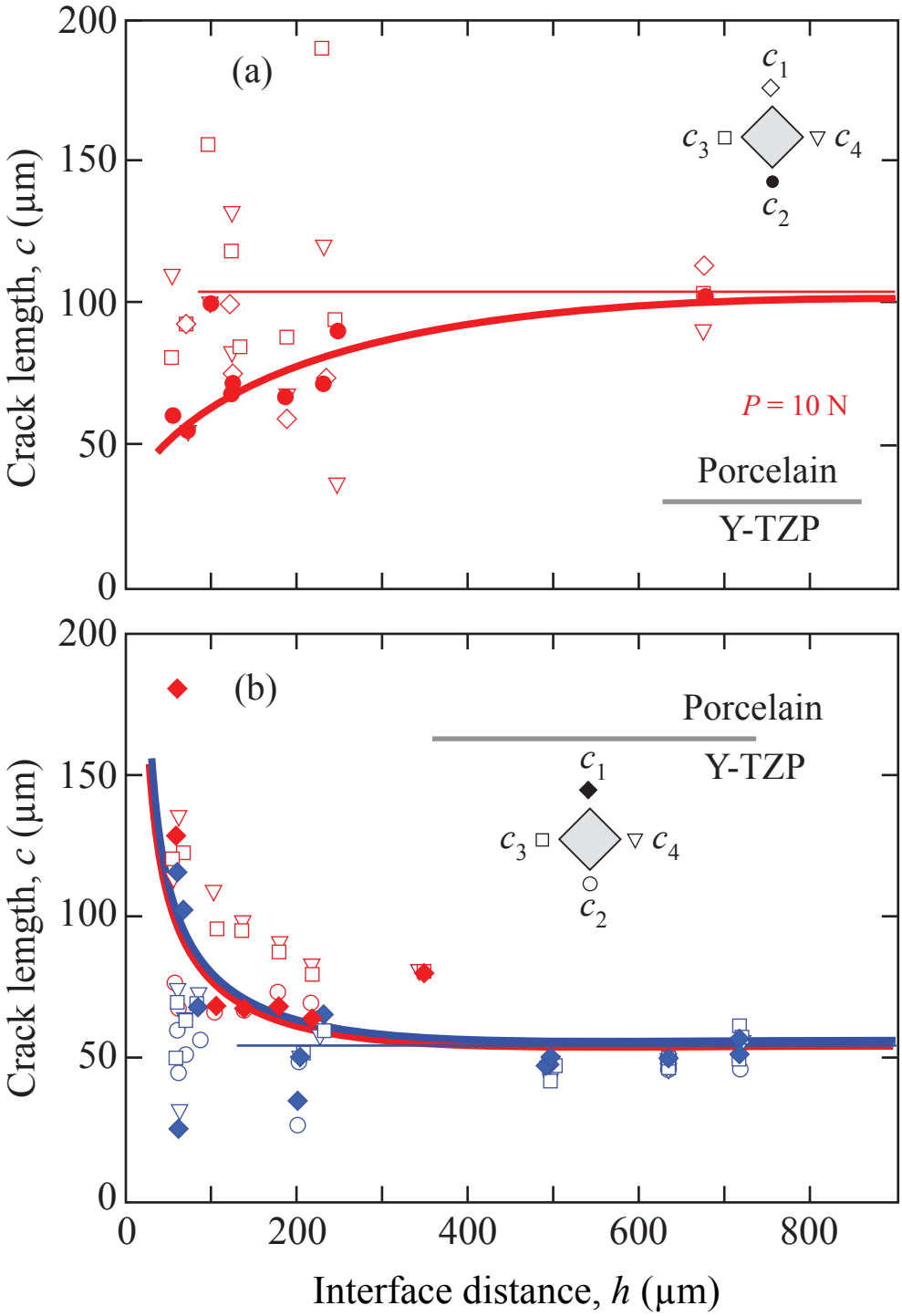

Figure 4.8 Crack sizes c_1, c_2, c_3 and c_4 *versus* distance h of indentation center to interface in glass-bonded porcelain veneer/ zirconia (Y-TZP) core systems. Indentations in (a) porcelain and (b) zirconia, orientation relative to interface indicated by inset. In zirconia graph, the red points represent glass AP1040, indents made at P = 40 N, while the blue points represent glass AP1020 indents madeat P = 35 N.

In the figures for zirconia system, Fig. 4.8, the data are for two bonding glasses, and different indentation loads (P = 35 N for AP1020 glass bonded specimen, and P = 40 N for AP1040 glass bonded specimen). Horizontal dashed lines on these plots indicate asymptotic limits $c_1 = c_2 = c_3 = c_4$ at large h, i.e. for indents away from the interface for remote indentations, although at small h (i.e. closer to the interface) there is wide scatter exacerbated by the different loads used. These crack sizes are similar to those measured in individual, unbonded ceramic specimens, in which no macroscopic CTE stresses exist.

Most interesting are the data for the lead indentations, c_1 in Figs. 4.7a and 4.8a and c_2 in Figs. 4.7b and 4.8b (indicated by the dark symbol at the respective insets). Solid curves through these data are empirical fits. As the indents approach the interface (diminishing h), there are tendencies for the lead cracks in the porcelains (Figs. 4.7a and 4.8a) to become smaller ('repulsion'). At very small I, the lead cracks arrest at the glass/core interface. In our case, we saw no delaminations at the interface, indicating very good bonding. This contrasts with observations by Kim et al. [53], in which delamination occurred at similar fused interfaces but without a glass bond. Conversely, lead cracks in the alumina and zirconia cores (Figs. 4.7b and 4.8b) become larger ('attraction'). This indicates that the cracks are sensing a lower modulus in the adjacent glass/veneer material. Cracks tend to accelerate when they approach a less stiff adjacent layer (and especially when approaching a free surface).

These interactive effects of crack repulsion and attraction has been interpreted by Kim et al. [52,53] in terms of an 'effective toughness'. Those authors begin by defining a stress intensity factor for a Vickers corner crack

$$K_0 = \psi P/c^{3/2}$$

where $\psi = \zeta(E/H)^{1/2}$ is an elastic–plastic coefficient, E is Youngs modulus and H is hardness, and is ζ a dimensionless constant. Figures 4.9 and 4.10 are plots of K_0 versus the distance $x = c - h$ of the lead crack tip from the glass/core interface (Fig. 4.2). The limit $x = 0$ corresponds to intersection of the crack tip with the interface origin. The vertical dashed lines represent asymptotic toughness values T measured for the individual porcelain and core materials. Note that the data deviate away from these limits as the interface is approached, suggesting a change in the toughness values. However, the toughness does not change—instead, the deviations are a measure of the interfacial influence on the crack, a factor not built in to the K_0 equation above. This influence is analyzed more closely in the work of Kim et al. [53], and is not of direct interest here. Of more importance is that the toughness of the porcelains is considerably less than that of the core materials, so that a crack in the porcelain will arrest, and that in the core will penetrate, the interface. This is in accord with the observations in Figs. 4.5 and 4.6.

We may take the analysis of Kim et al. one stage further, using a well documented scheme by He and Hutchinson [51], to determine a lower bound to the toughness of our interfaces. Basically, delamination will not occur if the interfacial toughness is less than about one half that of the adjacent layer material. For indents in the porcelain, the cracks arrest at the interface. They do not penetrate into the core because of the relatively high toughness of the latter material.

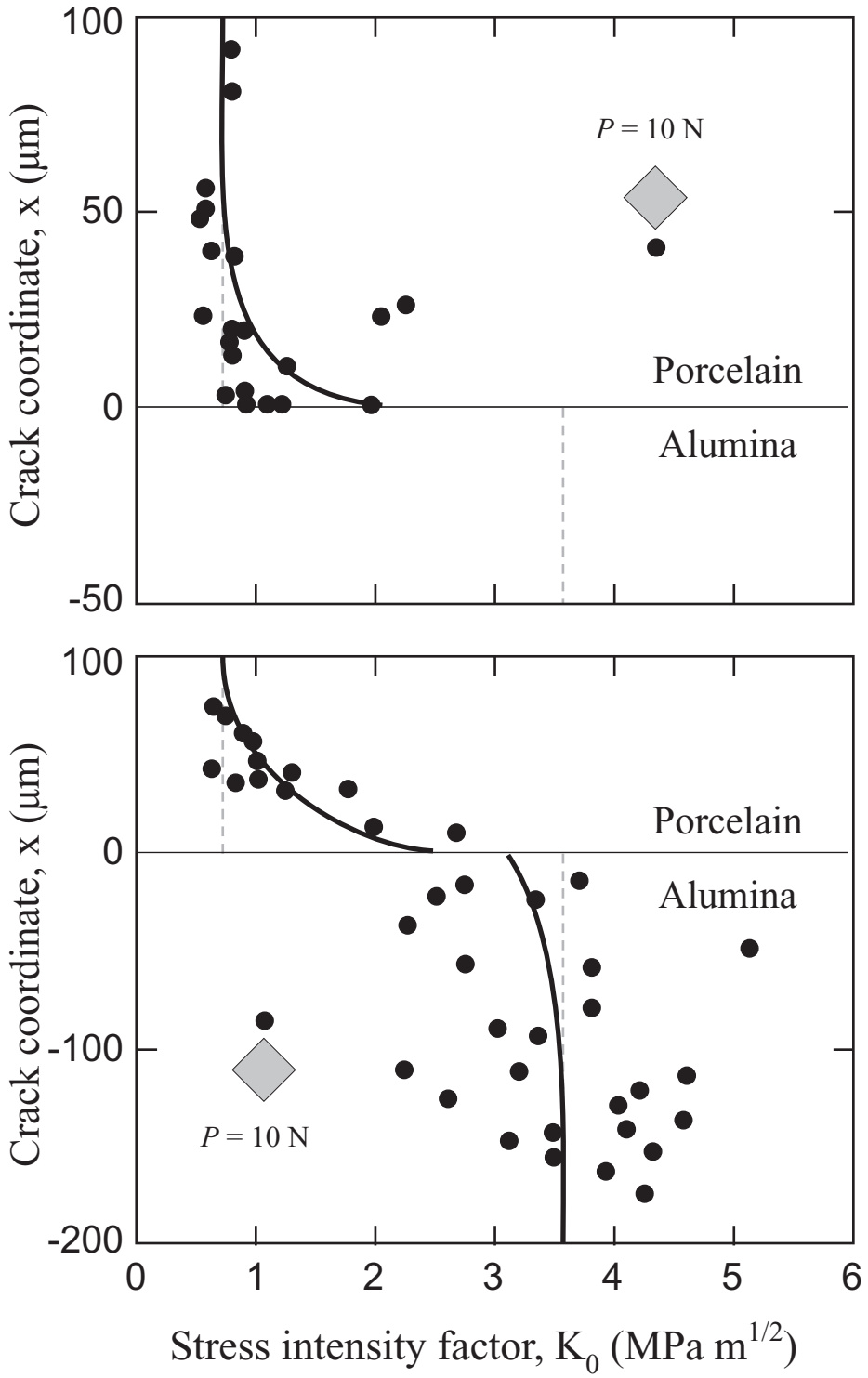

Figure 4.9 Stress intensity factor as function at different location $x = c - h$ from interface, for glass-bonded alumina veneer/core system. Indentation corner cracks in (a) porcelain ($x = h - c_2$) and (b) alumina ($x = c_1 - h$), indicated by inset. Solid lines are empirical fits to data, dashed lines are asymptotic toughness bounds.

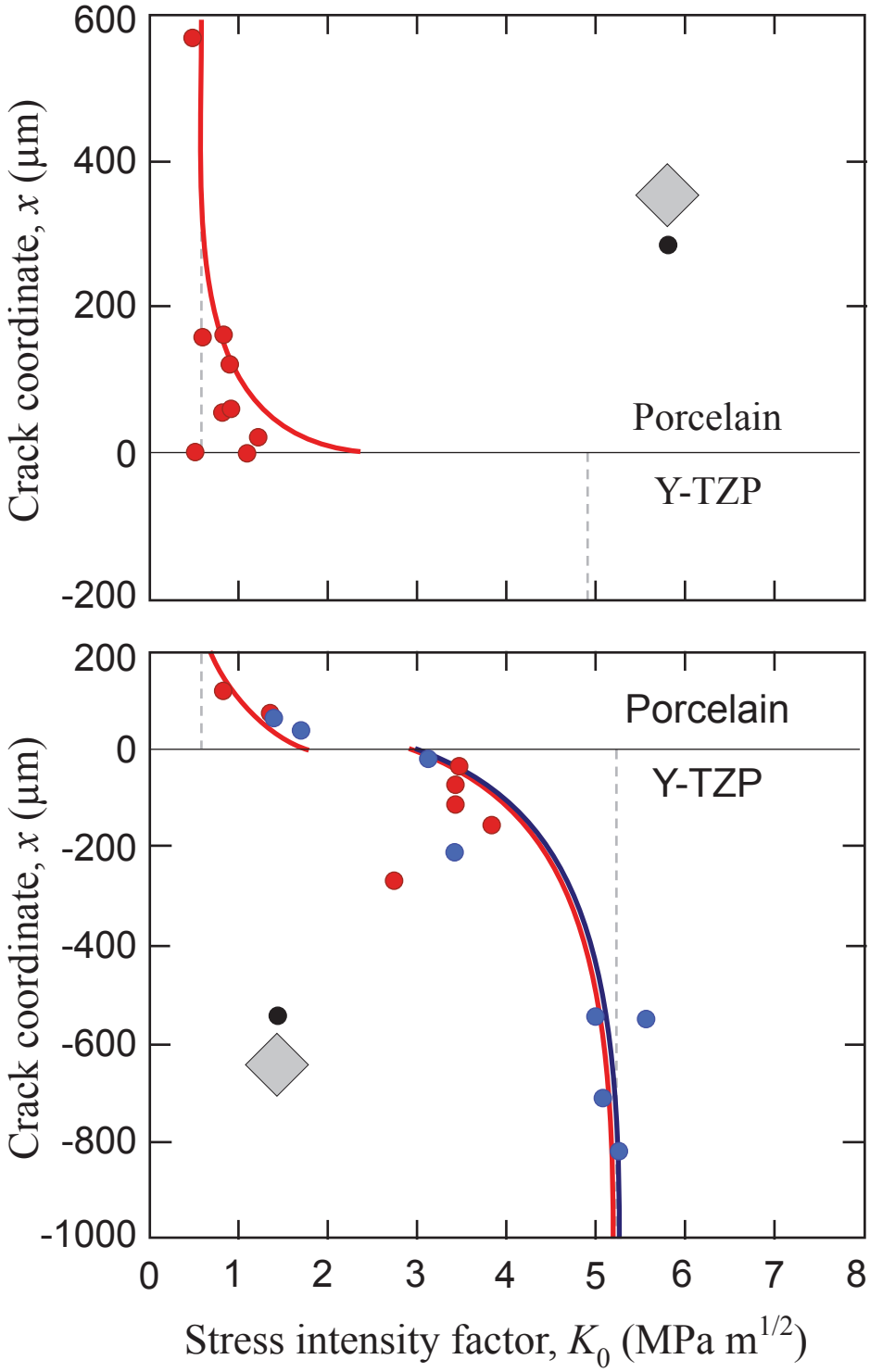

Figure 4.10 Stress intensity factor as function at different location $x = c_{1,2} - h$ from interface, for glass-bonded zirconia veneer/core system. Indentation corner cracks in (a) porcelain ($x = h - c_2$) and (b) zirconia ($x = c_1 - h$), indicated by inset. Solid lines are empirical fits to data, dashed lines are asymptotic toughness bounds. In b) for zirconia, the red points represent glass AP1040, indents made at $P = 40$ N, while the blue points represent glass AP1020 indents made at $P = 35$ N. Note the toughness values converging towards the same values.

Presumably, if we could get the indents closer to the interface, with very high contact loads, we might be able to get delamination to occur. However, we were never able to achieve that in any of our experiments. For indents in the core materials, the cracks always penetrated into the veneer, meaning that the toughness of the interfaces was at least one half that of the bulk veneer (Table 2.1), i.e. around 0.5 MPa $m^{1/2}$. This is a very respectable toughness for any interface, and confirms the mechanical integrity of our glass bonding.

4.5 Discussion and Summary

In this chapter, Vickers indentations were used to probe the effect of a glassy join interlayer on the mechanical behavior of layered dental ceramics. The interfaces of porcelains bonded by glass to alumina and zirconia were indented, and crack lengths were measured as a function of the distance to the glass/core interface. Lead cracks originating in the porcelain layer crossed the glass join, arresting at the core interface. Lead cracks originating in the stiffer, tougher core were increasingly attracted to the weaker porcelain, and penetrated the glass join, extending abruptly into the porcelain. No delamination was observed, confirming good bonding at the interface. Measured toughness values tended to asymptotic limits of 3.5 MPa in the alumina, and 5 MPa in zirconia, with values of both veneers tending to 1 MPa, corresponding to measured values of toughness for these two material. Propagation of the crack from the core ceramic into the veneer across the interface indicated an interface toughness greater than one half the toughness of the veneer, i.e. $\geq$ 0.5 MPa.

Most importantly, the interfaces never delaminated in our joined specimens, attesting to the mechanical integrity of the joins.

A comparison with previous work on resin-based adhesives, specifically polymer matrix particle-filled joins, is of interest. Such adhesives have the advantage of simple processing, without the need for high temperature fusion. In an exhaustive study of such adhesives, Wang et al used a BisGMA-TEGDMA matrix filled with Al_2O_3, SiO_2 and diamond particles to increase the elastic modulus of the join, and at the same time effect good bonding. However, a problem faced by resin-based adhesives is the degree of integrity within the join material—they tend to be much weaker that fused interfaces. They are also susceptible to chemical degradation, and to loss of strength during cyclic loading. In our work, we do not have this integrity issue as the glass is well-homogenized by the stage of application as a join, although the need for high fusion temperatures is an offset. Another advantage of glass joins is that the properties of the glass can be matched more closely to that of the typical dental porcelain, eliminating the prospect of catastrophic radial cracking from flexure of the porcelain on a soft interface support [69].

In high temperature joining, residual stresses due to CTE mismatch between adjacent materials is a frequent problem, one which we have avoided by compositional CTE matching of the glass join. Residual stresses arising from the effect of CTE mismatch in dental systems can be calculated from finite element calculations, as has been demonstrated by Hermann et al. [54]. As we have seen, CTE mismatches below $1x10^{-6}$ C^{-1} are unlikely to result in residual stresses above 30 MPa, and our crack size measurements indicate well below that level. This is very

important, because large stresses can lead to catastrophic fracture of the layer system, either spontaneously or in long-term service, especially in cyclic loading in reactive environments.

Finally, some comments on clinical relevance are in order. This issue has been discussed by Kim et al., but only for fused layers without a glass bonding phase [53]. Recall from Fig. 4.1 the various modes of fracture that compete in top-loaded layer structures. These include inner and outer cone cracks and median cracks that initiate in the occlusal contact region and propagate downwards into the top layer (i.e. the porcelain veneer), driven by Hertzian stresses. There are also radial cracks that initiate at the bottom surface of the lower layer (the core) and propagate upwards, driven by flexure on the compliant dentin underlayer. Our experiments with Vickers corner cracks simulate the likely response of such cracks as they approach an intervening interface, in our case the glass bond interlayer. Cracks in the veneer layer may then be expected to intersect the glass join layer, continue growing, and ultimately arrest at the core interface. Only at exceptionally high loads would such cracks deflect along the interface to cause delamination. It is worth repeating that we saw no such delaminations in our tests, suggesting an entirely adequate bond. Coupled with this is the chemical intermixing evident in the veneer/glass join/core diffusion profiles considered in Chapter 3, which adds an element of strength to the veneer/core bond. On the other hand, cracks that initiate in the core layer will be expected to penetrate directly into the veneer, and potentially proceed through the veneer layer to the occlusal surface, exposing the tooth interior to the oral environment [70]. However, flexural stresses in the tooth are expected to be

compressive at the top surface, thereby inhibiting full fracture.

We can conclude that glass bonding is an effective way of joining veneer and core layers, with inbuilt provisions to resist catastrophic fracture in dental crown applications.

Chapter 5: Summary and Future Work

5.1 Summary

This thesis has outlined how to fabricate and test veneer porcelain and ceramic core joined by glass fusion, for potential applications in dental crowns. The methodology has involved processing of new glass types, optimizing fusion processes, and mechanical evaluation of the finished layer system.

Glass preparation and selection has been discussed in Chapter 2. This part proved to be a daunting task, because great care had to be taken to match properties of the glass to both veneer and core materials. Commercial glasses were found to be inadequate for this purpose, so new glass compositions had to be designed and fabricated. Sol gel processing formed the basis of the processing route. Different glass compositions led to various degrees of wetting, crazing and porosity on the ceramic substrates, so the composition and processing route itself had to be optimized.

The actual joining process has been considered in Chapter 3. Again, the process of joining, firing times and temperatures, along with compositional considerations, have been discussed. Some of the combinations produced intact interfaces with good characteristics, as determined by optical microscopy. Simple mechanical screening tests were used to eliminate unsatisfactory layer systems. Detailed microprobe analysis has been applied to determine interdiffusional layers at the veneer/glass and glass/core interfaces.

In Chapter 4, the mechanical integrity of the glass joins investigated. A Vickers indentation probe method has been used to introduce controlled cracks in veneer/glass/core sections, to investigate the integrity of the join interfaces. No delamination was observed in any of our experiments, confirming strong bonding. The indentation method also enabled confirmation of insignificant residual stresses, as well as providing an estimate of the join interface toughness.

5.2 Future Work

This work has provided the first steps in demonstrating the feasibility of glass joining in the preparation of dental crowns. There is room for further study of this methodology. Further refinement of the sol gel processing route is in order, e.g. role of finer glass frits in the joining process. Our work has examined only porcelain fused to alumina and zirconia cores, but other material systems could be explored. The possibility of developing a graded structure, by fusing together several layers with gradually changing modulus from veneer top surface to core bottom surface is a potential future development.

From the mechanical evaluation standpoint, there is a need to look more closely at the role of water and other chemical species on the aging properties of glass joins. All ceramics are notoriously susceptible to chemical degradation. The possible role of cyclic loading is another issue that should be investigated.

Finally, there needs to be some attempt to demonstrate transferability of the glass fusion technology to the dental laboratory. This would involve dental

clinicians, to see if the new fabrication methods can withstand oral environments.

This is work for the next generation of researchers.

Appendix

CTE Calculations

a) Winkelmann Schott and Appen factors table. This table was hyperlinked to the next, the Calculation sheet for compositions, to provide a linear correlation between composition and CTE. In the table we see the effect of each oxide on the CTE, by wt or mol % as denoted. Network formers SiO_2, B_2O_3 have the smallest effects for both sets of factors (W-S & AA). Al2O3's behavior as an intermediate oxide, has a deleterious effect on CTE above certain mol %s.

Oxide	Winkelmann & Schott Factors (wt %)	*Molec Wt.*	W & S Factors per mol	Appen Factor per mol	Appen Factor per mol *(10^-7)
B2O3	0.1	69.62	2.32E-07	1.00E-07	1.00
MgO	0.1				
SiO2	0.8	60.09	1.60E-06	3.80E-06	38.00
ZnO	1.8				
As2O3	2				
Li2O	2				
P2O5	2				
BaO	3	153.33	1.53E-05	2.00E-05	200.00
PbO	3				
Al2O3	5	101.78	1.70E-05	-3.00E-06	-30.00
CaO	5	56.09	9.35E-06	1.30E-05	130.00
K2O	8.5				
Na2O	10	61.98	2.07E-05	3.95E-05	395.00

b) Example calculation sheet for compositions. By keeping the volume of TEOS constant (20 ml), and translating that to a constant mol % (60 or 65 mol %), then varying the mol % of the other components, we arrived at the desired CTE. Then, composition for that CTE, was converted to weight % of constituent salts (nitrates, some acetates). Note that the same CTE could be attained via various compositions, however, we had to take chemical durability (B, Ca and Na components), melting temperature (Al, B, Na components), and CTE (Ba, B, Na) into account. So we used compositions that kept these different components within appropriate ranges.

Base glass

Example glass

Goal: Max. CTE 1														
Oxide	**Original Mol %**	**# of Mols**	**Mol %**	**%*AF***		**For Theoretical calculation:**								
SiO2	60	60.00	60.00	2.28E-06		*Liquids*	*Volume (ml)*	*Density*	*Molec Wei*	*Moles*	*Mole Fraction of Total*			
Al2O3	3	3.32	3.32	-9.97E-08		**TEOS (98% purity)**	20	0.934	208.33	0.087872126	0.6			
CaO	8	9.20	9.20	1.20E-06						**Total Moles**	0.146454			
Na2O	7	5.54	5.54	2.19E-06										
BaO	6	2.22	2.22	4.43E-07		**water**	4	1	18.016					
B2O3	16	19.72	19.72	-8.64E-09		**etOH**	56							
	100	*40*		6.00E-06		*Oxide*	*Ox. Mol. Frac*	*Moles Nee*	*Conversion*	*Solids*	*Molecular*	***Mass Needed (g)***		
		100	100.00	is10^7 times 3A		Na2O	0.06	0.01	2.00	**NaNO3**	84.99	1.379		
				6.00E-06	is theoreti	CaO	0.09	0.01	1.00	**Ca(NO3)2*4H2O**	236.09	3.180		
Start with 20 ml of 98% TEOS						Al2O3	0.03	0.00	2.00	**Al(NO3)3*9H2O**	375.13	3.652		
						B2O3	0.20	0.03	2.00	**H3BO3**	61.83	3.572		
						BaO	0.02	0.00	1.00	**Ba(CH3CO2)2**	255.416	0.829		
										Ba(NO3)2	261.35	0.848		
						For experimental calc.:								
						Solids	*Mass (g)*	*MW*	*Moles*	*Oxide*	*Conversion*	*Mol Oxide*	*Ox. Mol. %*	
						NaNO3	2.1904	84.99	0.025772	**Na2O**	2	0.012886	**9.557033**	
						Ca(NO3)2*4H2O	1.1332	236.09	0.0048	**CaO**	1	0.0048	**3.559807**	
						Al(NO3)3*9H2O	4.3948	375.13	0.011715	**Al2O3**	2	0.005858	**4.34435**	
						H3BO3	2.896	61.83	0.046838	**B2O3**	2	0.023419	**17.36868**	
						Liquids	*Volume (ml)*				*Density*			
						TEOS	20	208.33	0.087872	**SiO2**	0.934	0.087872	**65.17013**	
						water	50	18.016	2.775311	n/a	1			
						ethanol	56							
						total mol oxide	0.13483497		**r (H2O:TE**	31.58351758				

** AA Factor X mol% constituent*

c) Some of our compositions, as calculated by the Appen factor method.

Starting Composition

Oxide	mol% needed	Solids	wt. needed	4 X WT NEEDED	AF	
SiO2	60.00				2.28E-06	
Al2O3	2.67	Al(NO3)3*9H2O	2.93	***11.72***	-8.00E-08	
CaO	8.00	Ca(NO3)2*4H2O	2.77	***11.08***	1.04E-06	
Na2O	12.44	NaNO3	3.10	***12.40***	4.92E-06	
BaO	11.56	Ba(CH3CO2)2	4.32	***17.28***	2.31E-06	***Calculated CTE***
B2O3	5.33	H3BO3	0.97	***3.88***	-6.88E-08	1.04E-05
						6.52E-06 SF
						8.70E-06 Orig_SF

BaO **reduced**

Oxide	mol% needed	Solids	wt. needed	4 X WT NEEDED	% AF	
SiO2	60.00				2.28E-06	
Al2O3	3.13	Al(NO3)3*9H2O	3.44	***13.76***	-9.40E-08	
CaO	9.40	Ca(NO3)2*4H2O	3.25	***13.00***	1.22E-06	
Na2O	14.63	NaNO3	3.64	***14.56***	5.78E-06	
BaO	6.56	Ba(CH3CO2)2	2.45	***9.80***	1.31E-06	***Calculated CTE***
B2O3	6.27	H3BO3	1.14	***4.56***	-5.48E-08	1.04E-05
						6.42E-06
						9.24E-06

BaO **increased**

Oxide	mol% needed	Solids	wt. needed	4 X WT NEEDED	% AF	
SiO2	60.00				2.28E-06	
Al2O3	2.20	Al(NO3)3*9H2O	2.41	***9.64***	-6.59E-08	
CaO	6.59	Ca(NO3)2*4H2O	2.28	***9.12***	8.57E-07	
Na2O	10.25	NaNO3	2.55	***10.20***	4.05E-06	
BaO	16.56	Ba(CH3CO2)2	6.19	***24.76***	3.31E-06	***Calculated CTE***
B2O3	4.39	H3BO3	0.80	***3.20***	-8.88E-08	1.03E-05

References

1. Aboushelib MN, de Jager N, Kleverlaan CJ, Feilzer AJ. Microtensile bond strength of different components of core veneered all-ceramic restorations. Dental Materials 2005 21**:**984.
2. Wang YJ, Lee JJ, Lloyd IK, Wilson OC, Rosenblum M, Thompson V. High modulus nanopowder reinforced dimethacrylate matrix composites for dental cement applications. Journal of Biomedical Materials Research Part A 2007;82A**:**651.
3. Lee JJW, Wang Y, Lloyd IK, Lawn BR. Joining veneers to ceramic cores and dentition with adhesive interlayers. Journal of Dental Research 2007;86**:**745.
4. Lee JJW, Lloyd IK, Chai H, Jung YG, Lawn BR. Arrest, deflection, penetration and reinitiation of cracks in brittle layers across adhesive interlayers. Acta Materialia 2007;55**:**5859.
5. Lee JJW, Chai H, Lloyd IK, Lawn BR. Crack propagation across an adhesive interlayer in flexural loading. Scripta Materialia 2007;57**:**1077.
6. Rekow ED, Thompson VP. Engineering long term clinical success of advanced ceramic prostheses. Journal of Materials Science: Materials in Medicine 2007;18**:**47.
7. Partridge JH. Glass to metal seals. 1949.
8. Doremus RH. Glass science. 1973.
9. Choi SY. Stable sealing glass for planar oxide fuel cell. Journal of Non-Crystalline Solids 2002;103.

10. Pascual MJ. Glass-forming ability, sinterability and thermal properties in the systems RO-BaO-SiO_2 (R=Mg, Zn). Journal of Non-Crystalline Solids 2004;149.

11. Jean JH. Crystallization kinetics and mechanism of low-dielectric, low-temperature, cofirable $CaO–B_2O_3–SiO_2$ glass-ceramics. Journal of the American Ceramic Society 1999;82**:**1725.

12. Fujinu S. Density, surface tension, and viscosity of $PbO–B_2O_3–SiO_2$ glass melts. Journal of the American Ceramic Society 2004;87**:**p. 10.

13. Saied M, Wang Y, Dreyer E, Lloyd I, OC Wilson J, Rosenblum M. Glassy ceramic-ceramic joins for laminar dental restorations. IADR/AADR/CADR 83rd General Session (March 9-12, 2005).

14. Saied M, Wang Y, Lloyd I, OC Wilson J, Rosenblum M, Thompson V. Progress on glassy joins for laminar dental all-ceramic restorations. ADEA/AADR/CADR Meeting & Exhibition (March 8-11, 2006).

15. Saied M, Slepitza J, Lloyd I, OC Wilson J, Janal M. Characteristics of glass-joined veneer-core layers for dental applications. IADR/AADR/CADR 85th General Session and Exhibition.

16. Saied M, Lloyd I, Rekow E. Investigating the use of glass joins for dental restoration systems. AADR 37th Annual Meeting and Exhibition.

17. Norton MG. Selection criteria for sealing glasses for sic packaging. Journal of Non-Crystalline Solids 2004;173.

18. Ley KE. Glass-ceramic sealants for solid oxide fuel cells: Part I. Physical properties. Journal of Materials Research 1997;11**:**1489.

19. Babcock CL. Silicate glass technology methods. 1977.

20. Mysen B, Richet P. Silicate glasses and melts: Properties and structure. Elsevier; 2005.

21. Yoldas BE. Modification of polymer-gel structures. Journal of Non-Crystalline Solids 1984;63**:**145.

22. Yoldas BE. Monolithic glass-formation by chemical polymerization. Journal of Materials Science 1979;14**:**1843.

23. Yoldas BE. Alumina sol preparation from alkoxides. American Ceramic Society Bulletin 1975;54**:**289.

24. Winkelmann A, Schott O. Über die elastizität und über die druckfestigkeit verschiedener neuer gläser in ihrer abhängigkeit von der chemischen zusammensetzung. Ann. Physik Chemie 1894;51**:**697

25. Winkelmann A, Schott O. Über thermische widerstandscoefficienten verschiedener gläser in ihrer abhängigkeit von der chemischen zusammensetzung. Ann. Physik Chemie 1894;51**:**730

26. Winkelmann A, Schott O. Über die specifischen wärmen verschieden zusammengesetzter gläser. Ann. Physik Chemie 1893;49**:**401

27. Appen AA. Calculating the properties of silicate glasses. 1956.

28. Appen AA. "Khimiya stekla" (glass chemistry). Leningrad: 1959.

29. Appen AA. The chemistry of glass (in Russian). Leningrad: 1970.

30. Priven AI. General method for calculating the properties of oxide glasses and glass-forming melts from their composition and temperature. Glass Technology 2004;45**:**244.

31. Gehlhoff G, Thomas M. The physical properties of glass in relation to its composition. I. The electrical conductivity of glass. Z. techn. Physik 1925;6**:**544.

32. Gehlhoff G, Thomas M. The physical properties of glass in relation to its composition. Ii. The mechanical properties of glass. Z. techn. Physik 1926;7**:**105.

33. Gehlhoff G, Thomas M. The physical properties of glass and their relation to glass composition. Iii. Viscosity of glass. Z. techn. Physik 1926;7**:**260.

34. Volf MB. Mathematical approach to glass. Elsevier; 1988.

35. Fluegel A. Glass viscosity calculation based on a global statistical modeling approach. European Journal of Glass Science and Technology Part A, 2007;48,**:**p 13.

36. Fluegel A, Varshneya AK, Earl DA, Seward TP, Oksoy D. Improved composition-property relations in silicate glasses, part I: Viscosity. In: editor. Proceedings of the 106th Annual Meeting of the American Ceramic Society. City: Year. p. 129.

37. Yoldas BE. Formation of titania-silica glasses by low-temperature chemical polymerization. Journal of Non-Crystalline Solids 1980;38-9**:**81.

38. Yoldas BE, D.P. P. Colloidal versus polymer gels and monolithic transformation in glass-forming systems. Journal of Non-Crystalline Solids 1981 46 153.

39. Yoldas BE. Preparation of glasses and ceramics from metal-organic compounds. Journal of Materials Science 1977; 12 1203.

40. Lombardo SJ, Westa AC. The role of thermal and transport properties on the binder burnout of injection-molded ceramic components. Chemical Engineering Journal 1998; 71 243.

41. Smay JE, Gratson GM, Shepherd RF, Cesarano J, Lewis JA. Directed colloidal assembly of 3d periodic structures. Advanced Materials 2002;14**:**1279.

42. Smay JE, Cesarano J, Lewis JA. Colloidal inks for directed assembly of 3-d periodic structures. Langmuir 2002;18**:**5429.

43. Lewis JA, Smay JE, Stuecker J, Cesarano J. Direct ink writing of three-dimensional ceramic structures. Journal of the American Ceramic Society 2006;89**:**3599.

44. Verne E, Brovarone CV, Moisescu C. Glazing of alumina by a fluoroapatite-containing glass-ceramic. Journal of Materials Science 2005;40**:**1209.

45. Faaland S. Reactions between calcium- and strontium-substituted lanthanum cobaltite ceramic membranes and calcium silicate sealing materials. Chemical Materials 2001;13**:** 723

46. Nielsen KA, Solvang M, Nielsen AR, Dinesen AR, Beeaff D, Larsen PH. Glass composite seals for SOFC application. Journal of the European Ceramic Society 2007;27**:**1817.

47. Lawn BR, Jung Y-G, Peterson IM, Kim DK. Lifetime-limiting strength degradation from contact fatigue in dental ceramics. Journal of Dental Research 2000; 79**:**722.

48. Guazzatoa M, Albakrya M, Ringer SP, Swaina MV. Strength, fracture toughness and microstructure of a selection of all-ceramic materials. Part I. Pressable and alumina glass-infiltrated ceramics. Dental Materials 2004;20**:**441.

49. Guazzatoa M, Albakrya M, Ringer SP, Swaina MV. Strength, fracture toughness and microstructure of a selection of all-ceramic materials. Part ii. Zirconia-based dental ceramics. Dental Materials 2004;20**:**449.

50. Denry I, Rosenstiel S. Flexural strength and fracture toughness of Dicor glass-ceramic after embedment modification. . Journal of Dental Research 1993; 72**:**572.

51. He M-Y, Hutchinson JW. Crack deflection at an interface between dissimilar elastic materials. International Journal of Solids and Structures 1989;25**:**1053.

52. Wuttiphan S, Lawn BR, Padture NP. Crack suppression in strongly-bonded homogeneous/heterogeneous laminates: A study on glass/glass-ceramic bilayers. Journal of the American Ceramic Society 1996;79**:**634.

53. Kim J-W, Bhowmick S, Hermann I, Lawn BR. Transverse fracture of brittle layers: Relevance to failure of all-ceramic dental crowns. Journal of Biomedical Materials Research 2006;79B**:**58.

54. Hermann I, Bhowmick S. Competing fracture modes in brittle materials subject to concentrated cyclic loading in liquid environments: Trilayer structures. Journal of Materials Research 2006;21**:**512.

55. Kim JH, Miranda P, Kim DK, Lawn BR. Effect of an adhesive interlayer on the fracture of a brittle coating on a supporting substrate. Journal of Materials Research 2003;18**:**222.

56. Lawn BR, Deng Y, Thompson VP. Use of contact testing in the characterization and design of all-ceramic crown-like layer structures: A review. Journal of Prosthetic Dentistry 2001;86**:**495.

57. Lawn BR, Pajares A, Zhang Y, Deng Y, Polack MA, Lloyd IK, Rekow ED, Thompson V. Materials design in the performance of all-ceramic crowns. Biomaterials 2004;25**:**2885.

58. Frank FC, Lawn BR. On the theory of Hertzian fracture. Proceedings of the Royal Society of London 1967;A299**:**291.

59. Chai H, Lawn BR. Hydraulically pumped cone fractures in brittle solids. Acta Materialia 2005;53**:**4237.

60. Zhang Y, Song JK, Lawn BR. Deep-penetrating conical cracks in brittle layers from hydraulic cyclic contact. Journal of Biomedical Material Research B Applied Biomaterials 2005;73**:**186.

61. Lawn BR, Padture NP, Cai H, Guiberteau F. Making ceramics 'ductile'. Science 1994;263**:**1114.

62. Guiberteau F, Padture NP, Cai H, Lawn BR. Indentation fatigue: A simple cyclic Hertzian test for measuring damage accumulation in polycrystalline ceramics. Philosophical Magazine 1993;A 68**:**1003.

63. Cai H, Kalceff MAS, Hooks BM, Lawn BR, Chyung K. Cyclic fatigue of a mica-containing glass–ceramic at Hertzian contacts. Journal of Materials Research 1994;9**:**2654.

64. Jung Y-G, Peterson IM, Kim DK, Lawn BR. Lifetime-limiting strength degradation from contact fatigue in dental ceramics. Journal of Dental Research 2000;79**:**722.

65. Chai H, Lawn BR, Wuttiphan S. Fracture modes in brittle coatings with large interlayer modulus mismatch. Journal of Materials Research 1999;14**:**3805.

66. Anstis GR, Chantikul P, Marshall DB, Lawn BR. A critical evaluation of indentation techniques for measuring fracture toughness: I. Direct crack measurements. Journal of the American Ceramic Society 1981;64**:**533.

67. Marshall DB, Lawn BR. An indentation technique for measuring stresses in tempered glass surfaces. Journal of the American Ceramic Society 1977;60**:**86.

68. Lardner TJ, Ritter JE, Shiao ML, Lin MR. Behavior of indentation cracks near free surfaces and interfaces. International Journal of Fracture 1990;44**:**133.

69. Chai H, Lawn BR. Role of adhesive interlayer in transverse fracture of brittle layer structures. Journal of Materials Research 2000;15**:**1017.

70. Miranda P, Pajares A, Guiberteau F, Cumbrera FL, Lawn BR. Contact fracture of brittle bilayer coatings on soft substrates. Journal of Materials Research 2001;16**:**115.

Curriculum Vitae

MEY SAIED
4319 Rowalt Dr, Apt. 302, College Park, MD 207
Cell: 617.821.3724, meysaied@umd.edu

EDUCATION

University of Maryland -	Ph.D. Mater. Sci. & Eng.	12 - 2008 *College Park, MD*
Royal College of Art -	M.Phil Ceramics Research,	01 - 1997 *London, UK*
Imperial College -	B.Eng. Mater. Sci. & Eng,	06 - 1994 *London, UK*

EXPERIENCE

University of Maryland, College Park, MD *(Aug 2003- present)*

- *Graduate Research Assistant & PhD Candidate*
- *PROMISE Peer Mentor (Aug 2004-May 2005)*
- *Eleanor Roosevelt High School student research mentor (Aug 2006 – May 2007)*

Harvard University Cambridge, MA *(Jul 2002-Aug 2003)*

Lab Administrator

- Grant management, purchasing, and administration.

Nubian Studies Proceedings Boston, MA *(Jan 2002- Oct 2002, pt/time)*

Editing & Publishing Assistant,

- Layout & desktop publishing of 1998 Nubian Studies Conference Proceedings

Education Development Center Newton, MA *(Sept 2001-Dec 2001)*

Consultant

- NSF-funded project DigNubia: ancient ceramics & archaeological materials characterization.

Juneteenth Productions North State, Sudan *(Dec 2002- Feb 2001)*

Production Coordinator, "Nubia & the Mysteries of Kush" Documentary

National Council for Antiquities & Museums Bayuda Desert, Northern State, Sudan

Interpreter and Assisting Archaeologist

United Nations World Food Program Khartoum, Sudan *(Apr 1999-Dec 2000)*

Reports & Information Assistant, Gender Task Force Member

Rupert Spira Ceramics Shropshire, UK *(Oct 1997- May 1998)*

Ceramics Apprentice

AWARDS

- Ruth L. Kirschstein NRSA/NIH Individual Predoctoral Minority Fellowship Award

  (May 2006 –May 2010)
- University of Maryland Centre for Women & Minorities Graduate School Fellowship

  (Oct 2003- Aug 2005)

CONFERENCES

- Saied M, Lloyd I, Rekow E, "Investigating the use of glass joins for dental restoration systems", # 0658, AADR Dallas, TX, 2008,
- Saied M, Slepitza J, Lloyd I, OC Wilson J, Janal M, "Characteristics of glass-joined veneer-core layers for dental applications", #2016, IADR New Orleans, LA, 2007
- Saied M, Wang Y, Lloyd I, OC Wilson J, Rosenblum M, Thompson V, "Progress on glassy joins for laminar dental all-ceramic restorations", #1880, AADR Orlando, FL, 2006
- Saied M, Wang Y, Dreyer E, Lloyd I, OC Wilson J, Rosenblum M, "Glassy ceramic-ceramic joins for laminar dental restorations", #1770, IADR Baltimore, MD, 2005

JOURNAL PUBLICATIONS

- MA Saied, IK Lloyd, OC Wilson Jr. "Design of join glass composition for layered all ceramic restorations", Journal of Non-Crystalline Solids, *in progress*.
- MA Saied, IK Lloyd, BR Lawn, WK Haller, "Joining Dental Ceramic Layers by Use Of Lead-Free Glass", Journal of Dental Research, *in progress.*
- MA Saied, BR Lawn, IK Lloyd, "Interfacial Characterization of joined laminar ceramic restorations", Dental Materials, *in progress.*

THESES

- M.Phil. Thesis Title: *An Investigation of Sudanese Raw Materials for Ceramic Manufacture*
- B.Eng. Senior Dissertation: *Ceramic Matrices and Composites Fabricated by Processing of Silicate Sols and Gels*

LANGUAGES

Fluent in English and Arabic, Proficient in French

REFERENCES

Available upon request.